THE IMPACT OF EXTRACELLULAR MATRIX STIFFNESS ON ANGIOGENESIS

A Dissertation

by

PO-FENG LEE

Submitted to the Office of Graduate Studies of
Texas A&M University
in partial fulfillment of the requirements for the degree of

DOCTOR OF PHILOSOPHY

Approved by:

Chair of Committee,	Alvin T. Yeh
Committee Members,	Kayla J. Bayless
	Brian E. Applegate
	Roland R. Kaunas
Head of Department,	Gerard L. Cote

December 2012

Major Subject: Biomedical Engineering

ABSTRACT

Sprouting endothelial cells (ECs) use soluble and insoluble cues to guide migration and expand the existing vascular network to meet changing trophic needs of the tissue during angiogenesis. A noninvasive and non-destructive nonlinear optical microscopy (NLOM) technique was used to optically image endothelial sprouting morphogenesis in three dimensional (3D) collagen matrices with simultaneously captured signals from collagen fibers and endothelial cells using second harmonic generation (SHG) and two-photon excited fluorescence (TPF), respectively. Sprout advancement and lumen expansion companying with ECM alteration were the synergistic results of membrane-associated matrix metalloproteinase and cell traction evidenced by proteinase inhibition and Rho-associated kinase (p160ROCK) inhibition experiments. These physical EC-ECM interactions suggest that ECM mechanical properties may influence angiogenic responses. In a 3D angiogenesis model, we measure angiogenic responses as a function of collagen matrix stiffness by inducing collagen cross-linking with microbial transglutaminase (mTG). Collagen matrices stiffen with both mTG treatment and incubation time as evidenced with biaxial mechanical test results and collagen TPF intensity increases with mTG treatment and that the ratio of TPF/SHG correlates with biaxial tested mechanical stiffness. SHG and optical coherence microscopy (OCM) are further used to show that other physical properties of the matrix do not change with mTG treatment, thus providing the same density but different stiffness with which to measure angiogenic responses. Stiffer matrices promote angiogenesis with more

invading sprouts that invade deeper. No differences in lumen size were observed between control and mTG stiffened 3D cultures, but there was evidence of greater matrix remodeling in stiffer gels using NLOM. Results of this study show angiogenic responses are enhanced with increasing stiffness and suggest that these properties may be used in tissue engineering and regenerative medicine applications to engineer angiogenesis.

ACKNOWLEDGEMENTS

I would like to thank my committee chair, Dr. Yeh, and my committee members, Dr. Bayless, Dr. Applegate, Dr. Kaunas, and Prof. Humphrey, for their guidance and support throughout the course of this research.

Very appreciate Dr. George Davis (Columbia, MO) for the generous gift of in pLenti6/V5 vector expressing EGFP. This work was made possible from the support of funding sources from AHA SDG (#0530020N) and Public Health Science Grant HL-095786 to KJB, NIH EB008366 and NSF Career Award to ATY.

Thanks also go to my friends and colleagues and the department faculty and staff for making my time at Texas A&M University a great experience.

Finally, thanks to my mother and father for their encouragement.

NOMENCLATURE

SMC	Smooth Muscle Cell
MMP	Metalloproteinase
mTG	Microbial Transglutaminase
VEGF	Vascular Endothelial Growth Factor
FGF	Fibroblast Growth Factor
PDGF	Platelet Derived Growth Factor
TGF-β	Transforming Growth Factor-β
ADAMs	a Disintegrin and Metalloproteinase Domains
ADAMTs	a Disintegrin and Metalloproteinase with Thrombospondin motifs
TIMPs	Tissue Inhibitor of Metalloproteinases
ECM	Extracellular Matrix
EC	Endothelial Cell
NLOM	Nonlinear Optical Microscopy
SHG	Second Harmonic Generation
TPF	Two Photon Fluorescence
CIR	Collagen Intensity Ratio
CAI	Collagen Alteration Index
OCM	Optical Coherence Microscopy

TABLE OF CONTENTS

LIST OF FIGURES

LIST OF TABLES

CHAPTER I

INTRODUCTION AND LITERATURE REVIEW

Angiogenesis is defined as new blood vessel formation from pre-existing vessels and plays a key role in normal tissue growth, wound repair and the progression of malignant diseases. Several diseases related to excessive angiogenesis include cancer, atherosclerosis, chronic inflammation and diabetic retinopathy, while the diseases related to insufficient angiogenesis are myocardial infarction and chronic wound healing [1-4]. Regenerative medicine or tissue engineering aims at replacing or regenerating tissue to restore, maintain or improve tissue function [5]. Capillaries and the vascular system are required to supply nutrients, remove waste products, and control pressure and temperature through coordination of vasoconstriction and vasodilation [6-9]. Due to diffusion limitations, cells cannot survive more than few hundred micrometers away from nearby capillary [10-12]. To create thick tissue is still a major challenge in tissue engineering owing to lack of a functional vasculature to provide a nutrient supply [13]. *In vivo* vascularization includes angiogenesis and vasculogenesis, which are different processes. *In vivo* angiogenesis consists of 6 steps: vasodilation, basement membrane degradation, adherent cell migration, lumen formation, synthesis of basement membrane, and recruitment of pericytes or smooth muscle cells (SMCs) [6, 8, 14-18]. *In vivo* vasculogenesis can be divided into 6 steps as well: differentiation of mesodermal cells into angioblasts, endothelial cell (EC) generation from angioblasts, primordial vessel formation by ECs that lack lumens, formation of nascent of endothelial tube composed

of polarized ECs, primary vascular network formation from an array of nascent endothelial tubes, and recruitment of pericytes and SMCs [8, 19]. Therefore, a complete understanding of angiogenesis is necessary to prevent disease progression and for proper tissue engineering [13]. ECs are the primary cells responsible for initiating angiogenesis under the influence of soluble and insoluble biochemical factors. Growth factors and lipids deliver potent pro-angiogenic signals that stimulate endothelial outgrowth and invasion events which require membrane-associated matrix metalloproteinases (MMPs). The extracellular matrix (ECM) is a scaffold that provides mechanical support and adhesive contact sites, along with mechanical signals, that combine with biochemical cues to promote angiogenesis. In additional to biochemical influences, angiogenesis is also affected by mechanical stimuli, such as shear stress and cyclic strain [20-25]. ECM stiffness can affect cell behavior but how that affects the interactions between ECs and ECM is still not clear. Here, we will brief review various factors that influence angiogenesis, such as soluble biochemical cues, proteinases, and insoluble cues (with a particular focus on collagen 3D scaffolds). Further, we will discuss how to tune collagen topographical properties and mechanical properties and how other groups use nonlinear optical microscopy or confocal microscopy to probe optical/topographical/mechanical properties of collagen. Finally we will go over other groups' work on tuning 3D scaffold stiffness and its influence on angiogenesis. In chapter II, we elucidated how ECs interact with collagen matrices during angiogenesis and lumenogenesis. In chapter III, one enzymatic crosslinking method is used, where microbial transglutaminase (mTG) was applied to decouple collagen stiffness from its topographical properties and further

investigated angiogenic responses and ECs-matrix interactions during lumenogenesis. The last chapter includes conclusions from these studies and also possible future experiments. The uniqueness of this work is we successfully used mTG to strengthen collagen stiffness without changing its microstructure, evidenced with its associated mechanical, optical and topographical properties measured with our biaxial bioreactor and NLOM-OCM combined system and further proven stiffness of mTG treated collagen enhanced angiogenic responses in vitro. Not only capable of characterizing optical property and microstructure of ECM noninvasively and nondestructively, NLOM also provided spatial and temporal information of EC-matrix and revealed collagen alterations during lumenogenesis were associated with lumen size and ECM stiffness enhanced EC-matrix interactions around lumens. The linear relationship between TPF/SHG (optical property) and stiffness (mechanical property) shed a light to measure ECM with NLOM noninvasively.

Soluble Biochemical Cues for Angiogenesis

Vascular Endothelial Growth Factor (VEGF)

The VEGF family contains 5 members, which are secreted and dimeric glycoproteins of approximately 40 kDa. The isoforms are VEGF-A (VEGF), -B, -C, -D and placenta growth factor (PLGF) [26-31]. The VEGF family of receptors includes three protein-tyrosine kinases (vascular growth factor receptor-1 (VEGFR-1), VEGFR-2 and VEGFR-3) and two non-protein kinase co-receptors (neuropilin-1 and neuropilin-2) [29-31].

VEGF binding causes VEGFR activation and the activated VEGFR leads to different cellular and angiogenic responses, such as increased EC permeability [32, 33], inhibition of EC apoptosis [34], stimulation of EC proliferation [35], enhancement of EC migration [36], production of ECM proteases and protease inhibitors from ECs [37], and production of nitric oxide synthase [38]. VEGF production is regulated by hypoxia, and VEGF isoforms are produced by various cell types, including ECs and tumor cells [27, 28, 31, 39]. Overall, all human VEGF receptors, their ligands and functions are summarized in Table 1-1 [29].

Fibroblast Growth Factor (FGF)

FGF-1 (acidic FGF) and FGF-2 (basic FGF) both are capable of stimulating angiogenesis [40, 41]. The receptor of FGF is FGFR, and there are 4 different types of FGFR [42, 43]. The action of FGF is not specific to ECs, and FGFs act on cells derived from mesoderm and neuroectoderm, such as ECs, fibroblasts and pericytes [44]. There are several EC activities modulated by FGF, which including stimulation of *in vivo* and in vitro angiogenesis [41, 45], stimulation of EC proliferation [46], enhancement of EC migration [41, 47] and stimulation of matrix protease production in ECs [48].

Platelet-derived Growth Factor (PDGF)

PDGF receptors, members of RTK (receptor tyrosine kinase) superfamily, are found in ECs, pericytes and SMCs [49-52]. PDGF isoforms are produced by various cells, such ECs, fibroblasts, and macrophages [53]. PDGF, the mitogen and chemoattractant for most mesenchymal cells [53], stimulates pericyte proliferation [52] and increases capillary stability [54-57].

Table 1- 1. Human VEGF receptors, ligands and functions

receptors	ligands	functions
VEGFR1	VEGF-A, VEGF-B, PIGF	Vasculogenesis, angiogenesis, and monocyte/macrophage motility
VEGFR2	VEGF-A, VEGF-C, VEGF-D	Vasculogenesis, angiogenesis, vascular permeability and endothelial cell motility
VEGFR3	VEGF-C, VEGF-D	Vascular and lymphatic development and maintenance
Neuropilin-1	VEGF-A, VEGF-B, VEGF-C, VEGF-D, PIGF	Vascular maturation, branching and heart development
Neuropilin-2	VEGF-A, VEGF-C, VEGF-D	lymphangiogenesis

Table 1- 2. Comparison between synthetic and natural polymeric materials

	synthetic polymeric material	natural polymeric material
physical properties	pure elasticity no physical architecture small porosity non-biodegradable	viscoelasticity physical architecture porosity (nm to μm) biodegradable
biochemical properties	no natural ligands	with natural ligands
disadvantages	stability over time	difficult to decouple mechanics and biochemistry
advantages	versatile to control	Biomimic

Transforming Growth Factor-β (TGF-β)

TGF-β receptors are receptor-type serine/threonine kinases [58, 59]. Both TGF-β and its receptors are expressed in full spectrum of vascular cell types, including ECs, smooth muscle cells, and pericytes [60]. TGF-β induces angiogenesis via recruiting inflammatory cells (monocytes and macrophages) that produce VEGF, FGF-2 and PDGF [61-65]. In a co-culture system, TGF-β inhibits EC proliferation upon EC-pericyte contact [60]. Thus, TGF-β can have both stimulatory and inhibitory effect on angiogenesis.

Proteinases Required for Angiogenesis

ECM is composed of many proteins. Some of these include collagen, elastin, fibronectin, laminin and nidogen, as well as proteoglycans and glycoproteins that can be degraded by proteases. Proteases have been classified into metalloproteinases, serine proteases, and cathepsin cysteine proteases. Metalloproteinases are composed of three major families: (1) matrix metalloproteinases (MMPs), (2) a disintegrin and metalloproteinase domains (ADAMs), and (3) a disintegrin and metalloproteinase with thrombospondin motifs (ADAMTs).

Matrix Metalloproteinases (MMPs)

There are 23 members of MMP family that share three basic domains, a prodomain (at amino terminus), catalytic domain, and hemopexin containing ancillary domains (at carboxyl terminus) but some have extra variations. In addition to matrix protein

specificity for degradation, MMPs cleave membrane-bound adhesion molecules, matrix-bound growth factors and other soluble enzymes [66-68]. Therefore, MMPs are divided into soluble MMPs and membrane-type MMPs (MT-MMPs). Soluble MMP include collagenases (MMP-1, MMP-8, and MMP-13), gelatinases (MMP-2, MMP-9), stromelysins (MMP-3, MMP-10 and MMP-11), matrilysins (MMP-7, MMP-26) and metalloelastase (MMP12). The MT-MMPs have 6 members (MMP-14/15/16/17/24/25 also called MT1/2/3/4/5/6-MMP, respectively), and they are either a type I transmembrane domain (MT1/2/3/5-MMP) or a glycosylphosphatidylinositol (GPI) anchor (MT4/6-MMP). In collagenases, MMP-1 cleaves type I and type III collagens, and MMP-8 and MMP-13 selectively target type I and type II collagens. Three principles are required for collagenases to degrade collagen, which include the ability to bind collagen molecules, unwind the three α chains, and cleave each strand of the triple helix [69, 70]. Regarding gelatinases, MMP-2 and MMP-9 degrades gelatin or denatured collagens [71]. MT-MMPs degrade various ECM proteins, such as different types of collagen, fibrinectin, gelatin, laminin and fibrin [72]. Five out of six MT-MMPs (not MT4-MMP) activate pro MMP-2 [68, 73-76]. ECs produce different MMPs, including MMP-1/2/9/13/14. In particular, MMP-2 and MMP-14 (MT1-MMP) have been proven in promoting EC migration and capillary network formation [77-80]. After activation by a furin-linked enzyme through intracellular cleavage of the pro-peptide domain, MT1-MMP can cleave ECM or form ternary complexes with tissue inhibitor of matrix metalloproteinase-2 (TIMP-2) and pro-MMP-2 (72kDa) to activate pro-MMP-2 into an active form (62kDa) [81, 82].

ADAMS and ADAMTS

ADAM and ADAMTS family members have several common structural domains, i.e. a pro-domain, disintegrin domain, and metalloproteinase domain. The difference between ADAMs and ADAMTSs is that ADAMTSs lack a cysteine-rich domain and ADAMTSs are secreted into interstitial space and bind with ECM proteins but not ADAMs (membrane-spanning proteins) [83, 84]. 19 out of 34 ADAMs have proteolytic activity [83, 85]. ADAMs are also involved in cytokine processing or growth factor receptor shedding [86]. Within the ADAMs family, ADAM -10, -15 and -17 are known to be involved in angiogenesis [87]. There are 19 members in ADAMTS family and ADAMTS-1, -4, -5, -8, -9, -15 and -16 are considered as proteoglycanases [88]. In angiogenesis, ADAMTS-1 and ADAMTS-8 have an inhibitory effect and ADAMTS-4 expressed in ECs promotes formation of capillary tube structures in fibrin matrices [89-91].

Serine Proteases

Among serine proteases, urokinase-type plasminogen activator (uPA) and plasmin regulate endothelial cell migration [92]. uPA activates plasminogen to generate the active protease plasmin to degrade matrix proteins such as fibrin, fibronectin, and laminin [93]. This activation process could be accelerated by presence of uPA receptor (u-PAR) [94]. Besides uPA, mammalian tissues also express tissue-type plasminogen activator (tPA), which activates plasminogen in presence of fibrin [95] and tPA is primary expressed by ECs and plays a key role in blood clotting [93]. Both uPA and tPA

are inhibited by plasminogen activator inhibitor (PAI). Plasmin, uPA and PAI-1 all participate in angiogenic processes [96, 97].

Tissue Inhibitors of Metalloproteinases (TIMPs)

There are 4 different tissue inhibitors of metalloproteinases (TIMPs) which specifically block MMP activity. TIMPs are secreted proteins with molecular weights from 20 to 29kDa that bind to MMPs in 1:1 ratio to form a complex which will be engulfed by macrophages [98]. TIMPs also inhibit proteinases of ADAMs and ADAMTSs families [86]. Among all TIMPs, TIMP-1 poorly inhibits membrane-type MMPs, such as MT1/2/3/4/5-MMP [99, 100]. Other than mediating pro-MMP2 activation with MT1-MMP, TIMP-2 inhibits MMPs via an N-terminal region and suppresses angiogenesis via a C-terminal region [101]. Among all TIMPs, TIMP-3 is unique because it inhibits ADAMs activity, blocks the binding of VEGF to VEGFR-2 [102], and is bound to sulfated glycosaminoglycans through a heparin binding sequence and is not freely diffusible [103]. Compared with TIMP-2, TIMP-4 doesn't reduce EC proliferation but restrict EC motility in vitro, but not *in vivo* [104], although TIMP-2 and TIMP-4 share specificity for inhibiting MMPs and can inhibit not only soluble, but also MT-MMPs.

Insoluble Cues-3D Scaffolds

Cells behave differently in 3D than 2D tissues [105-110], specifically migration [107], drug responsiveness [108] and differentiation [109]. There is growing interest in

tissue engineering in designing the physical properties of a biomaterial scaffold, including topographical and mechanical properties, to influence cell behavior [106, 111-118]. Topographical properties represent information of ECM architecture in micrometer or nanometer scale that cells sense, such as fiber thickness, pore size or porosity [119].

Synthetic and Natural Polymeric Materials

2D/3D polymeric biomaterials used for tissue engineering or mechano-sensitivity studies consist of synthetic and natural polymeric materials. Synthetic polymeric material includes polyacrylamide (PA) [117, 120-122], polyelectrolyte multilayer film (PEM) [123-125], polydimethylsiloxane (PDMS) [126-128] and polyethylene glycol (PEG) [129-132]. Natural polymeric materials include collagen [133-135], fibrin [136-138], hyaluronan (HA) [139-141] and alginate [142-147]. Except PEG [129], very few synthetic polymeric biomaterials were used for 3D studies owing to their high density, low porosity, and lack of biocompatibility and biodegradability. Compared with other polymeric scaffolds, the advantage of using natural polymeric materials is that they occur naturally, are synthesized naturally, and are nontoxic. The differences between synthetic and natural polymeric materials are summarized in Table 1-2.

Collagen

Collagen fibrillogenesis

Collagen gels have been applied in various tissue engineering applications, such as skin, cartilage, blood vessels and other tissue replacements. Collagen, the most abundant protein in vertebrates, constitutes one quarter of total protein mass of animals. Collagen molecule contains a unique triple-helical structure which is constituted by three

polypeptide chains (α-chain). The triple helix, known as procollagen, is secreted from cells and soluble under physiological conditions. Tropocollagen is formed after removing loose ends of the procollagen by collagen peptidases. Glycine presents at every third residue along each chain to allow a tight packaging of three α chains in the tropocollagen. Therefore, each of three α chains has the repeating structure Gly-X-Y where X, Y could be any amino acid but they are usually proline and hydroxyproline [148, 149]. The fibril-forming collagen molecule consists of an uninterrupted triple helix that is 300nm in length and 1.5 nm in diameter flanked by an extra telopeptide, which is critical for fibril formation. The assembly of collagen from molecules to fibril and into fibers occurs through a protein self-assembly and entropy driven process, i.e. collagen molecules exclude water and lower surface energy by aggregating [150]. There are 29 different collagen chains that exist in animals [151]. Collagen types I, II, III, V and XI are all characterized with D-periodic cross-striated fibrils (67nm in diameter) [152-155] and form fibrous structure. Type I collagen (fibril forming), the major collagen in skin and bone, accounts for 90% of total collagen in body. Type II collagen (fibril forming) is found in cartilage. Type III collagen (fibril forming) is observed in wound healing and developing skin [151]. Type IV collagen (nonfibrillar meshwork) is located in basal lamina and basement membranes of blood vessels. Altogether, type I collagen matrices will be the major focus of subsequent studies included here.

Table 1- 3. Methods to control topographical properties of type I collagen

	collagen concentration	topographical characteristics	collagen source	reference
collagen concentration	<5 mg/ml	fibril diameter increase with concentration	collagen type I	[156, 157]
	10-80 mg/ml	fibril diameter increase with concentration (20-80nm)	collagen type I	[158, 159]
	90-150 mg/ml	fibril diameter increase with increasing concentration	collagen type I from young Wistar rat tail	[160, 161]
	200-300 mg/ml	fibril diameter decrease with increasing concentration	collagen type I from young Wistar rat tail	[160, 161]
	0.5, 1.5, 2.5, 3.5 mg/ml	fibril density increased with increasing collagen concentration. average fibril diameter did not change significantly with collagen concentration.	collagen type I	[162]
temperature	4°C, 22°C, 37°C	lack of gelation and fiber formation at low temperature (4, 22°C) but not 37°C	porcine myocardial matrix	[163]
	22°C, 27°C, 32°C	matrices with small pore size associated with lower temperature.	rat tail tendon (BD)	[164]
	25°C, 30°C, 37°C	no influence on fibril diameter	collagen type I rat tail tendon	[159]
	4°C, 14°C, 24°C, 37°C	fiber diameter and pore size decrease with increasing temperature	collagen type I rat tail tendon	[165]
	22°C, 37°C	pore size decrease with increasing temperature with precise control two-step fibrillogenesis (lag and growth state), difference of fiber diameter could be minimized.	collagen type I Rat tail tendon	[164]
pH	7.5, 8.5	fiber diameter doesn't change	porcine myocardial matrix	[163]
	from 7.0 to 5.0	fiber diameter decreases from pH 7.0 to pH 5.0		[159]
	5.5-7.5	fiber diameter decreases (3.7±0.7μm-1.6±0.3 μm) Pore size decreases (81.7±3.7μm^2-7.8±0.4 μm^2)	rat tail tendon (BD)	[166]
	5.0-8.5	fibril diameter decreases	collagen type I rat tail tendon	[159]
	5, 7, 9	fibril diameter decreases	collagen type I rat tail tendon	[133]
Ionic strength	>24 mM 127-291mM	low ionic strength limits fibril size, at higher ionic strength, fibrils are larger and aggregated in bundles.	collagen type I from young Wistar rat tail	[161]

Method to control topographical properties of type I collagen

Topographical properties include porosity, pore size and fiber thickness, which is what cells sense in their local environment. During collagen self-assembly fibrillogenesis, the sigmoidal shape of a rheometric measurement revealed a two phase mechanism (nucleation phase and growth phase) [157, 167]. The nucleation step is temperature dependent and also able to control the number and diameter of collagen fibrils [156, 157, 164, 168]. Topographic properties and gelation kinematics of polymerized collagen matrices can be altered via varying temperature, ion concentration, phosphate content, pH, and protein concentration during self-assembly [161, 166, 169-172] (see Table 1-3). Importantly, pore sizes of 10-100 μm allow cells to migrate through a scaffold, and pore sizes less than 1 μm allows molecules to diffuse freely. Different methods to control topographical properties of type I collagen are summarized in Table 1-3. Varying concentration will couple both angiogenesis influencing factor, topographical property and stiffness, at the same time (see Figure 1-1). Even collagen I and II can form fibrils in vitro, but *in vivo*, they require fibronectin and integrins as organizer to determine the site of fibril assembly and collagen V and XI as the nucleators to initiate collagen fibrillogenesis [173].

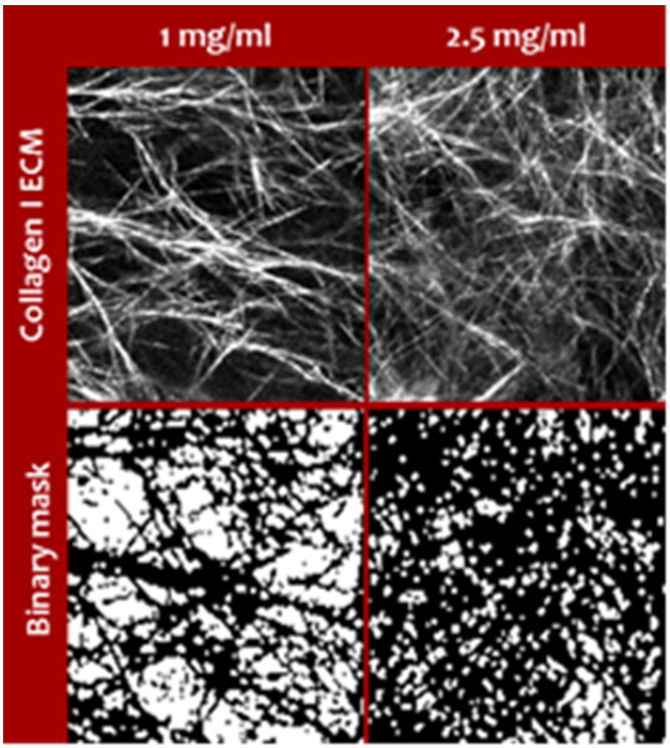

Figure 1- 1. ECM morphology of 1 vs. 2.5 mg/ml type I collagen captured with NLOM.

Table 1- 4. Methods to crosslink type I collagen

method	crosslinker	observation	reference
physical	UV irradiation	only effective for thin/transparent scaffold	[174-176]
chemical	glutaraldehyde	potential toxic	[163, 177-180]
chemical	carbodiimide	potential toxic	[181-184]
enzymatic	transglutaminase	nontoxic	[185-187]
enzymatic	mTG	nontoxic	[188]
enzymatic	lysyl oxidase	nontoxic	[189]
nonenzymatic	glycation	nontoxic	[190-198]

Method to control type I collagen mechanical properties

Decoupling biochemical, topological and mechanical properties in a 3D environment is challenging. Although the stiffness of collagen is strengthened by increasing protein density, that will also change other ECM topological properties, such as fiber thickness, pore size, and porosity (see Figure 1.1). Instead of varying collagen concentration, the stiffness can be modulated via physical, chemical, enzymatical or nonenzymatical crosslinkings independent of density [196, 197]. Various methods to crosslink type I collagen ECM are summarized in Table 1-4. Among them, tissue transglutaminase (tTG) and lysyl oxidase (LOX) are physiologic and all nontoxic for cell. There merits [199, 200] to use mTG over tTG are (1) Ca^{2+} independence, (2) higher reaction rate and (3) broader substrate specificity. In chapter II, we characterized how mTG modulated collagen stiffness without changing topographical properties optically and mechanically with our NLOM-OCM combined system and biaxial bioreactor.

Characterizing mechanical and optical properties of type I collagen scaffolds

characterizing mechanical properties of type I collagen scaffolds

There are several mechanical tests that can be used to evaluate collagen gel mechanics, such as shear rheometry, uniaxial testing, and planar biaxial testing, but each has its own merits and limitations.

Shear rheometry has been extensively applied in studying collagen fibrillation dynamics and bulk viscoelastic properties of collagen gels [165, 166, 201, 202]. Briefly, collagen fibrillation begins with a lag phase during nucleation with constant turbidity and shear modulus (shear modulus G”> storage modulus G’), followed by a growth

phase where turbidity and shear modulus rapidly increases (G' crossing over G") until finally reaching a plateau where collagen monomers assemble successfully [167]. Because this method cannot be performed while maintaining sterility, shear rheometry is not suitable for studying collagen matrices remodeled by cells.

Uniaxial testing is a simple method that has been exploited in large deformation analyses and cell-remodeled collagen gel characterization [203, 204]. The dog bone shape with at least 5:1 in aspect ratio is required for homogeneous strain and the shape will minimize the stress concentration at grips [203]. Collagen matrices undergoing uniaxial tests usually reveals more linear response and less elastic return than native collagen tissue due to its less mature and complex collagen fiber microstructure [203].

Planar biaxial testing: compared with uniaxial testing, biaxial testing is more close to physiological condition and sufficient to elucidate the anisotropic mechanical properties of biological tissues [205-208]. Other than square collagen gel [205, 206], cruciform shaped collagen gel [207, 208] has an advantage of minimizing edge effect and has been exploited in biaxial mechanical testing combing with polarized light microscopy [207] and NLOM [208].

Table 1- 5. Comparison between light microscopy and nonlinear microscopy

light microscopy	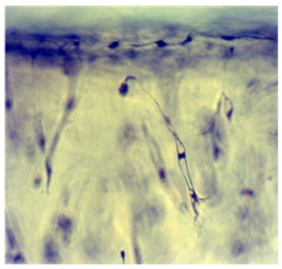	• have to fix tissue • have to stain tissue with toluidine blue • no information about ECM
nonlinear microscopy	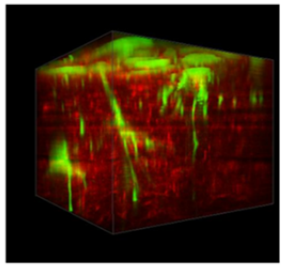	• no need to fix tissue • no stain or dye • sensitive in defining cell and ECM morphology • permit 3D imaging of culture

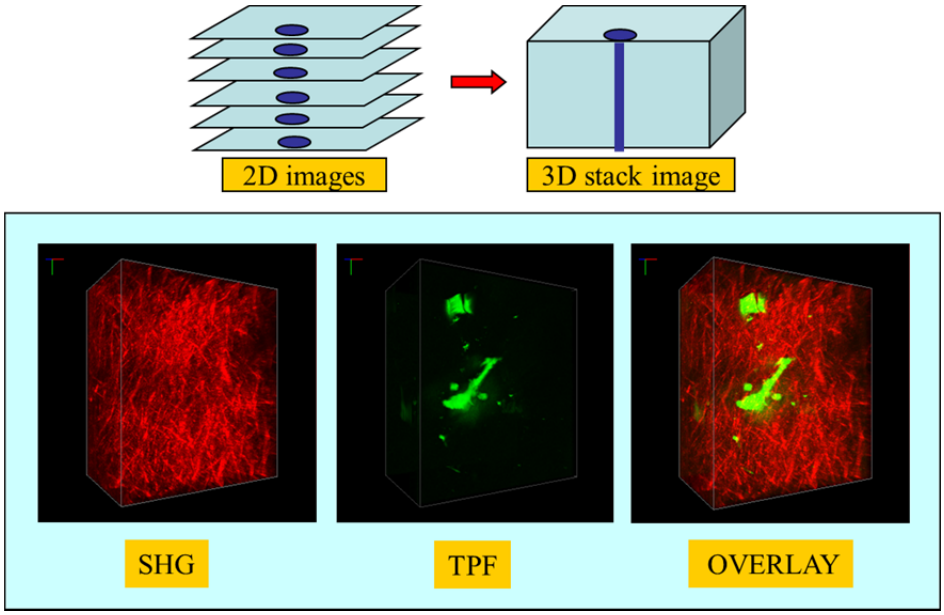

Figure 1- 2. Noninvasive 3D image construction with NLOM

optical characterization of type I collagen scaffolds with Nonlinear Optical Microscopy (NLOM)

NLOM uses two different types of signals, two photon fluorescence (TPF) and second harmonic generation (SHG), to image biological structures with subcellular resolution. TPF is used to monitor the dynamic behavior of the chemical components of tissue, whereas SHG provides novel ways to investigate their spatial organization. SHG doesn't involve absorption of incident photons; hence, SHG imaging is not compromised significantly by photobleaching or phototoxicity. Signals of TPF are emitted isotropically but those of SHG are anisotropic. TPF is a nonlinear process since TPF depends nonlinearly on the laser intensity, not linearly on fluorescence. Specifically, doubling the incident laser intensity produces four times the fluorescence [209]. SHG intensity is proportional to the square of the incident light intensity. The reason why we adapted NLOM for our study is that compared to traditional light microscopy, there is no need to fix tissue or use stain or dye to visualize cell and NLOM also provide information of ECM (see Table 1-5). Also, scanning the focus with NLOM generates a 2D image and by incrementally changing the depth of focus, a stack of images was generated and used to reconstruct a 3D view of the tissue (see Figure 1.2). Therefore NLOM is a suitable intra-vital microscopy to provide spatial and temporal information of cell-matrix interaction during angiogenesis nondestructively and noninvasively.

Even confocal microscopy also has ability to create 3D image noninvasively, NLOM has multiple advantages over traditional confocal microscopy (one photon fluorescence) including [209-213]:

1. greater tissue penetration up to the couple hundred micrometer range due to near-infrared excitation compared with confocal (near 50 μm) and consequently, less scatter .

2. minimize phototoxicity, photobleaching and photodamaging imposed onto cells and tissues due to fluorophores excitation localizing in the focal plane and improve optical detection efficiency due to the lack of a detector pinhole, which is necessary for confocal.

3. broader excitation range of multiple fluorophores, compared to single photon excitation, allowing multicolor imaging using the same excitation wavelength.

4. generation of other optical contrast based on nonlinear interactions between light and molecules without leading to fluorescence, such as second harmonic generation (SHG). Therefore, increase the possibility of combining fluorescence microscopy with other detection modes, including higher harmonic generation microscopy and fluorescent lifetime imaging.

two photon fluorescence (TPF)

TPF involves simultaneously absorption of low energy photons to excite a fluorophore, followed by an incoherent emission of fluorescence. There are several types of endogenous fluorescence in tissues, such as NADH, keratin, melanin, collagen and elastin [212, 214-216]. The major cellular endogenous autofluorescence are from the reduced pyridine nucleotides, NADH (reduced form of nicotinamide adenine dinucleotide), NADPH (reduced form of nicotinamide adenine dinucleotide phosphate), riboflavins and tryptophan [212, 216]. Autofluorescence is also captured from serotonin

[217-219], keratin [220], elastin [221-223] and melanin [216, 224, 225]. Fluorescence lifetime is specific for fluorophore and its micro environment and does not depend on fluorophore concentration [226]. The fluorophore of collagen are fluorescent amino acids phenylalanine and tyrosine, the pyridinoline crosslinks and advanced glycated endproducts (AGEs) [227]. The pyridolamine crosslink in elastin and collagen is another extracellular fluorophore [216]. For collagen I, about 1.7% of all amino acids (55 out of 3156) are the fluorescent ones, namely phenylalanine and tyrosine [227]. The fluorescent amino acid tryptophane is not part of the mature collagen molecule as it contributes only to the propeptide that is cleaved during maturation. Collagens I and III differ in their amino acid sequence. Collagen I consists of 13 tyrosines, 42 phenylalanines, 107 lysines and 1040 glycines in contrast to collagen III which is composed of 18 tyrosines, 27 phenylalanines, 120 lysines and 1263 glycines per molecules. The emission maxima of both collagen I and III are the same around 460nm [228]. Compared with fluorescent component of collagen I and III, phenylalanine (2750 ps) has a longer fluorescence lifetime than tyrosine (2393 ps). Collagen I is composed of a relative ratio of 76% phenylalanine to 24% tyrosine (42-13) in contrast to a collagen III that has 60% phenylalanine to 40% tyrosine (27-18). The difference in molecular structure of the fluorescent amino acids, phenylalanine and tyrosine, is only addition of hydroxyl group to the end of the 6-carbon aromatic ring of phenylalanine. Another fluorescent component of collagen is AGE pentosidine and the autofluorescence of collagen in skin seems to correlate with the level of pentosidine [227] but placental collagen doesn't

Table 1- 6. Application of NLOM in imaging type I collagen scaffold

ECM	crosslinker	Mechanical test	observation	reference
collagen I	N/A	N/A	1. The trend of collagen fluorescence over time is dependent on excitation wavelength. 2. Collagen fluorescence spectrum is dependent on excitation wavelength, polymerize temperature and pH.	[229]
collagen I	glutaraldehyde (GTA)	rheology	1.with polymerization temperature decreasing, fiber diameter and pore size increase but storage modulus and SHG decrease (minimal effect on TPF) 2. fiber diameter accessed from SHG is linearly correlated with that accessed from SEM but with an order of magnitude larger. 3. crosslinker, GTA increases the mean TPF (but not mean SHG) and storage modulus.	[165]
collagen I	N/A	rheology	1. with polymerization pH increasing from 5.5 to 8.5, mean fiber diameter and pore size decrease but storage and shear modulus increase. 2. bulk storage modulus depends on pore size and fiber diameter which are estimated from SHG.	[166]
collagen I	glutaraldehyde	Synergie 100 (stress-strain calibration)	With TPF and SHG images, skewiness and speckle contrast from cellularized collagen gels can predict E.	[230]
collagen I	genipin	N/A	1. emission spectrum of genipin treated collagen gel is dependent on excitation wavelength and also incubation time. 2. fluorescent image revealed that genipin induced formation of fluorescent strand throughout the depth of scaffold.	[231]
collagen I	glycation	N/A	1. during the course of glycation, there is an increase in fluorescence and structural alterations within scaffold. 2. with measuring the fluorescence intensity at 460 nm max, glycation with glyceraldehyde was faster compared to ribose and generated strong fluorescence signals.	[232]
collagen I	N/A	N/A	A unified relationship between SHG directionality, collagen fibril morphology and fibril sizes are not likely.	[233]

contain pentosidine. A collagen crosslink, pyridinoline, also generates fluorescence but that is not detectable in skin in relevant amounts [234].

second harmonic generation (SHG)

SHG involves conversion of two incident photons with same excitation energy into a single photon at twice the excitation energy emitted coherently. The ability to generate SHG is peculiar to molecules which are not centrosymmetric. Collage has highly crystalline triple-helix structure which is not centrosymmetric; hence it's very effective generator of SHG [235]. SHG is nonlinear process in which two photons of lower energy generate a photon of higher energy with twice the frequency (or half the wavelength) of incident photon. Besides metal and ion crystals, several biological materials contain repetitive or symmetric structural units, including coiled-coil structures and polymeric proteins. In addition to fibrillar collagen [235-237], other biological structures also produce SHG, such as tubulin [238], myosin [239, 240], cellulose[241], starch [241] and DNA [242].

Therefore, NLOM is suitable for in vitro, *in vivo* imaging that requires multicolor imaging, deep tissue penetration, low photo toxicity and high resolution. NLOM has been exploited in imaging various tissues, such as rat tail tendon [240, 243], skin [221, 244], and cornea [245, 246]. The intrinsic collagen fluorescence arises from enzymatic crosslinks between collagen fibers [247-250], such as pyridinium-type crosslink or from nonenzymatic crosslinks, such as glycation. Studies of collagen scaffold optical or physcial properties with applying NLOM and confocal microscopy are summarized in Table 1-6 and Table 1-7, respectively. Among these comparison tables, we can see that both NLOM and confocal microscopy can be used to characterize microstructure but NLOM more merits over confocal microscopy, such as characterization intrinsic fluorescence of collagen and crosslinker.

Table 1- 7. Application of confocal microscopy in imaging type I collagen scaffold

ECM	crosslinker	Mechanical test	observation	reference
collagen I	N/A	rheology	1. fibril diameter assessed from CRM (confocal reflectance microscopy) or CFM (confocal fluorescence microscopy) correlates well with the result from SEM. 2. average structure diameter, rather than fibril diameter, is the length scale that sets that magnitude of the gel elastic modulus.	[201]
collagen I	Hyaluronan (HA)	rheology	Addition of HA subtly altered the mechanical properties and structure of the composite during gelation process and at equilibrium.	[202]

Influence of 3D ECM Stiffness on Angiogenesis

In 2D angiogenesis, tube formation was decreased with increasing matrix stiffness via changing type I collagen concentration [251], matrigel concentration [252], changing polyacrylamide (PA) rigidity underneath collagen coating [253] or inducing glycation [254]. Compared with 2D models, 3D angiogenesis models more closely mimic physiological conditions since cells reside in 3D ECM. In 3D *in vitro* models, ECs are either cultured on top of 3D gels or mixed inside 3D gels for them to migrate into 3D ECM to form capillary tubular networks [45, 255-258]. When cultured inside 3D ECM, ECs can be resuspended as individual cells [259-261], aggregates [20, 262, 263] or EC-coated beads [264-266]. In our studies, we used a 3D angiogenesis model that incorporates a proangiogenic lipid, sphingosine-1-phosphate (S1P) [267-270], inside collagen matrices. ECs were cultured on top of each matrix as monolayer in media containing VEGF and bFGF to establish serum-free 3D angiogenesis *in vitro* model. Table 1-8 summarizes various models of 3D angiogenesis used to study alterations in matrix stiffness. This list includes multiple studies that use traditional method (vary ECM concentration) to vary ECM stiffness which also induce changes of topographical and mechanical properties. The studies described here aim to change only matrix stiffness (i.e. mechanical property) without changing topographical properties (such as pore size, pore number, porosity …etc.).

Table 1- 8. Angiogenesis response to ECM stiffness

Cell type	ECM type	Method to vary stiffness	observation	reference
Endothelial colony forming cell (ECFC)	Collagen type I (0.5, 1.5, 2.5, 3.5 mg/ml)	Varying concentration (0.5-3.5 mg/ml)	In this *in vivo* study, total vessel density (host+ECFC) decreased with increasing collagen concentration. When counting ECFC vessel area only, average or total ECFC vessel area were increased with increasing collagen concentration.	[162]
Bovine pulmonary microvascular endothelial cell (BPMEC)	Collagen I (2.4 mg/ml)	Varying pH (5-10)	Neovessels penetrate deeper and have larger lumen in rigid gel than in soft gel.	[133]
Human umbilical vein endothelial cell (HUVEC) +HUASMC	Collagen I (2.5 mg/ml)	Varying Glucose-6-phosphate (G6P) concentration (0, 100, 375mM)	Compared with control, glycated gels resulted in shorter vessels with increasing branching and higher tortuosity.	[195]
HUVEC Human blood outgrowth endothelial cell (HBOEC)	Collagen I (1.5, 3.5 mg/ml)	Varying collagen concentration (1.5, 3.5 mg/ml) and gel boundary condition (float, constrained)	The balance between cell force and matrix stiffness played a role in regulating angiogenesis. Improved capillary morphogenesis is formed in more malleable environment.	[271]
Bovine aortic endothelial cell (BAEC)	Polyacrylamide (PA) Collagen I (1, 5, 10, 50, 100 µg/ml)	Varying PA stiffness (200, 1000, 2500, 5000, 10000pa) and varying collagen concentration on top of PA (1, 5, 10, 50, 100 µg/ml)	1. Cell network assembly could occur in compliant substrate with sufficient surface ligand or in stiffer substrate with less surface ligand. 2. Fibronectin polymerization stabilized cell-cell contacts and is necessary for network formation regardless of substrate stiffness or density of surface ligand.	[272]
EC	fibrin	Varying fibrin concentration (1, 1.5, 2.0, 2.5, 5, 10 mg/ml)	In 3D fibrin gel, the biphasic trend has been revealed in angiogenic sprouting and rate of ECM displacement and optimal rate will occurred at 2.5 mg/ml.	[136]
HUVEC	fibrin	Varying fibrin concentration (2.5, 5, 10 mg/ml)	Total capillary network length decreased with increasing fibrin density.	[137]
HUVEC	fibrin	Varying fibrin concentration (1, 2, 3 mg/ml)	1. For the intermediate fibrin concentration (2 mg/ml), the angiogenic sprouting proceeds faster (biphasic trend). 2. Rigidity is more important than adhesion ligand number.	2D [138]
HUVEC	fibrin	Varying fibrin concentration (2.5, 5, 10 mg/ml)	Increasing the matrix density could reduce neovessel network formation and that effect could be abrogated by distributing fibroblast throughout the matrix.	[273]

Influence of ECM Mechanics on Cell Traction

ECs reside within the inner layer of blood vessels above the basal lamina as a monolayer [274] and control vascular tone, vascular permeability, and prevent coagulation [275]. Capillaries are surrounded by pericytes, specialized mural cells, to confer stability and quiescence to capillaries [60, 276]. Larger vessels contain a layer of smooth muscle cells (SMC) within the media and connective tissue within the adventitia [277]. ECs are subjected to various mechanical stimuli on the apical cell membrane, which are transmitted through cell-cell contacts and ECM adventitial layers [275]. Those mechanical stimuli include shear and pressure stresses acting on the EC apical membrane, residual hoop stress in the vascular wall, external forces from surrounding tissues that impinge vessels [278], and mechanical input from surrounding ECM stiffness. In response to various mechanical stimuli, ECs are able to exert force against their ECM to remodel ECM [279], assist in cell adhesion and migration [280, 281] and influence cellular mechanotransduction [275, 282]. The ECM mechanics and mechanotransduction have been associated with various pathologies, such as cardiovascular diseases (hypertrophy, hypertension and atherosclerosis) [105, 275], tumorigenesis [283], metastasis and wound healing [284]. EC traction generation is enabled by stress fibers or bundles of actin filaments, myosins and integrins that anchor the cells to its substrate through focal adhesion (FA) [285]. FAs are large structurally polarized adhesion sites with their proximal ends linking with contractile actin bundles, i.e. stress fibers and their formation is associated with natural matrix proteins or

arginine-glycine-aspartate (RGD) motifs [286, 287]. Besides integrins, FAs are formed with other FA adapter proteins, including vinculin, paxillin, talin, α-actinin, zyxin [288-290], VASP [291], focal adhesion kinase (FAK) [292-294] and p130Cas [295, 296]. Contractile ability within the cell influences the growth and maintenance of FAs. For example, inhibition of myosin II activity induces disappearance of FAs [297-299] and activation of myosin II induces FA assembly [300-302]. Actin polymerization and FA formation are different in 3D versus 2D environments [110]. The Rho-family of GTPases includes RhoA, RhoB, RhoC, Rac1 and Cdc42. These small GTPases control integrin-mediating signaling [303-305], cell migration [306-308], and intracellular contractility and tension [309, 310]. Greater myosin light chain phosphorylation [311] mediated via activation of RhoA [312, 313] causes increase contractility. Rho-associated protein kinase (ROCK), downstream effector of RhoA, plays a role in actin contractility via regulating the phosphorylation of myosin light chain and hence the interaction between actin and myosin II [314]. The amount of traction generated by cells is dependent on ECM stiffness [113, 315, 316] where cell traction force increases with substrate stiffness [113]. Therefore, stiff ECM promotes cell spreading, large FAs, large stress fibers and strong traction forces [317, 318]. Califano et al. further confirmed that substrate stiffness and cell area could predict cell traction in single cells or even cells in contact [319]. Similar to FA, cadherin mediated cell-cell adherens junctions (AJ) also depends on myosin II driven contractility [320] and size of cell-cell AJs is regulated by mechanical tugging forces [321]. Modulation of ECM properties not only impacts cell-ECM traction but also alters cell-cell tension [322]. Liu et al. further proposed that cell-

cell tugging force is important in mediating AJs via myosin activation or inhibition [321]. Therefore, the dynamic coordination of traction at cell-ECM interface is critical to the maintenance of vascular integrity and ultimate control of vascular permeability.

CHAPTER II

NONLINEAR OPTICAL MICROSCOPY REVEALS INVADING ENDTHELIAL CELLS ANISOTROPICALLY ALTER THREE-DIMENSIONAL COLLAGEN MATRICES[*]

Overview

The interactions between endothelial cells (ECs) and the extracellular matrix (ECM) are fundamental in mediating various steps of angiogenesis, including cell adhesion, migration and sprout formation. Here, we used a noninvasive and non-destructive nonlinear optical microscopy (NLOM) technique to optically image endothelial sprouting morphogenesis in three dimensional (3D) collagen matrices. We simultaneously captured signals from collagen fibers and endothelial cells using second harmonic generation (SHG) and two-photon excited fluorescence (TPF), respectively. Dynamic 3D imaging revealed EC interactions with collagen fibers along with quantifiable alterations in collagen matrix density elicited by EC movement through and morphogenesis within the matrix. Specifically, we observed increased collagen density in the area between bifurcation points of sprouting structures and anisotropic increases in collagen density around the perimeter of lumenal structures, but not advancing sprout

[*] The content of chapter II is reprinted with permission from "Nonlinear Optical Microscopy Reveals Invading Endothelial Cells Anisotropically Alter Three-Dimensional Collagen Matrices" by Po-Feng Lee, Alvin T Yeh and Kayla J Bayless, 2009. Experimental Cell Research, Volume 35, P396-410, Copyright [2012] by ELSEVIER.

tips. Proteinase inhibition studies revealed membrane-associated matrix metalloproteinase were utilized for sprout advancement and lumen expansion. Rho-associated kinase (p160ROCK) inhibition demonstrated that the generation of cell tension increased collagen matrix alterations. This study followed sprouting ECs within a 3D matrix and revealed that the advancing structures recognize and significantly alter their extracellular environment at the periphery of lumens as they progress.

Introduction

Angiogenesis, the process of new blood vessel growth from existing structures, plays a key role in normal tissue growth, wound repair and the progression of malignant diseases [323, 324]. Cell migration, proliferation, intracellular alignment, adhesion, and lumen formation coordinate to allow ECs of existing vessels to detach from the vascular wall, degrade and penetrate the underlying basal lamina while invading the surrounding 3D interstitial ECM during angiogenesis [325-327]. The ECM is a scaffold that provides structural support and adhesive contact sites, along with mechanical signals, that combine with biochemical cues to promote angiogenesis.

Cell movement through 3D matrices is a precisely coordinated process. Growth factors and lipids, such as sphingosine-1-phosphate (S1P), deliver potent pro-angiogenic signals [270, 328, 329] that stimulate endothelial outgrowth and invasion events and require membrane-associated (but not soluble) matrix metalloproteinases (MMPs) [330].

In particular, these events require MT1-MMP [80, 331-333], which selectively degrades ECM proteins at the cell surface-ECM interface without affecting the integrity of the ECM scaffold. Thus, newly-sprouting ECs integrate signals from pro-angiogenic stimuli to initiate successful proteinase-dependent outgrowth in 3D matrices.

Here, we utilize an *in vitro* model [330] that mimics the sprouting step of angiogenesis where ECs are allowed to invade in 3D collagen matrices. Collagen is the most abundant ECM protein in the body and strongly promotes EC morphogenesis [327]. Collagen is a hierarchal structured protein with long range molecular order and appreciable nonlinear susceptibility for SHG [243, 334-339]. SHG in collagen can be utilized in NLOM for serial imaging of live tissue and defining ECM morphology without using exogenous stains or dyes [337]. SHG has been utilized to image collagen dynamics and structures of intact and explanted tumors [340-343], mammary glands [340, 344], cardiovascular structures [345, 346], skin [222, 342, 347], fibrotic lung tissue [348] and cornea [349]. The utility of NLOM for collagen imaging can be further enhanced using TPF. TPF can arise from the nonlinear excitation of cell endogenous molecular fluorescence [350] and TPF signal can be used in NLOM to observe cell morphology in detail [346]. In addition, TPF signal can be greatly enhanced by cellular expression of endogenous fluorophores, such as enhanced green fluorescent protein (EGFP). Although much work has been done to define the cellular signals required by ECs to undergo morphogenesis and mediate angiogenic events, less is known about the molecular and structural interactions that occur between ECs undergoing morphogenesis and the surrounding 3D ECM.

Cell migration in two dimensions requires the generation of tension. The small GTPase Rho promotes stress-fiber assembly and focal adhesions formation through Rho-associated kinase (p160ROCK) activation, which also increases contractility [314, 351-354]. In addition, p160ROCK signaling provides not only a framework to maintain cell shape, but also the driving force to alter cell morphology [355, 356] and promote directed cell migration [307, 357, 358]. In this study, we use metalloproteinase and p160ROCK inhibitors to demonstrate that proteolytic activity at the cell surface is coordinated with the generation of tensional forces at the periphery of lumens, where anisotropic forces are applied to the underlying collagen matrix. We utilize NLOM to quantify alterations in collagen matrices elicited by ECs with time.

Materials and Methods

Reagents and Chemicals

Rat-tail Collagen type I was obtained from BD Biosciences. Recombinant human vascular endothelial growth factor (VEGF) and fibroblast growth factor-2 (FGF-2) were purchased from Upstate Biotechnology. Medium 199 (M199) and fetal bovine serum (FBS) were from Invitrogen. Tumor promoting antigen (TPA, Phorbol 12-myristate 13-acetate) and ascorbic acid (AA) were purchased from Sigma (St. Louis, MO).

Sphingosine-1-phosphate (S1P) was purchased from Avanti Polar Lipids (Alabaster, AL).

Cell and Tissue Culture

Primary human umbilical vein endothelial cells (ECs) were purchased from Cambrex and used at passage 2-6. ECs were grown on gelatin-coated tissue culture flasks (1 mg/ml) in culture media that consisted of M199 containing 15% fetal bovine serum, 400 μg/ml bovine hypothalamic extract [359], 100 μg/ml heparin (Sigma), 0.1% gentamycin and 1% penicillin/streptomycin (Invitrogen). Cells were passaged once a week. Stable EC lines expressing EGFP were generated using a recombinant lentivirus system (Invitrogen). pLenti6/V5 clone expressing EGFP [333] was a generous gift of Dr. George Davis (University of Missouri, Columbia). Backbone plasmid (4.5 μg) along with Virapower plasmid (13.5 μg) was transfected into 293 FT packaging cell line (Invitrogen) in 75 cm^2 tissue culture flasks using 36 μl Lipofectamine 2000. Supernatants were collected at 72 hours, centrifuged at 350Xg for 3 minutes, filtered and used fresh to transfect passage 2 ECs. Following blasticidin selection (5 μg/ml) for 2 weeks, cells were frozen down at passage 3 or used in experiments.

EC Capillary Formation in Collagen Gels

3D angiogenesis invasion assays were generated in a two-step process. The collagen matrix was prepared prior to seeding an endothelial monolayer on the collagen surface. Fibrous collagen gels (3.6 mg/ml) were assembled with rat-tail type I collagen, 5xDMEM, reconstitution buffer and neutralized with 1M NaOH [339] before

incorporating 1 μM S1P, which enhances EC invasion [330]. To ensure matrix alterations were not due to nonhomogenous distribution of fibrous collagen, it was necessary to create homogeneous collagen matrices in which no fibers could be resolved by NLOM. To accomplish this, 300 mg of rat-tail type I collagen (BD Biosciences) was frozen and thawed prior to being lyophilized and resuspended at 7.1 mg/ml in 0.1% acetic acid. We determined empirically this result in formation of homogenous collagen fibers (data not shown). For all collagen matrices, after thorough mixing of components, 1ml of collagen mixture was added per well of a Falcon 12-well plate (Becton Dickinson). Gels were allowed to polymerize and equilibrate for 20 minutes at 37°C in a CO_2 incubator prior to seeding $3.6x10^5$ cells per well in serum-free Medium 199 containing reduced serum supplement II (RSII) [360], recombinant VEGF (40 ng/ml), recombinant FGF-2 (40 ng/ml), ascorbic acid (50 μg/ml) and TPA (50 ng/ml). After allowing ECs to attach to the collagen matrix for 20 minutes, an additional 3 ml of identical serum-free media was added to each well. Cultures were imaged live or allowed to proceed for the times indicated before fixing in 4% paraformaldehyde in PBS prior to imaging.

Nonlinear Optical Microscopy

System setup

Our custom-built NLOM system has been described previously [361]. Briefly, sub-10-fs pulses from a Ti:Al_2O_3 oscillator (Femtosource, Femtolasers) pumped by a Nd:YVO_4 solid state laser (Verdi, Coherent) are coupled into the epi-fluorescence port of an upright microscope (Axioskop2 MAT, Carl Zeiss GmBH) via dual-axis galvanometer driven mirrors (Model 6220, Cambridge Technology) mounted on an elevated breadboard. The beam is directed to the microscope objective by a short pass dichroic mirror (635dcspxruv3p, Chroma). Nonlinear optical signals are collected by the 40X focusing objective (NA=0.8) and directed to a custom built two channel detector unit mounted on one of the dual accessory ports of the binocular head. The detector unit houses two dichroic mirrors and bandpass filters (Chroma), focusing lenses (PCX, focal length: 50 mm, 312321, Linos Photonics), and a pair of photon-counting photomultiplier tubes (R7400P, Hamamatsu). Appropriate long pass dichroic mirrors and bandpass filters are used for SHG (430dcxru and HQ405/40, respectively; Chroma) and TPF detection (580dcxr and HQ480/40, respectively; Chroma). In imaging mode each photomultiplier tube is connected to a preamplifier/discriminator (F-100T, Advanced Research Technologies) that thresholds signal current and converts to TTL pulses for photon counting. Image intensities are displayed in photon counts per second on a PC (Optiplex GX280, Dell). Our laser spectrum is 133 nm FWHM centered at 800 nm.

Throughout this experiment, less than 40 mW of laser power was incident on the scanning mirror that is approximately10 mW at the sample.

Image processing

For morphogenesis studies, live EC invasion was imaged without stains using NLOM rendering en face, 2D intensity images. By incrementally changing the depth of focus, a stack of images was generated and used to reconstruct 3D visualization of the tissue. SHG and TPF signals were collected simultaneously with NLOM. Image files captured using NLOM were converted from 16-bit to 8-bit files via MATLAB by scaling the maximum pixel value to 255 and then processed in the MetaVue software to generate 3-D image.

Collagen density quantification

Collagen density was quantified from individual optical sections using Matlab software. Collagen intensity ratio (CIR) was calculated by normalizing SHG intensity at the region of interest against the surrounding reference intensity within the NLOM image. Reference intensity was obtained by dividing the SHG intensity by the overall pixel number outside the area of interest. To quantify collagen density around the perimeter of invading EC structures, optical sections of lumen and tip were selected and the cell profile within the image was delineated by TPF. A vertical (V) line was chosen to divide the cell profile along its longest axis symmetrically. The corresponding horizontal (H) line intersected the vertical line perpendicularly at the point of maximum cell width. These designations allowed the cell boundary and lumen dimensions to be

obtained. The lumen dimensions are defined as the mean value of lumen size along H and V axes. CIR values were calculated at the four regions intersecting the vertical and horizontal lines at cell periphery (designated $Lumen_{V1}$, $Lumen_{V2}$, $Lumen_{H1}$, $Lumen_{H2}$). Data values represent the average of the 5 maximum CIR values obtained from 10 pixels, which translates to approximately 7 microns beyond the cell boundary.

Invasion distance measurement

To quantify invasion distance, photographs of invading cells were taken from a side view with an Olympus CKX41 microscope equipped with a Q color 3 Olympus camera. Invasion distance measurement (n=50 cells) were measured digitally using QCapture software (Olympus/Leeds) and pixel values were converted to microns.

Transmitted light image acquisition

Toluidine blue staining was conducted on cultures fixed in 3% glutaraldehyde in PBS as previously described [9]. In live cultures, experiments were established for 24 hours in a tissue culture incubator (37°C, 5% CO_2, 85% humidity) using a slide assay previously described [362] prior to imaging. Slides were placed in an environmental chamber on a *Nikon TE2000 imaging system.* DIC images (10 micro sec exposure) were collected at 20x every 6 minutes for 24 hours. Selected images are shown.

NLOM time-lapse image acquisition

Cultures were established and incubated (37°C, 5% CO_2) for the times indicated in each experiment. For initial image analysis, culture media was removed and replaced

with sterile PBS and transported to the NLOM system, which was hooded with 5% CO_2 custom environmental chamber for imaging. Each structure required approximately 20-30 minutes. Following completion, PBS was removed and media replaced before returning to the humidified tissue culture incubator. The imaging position was recorded using the position readout of the motorized stage to capture the same field at the next time point.

Matrix Metalloproteinase Inhibition Experiments

To investigate whether matrix metalloproteinases (MMPs) are involved in generating collagen alterations, GM6001 (a universal MMP inhibitor) was used initially. To determine whether soluble or membrane-associated MMPs were involved in generating collagen alterations, tissue inhibitor of metalloproteinase-1 (TIMP-1) and TIMP-3 were applied. GM6001 (Calbiochem) was reconstituted in DMSO at 2.57 mM, aliquoted and stored at -80°C prior to use at a final dose of 2.5 μM. Cultures were established for 24 hours and imaged live with NLOM before adding DMSO or GM6001 to the media. Cultures of DMSO and GM6001 were allowed to proceed for additional 24 hours and then imaged again at 48 hours.

Recombinant TIMP-1 and TIMP-3 were isolated from 293 cells transfected with adenovirus delivering TIMP-1 and TIMP-3 fused to a C-terminal His tag (constructs will be described elsewhere). Confluent monolayers of 293 cells were seeded in duplicate 75 cm^2 flasks. Each flask was infected with 4×10^6 IFU/cm^2 and allowed to express for 48-72 hours. Successful transduction was monitored by expression of green fluorescence

protein. Prior to collecting M199 containing conditioned media, the cells were rinsed twice with M199 (15 ml). Heparin (100 μg/ml) was added and incubated for 14 hours. Conditioned media were purified using 0.5 ml Nickel affinity resin (Novagen) by incubating overnight with gentle shaking at 4°C. Proteins were eluted with 0.2 M Imidazole and dialyzed overnight against M199.

p160ROCK Inhibition Experiments

The p160ROCK inhibitor, H1152 (Calbiochem) was reconstituted in sterile deionized water at 12.7 mM, aliquoted and stored -80°C prior to use. Cultures were established for 48 hours and imaged live with NLOM before adding ddH_2O or H1152 (30 μM) to the media. Cultures were allowed to proceed for additional 24 hours and then imaged again at 72 hours.

Tandem GM6001 and p160ROCK Inhibition Experiments

Invasion cultures were established for 24 hours and imaged with NLOM prior to the addition of the global MMP inhibitor, GM6001 (2.5 μM). Cultures were allowed to develop from 24-48 hours. After imaging at 48 hours, the cultures were treated with vehicle or H1152 (30 μM) and imaged for the final time at 72 hours.

Statistics

Relative collagen intensities were compared at the lumen and tip sites from seven individual invading structures in a homogeneous collagen ECM. In GM6001 and p160ROCK inhibition experiments, comparisons are made between the number of invading structures indicated in each treatment group. The mean and standard deviation were calculated for four regions defined by horizontal and vertical axes at the lumen and tip and grouped in Table 2-1. In addition, mean relative collagen intensity values and their standard deviations were calculated for the four regions of EC structures with lumens, compared using Student's T-test and tabulated in Table 2-2. P-value < 0.05 was considered a significant difference.

Table 2- 9. Mean and standard deviation of CIR (Collagen Intensity Ratio) values at lumens and tips from 7 different invading structures and their corresponding P values using student's T-test

Sample#		mean	std	$Lumen_H$	$Lumen_V$	Tip_H	Tip_V
1	$Lumen_H$	4.7038	0.49981			P<0.0005	P<0.0005
	$Lumen_V$	4.0825	0.50165			P<0.0005	P<0.001
	Tip_H	1.2348	0.20867	P<0.0005	P<0.0005		
	Tip_V	1.5695	0.22619	P<0.0005	P<0.001		
2	$Lumen_H$	3.5466	0.51256		P<0.01	P<0.005	P<0.0005
	$Lumen_V$	5.1002	0.49148	P<0.01		P<0.0005	P<0.0005
	Tip_H	1.2494	0.45337	P<0.005	P<0.0005		
	Tip_V	0.62469	0.22669	P<0.0005	P<0.0005		
3	$Lumen_H$	4.9575	0.52438			P<0.0005	P<0.0005
	$Lumen_V$	5.4533	0.6665			P<0.0005	P<0.0005
	Tip_H	1.2494	0.45337	P<0.0005	P<0.0005		
	Tip_V	0.62469	0.22669	P<0.0005	P<0.0005		
4	$Lumen_H$	3.5469	0.18145		P<0.0005	P<0.0005	P<0.0005
	$Lumen_V$	2.3009	0.071465	P<0.0005		P<0.01	P<0.005
	Tip_H	1.6808	0.23753	P<0.0005	P<0.01		
	Tip_V	1.28	0.35819	P<0.0005	P<0.0005		
5	$Lumen_H$	3.0225	0.2374			P<0.001	P<0.01
	$Lumen_V$	3.1256	0.2055	P<0.001		P<0.0005	P<0.005
	Tip_H	1.9043	0.1173	P<0.01	P<0.0005		
	Tip_V	1.926	0.395	P<0.0005	P<0.005		
6	$Lumen_H$	2.7064	0.2059		P<0.0005	P<0.0005	P<0.0005
	$Lumen_V$	1.2952	0.1887	P<0.0005		P<0.01	P<0.005
	Tip_H	0.849	0.1279	P<0.0005	P<0.01		
	Tip_V	0.7525	0.0876	P<0.0005	P<0.005		
7	$Lumen_H$	2.4417	0.13026		P<0.05	P<0.001	P<0.005
	$Lumen_V$	2.113	0.16471	P<0.05		P<0.005	P<0.01
	Tip_H	1.2659	0.26899	P<0.001	P<0.005		
	Tip_V	1.3299	0.27276	P<0.005	P<0.01		

Table 2- 2. Mean and standard deviation of CIR (Collagen Intensity Ratio) values around lumens from 7 different invading structures and their corresponding P values using student's T-test

Sample#		mean	std	$Lumen_{H1}$	$Lumen_{H2}$	$Lumen_{V1}$	$Lumen_{V2}$
1	$Lumen_{H1}$	4.552	0.90104				P<0.025
	$Lumen_{H2}$	4.8555	0.85843				P<0.01
	$Lumen_{V1}$	5.0031	0.80636				P<0.01
	$Lumen_{V2}$	3.1618	0.39505	P<0.025	P<0.01	P<0.01	
2	$Lumen_{H1}$	3.3424	0.82926			P<0.0005	P<0.025
	$Lumen_{H2}$	3.7509	0.36775			P<0.0005	P<0.005
	$Lumen_{V1}$	8.1702	0.62358	P<0.0005	P<0.0005		P<0.0005
	$Lumen_{V2}$	2.0302	0.43854	P<0.025	P<0.0005	P<0.0005	
3	$Lumen_{H1}$	5.8939	0.38213		P<0.01	P<0.005	P<0.025
	$Lumen_{H2}$	4.0211	0.93601	P<0.01		P<0.005	P<0.005
	$Lumen_{V1}$	9.7498	1.3187	P<0.005	P<0.005		P<0.0005
	$Lumen_{V2}$	1.1568	0.33165	P<0.025	P<0.005	P<0.0005	
4	$Lumen_{H1}$	4.0744	0.33423		P<0.01	P<0.005	P<0.0005
	$Lumen_{H2}$	3.0195	0.42574	P<0.01			P<0.005
	$Lumen_{V1}$	2.9536	0.32766	P<0.005			P<0.005
	$Lumen_{V2}$	1.6482	0.34886	P<0.0005	P<0.005	P<0.005	
5	$Lumen_{H1}$	2.4864	0.3037		P<0.01	P<0.005	
	$Lumen_{H2}$	3.5587	0.4811	P<0.01			P<0.025
	$Lumen_{V1}$	3.706	0.2563	P<0.005			P<0.005
	$Lumen_{V2}$	2.5453	0.39		P<0.025	P<0.005	
6	$Lumen_{H1}$	2.4139	0.2526		P<0.05	P<0.005	P<0.0005
	$Lumen_{H2}$	2.9988	0.4053	P<0.05		P<0.005	P<0.0005
	$Lumen_{V1}$	1.2936	0.3002	P<0.005	P<0.005		
	$Lumen_{V2}$	1.2967	0.1134	P<0.0005	P<0.0005		
7	$Lumen_{H1}$	1.8548	0.2048		P<0.005	P<0.005	P<0.01
	$Lumen_{H2}$	3.0287	0.35907	P<0.005			P<0.0005
	$Lumen_{V1}$	2.9935	0.25075	P<0.005			P<0.0005
	$Lumen_{V2}$	1.2326	0.23108	P<0.01	P<0.0005	P<0.0005	

Results

NLOM captures signals from cells via TPF as well as individual collagen fibers by SHG, allowing simultaneous visualization of both constituents to better understand the interactions between them during angiogenic events. Here, we utilized a 3D model of EC invasion that mimics angiogenesis [330]. In this model, ECs stably EGFP were seeded on the upper surface of 3D collagen matrices and stimulated to invade using the pro-angiogenic molecules S1P, VEGF and bFGF. In these experiments, ECs migrated from the monolayer into the underlying collagen matrix (Figure 2-1). Figure 2-1A illustrates that capillary structures assemble to form multicellular structures containing lumens. A lumen forming an angiogenic sprout was captured extending from the surface monolayer (white arrowheads) with matrix interrogating cell processes (gray arrow) from the tip (Figure 2-1A). These invading structures are typically multicellular, as indicated by multiple stained nuclei (gray arrowheads). Further, photographs of live ECs migrating through 3D collagen matrices (Figure 2-1B) revealed that the invading structures appear to alter the collagen matrix as they migrate. Visible alterations were observed in the matrix following the migration of an invading endothelial structure (indicated by black arrowheads), which is consistent with previous work [330]. Although these studies with transmitted light were useful for revealing details about the morphology and architecture of invading cellular structures, subsequent studies with NLOM revealed clear orientation of collagen fibers along with EC architecture. In Figure 2-1C, TPF images were

collected, digitized and stacked to provide a 3D reconstruction of live invading ECs after 18 hours in culture. Angiogenic sprouts were observed to both extend from the surface monolayer (white arrowheads) and migrate into the matrix (gray arrows). Overlay of TPF signal (green) with SHG (red) allowed visualization of EC angiogenic structures, 3D organization of collagen fibers and their interspatial relationships (Figure 2-1D). NLOM resolved extended peripheral tip processes (gray arrow), small vacuoles (black arrow), and lumens formed inside invading structures (black arrowhead) (see Figure 2-1E). Thus, NLOM is useful to more closely define the nature of collagen matrix alterations induced by invading EC structures with high fidelity.

Collagen Fibers Dictate the Direction of Sprout Outgrowth

To investigate more closely the signals that dictate sprout extension and retraction, we utilized NLOM to observe interactions between the collagen matrix and invading cells (Figure 2-2). Analysis of individual sections of SHG and TPF data revealed that extended peripheral sprout processes extended along collagen fibers (black arrows) at 24 hours of culture (Figure 2-2A). This interaction of collagen fibers with sprout processes is evident in overlay images of SHG+TPF, where the invading ECs (green) track along collagen fibers (red). The collagen matrix presented a heterogeneous environment that must be navigated by ECs while exploring potential migratory routes. Examination of ECs at higher magnification revealed that extended peripheral processes also appeared to intersect with collagen fibers (black arrows), at times extending processes beyond areas

of intersection (gray arrows) that extended further into the interstitial space (Figure 2-2B).

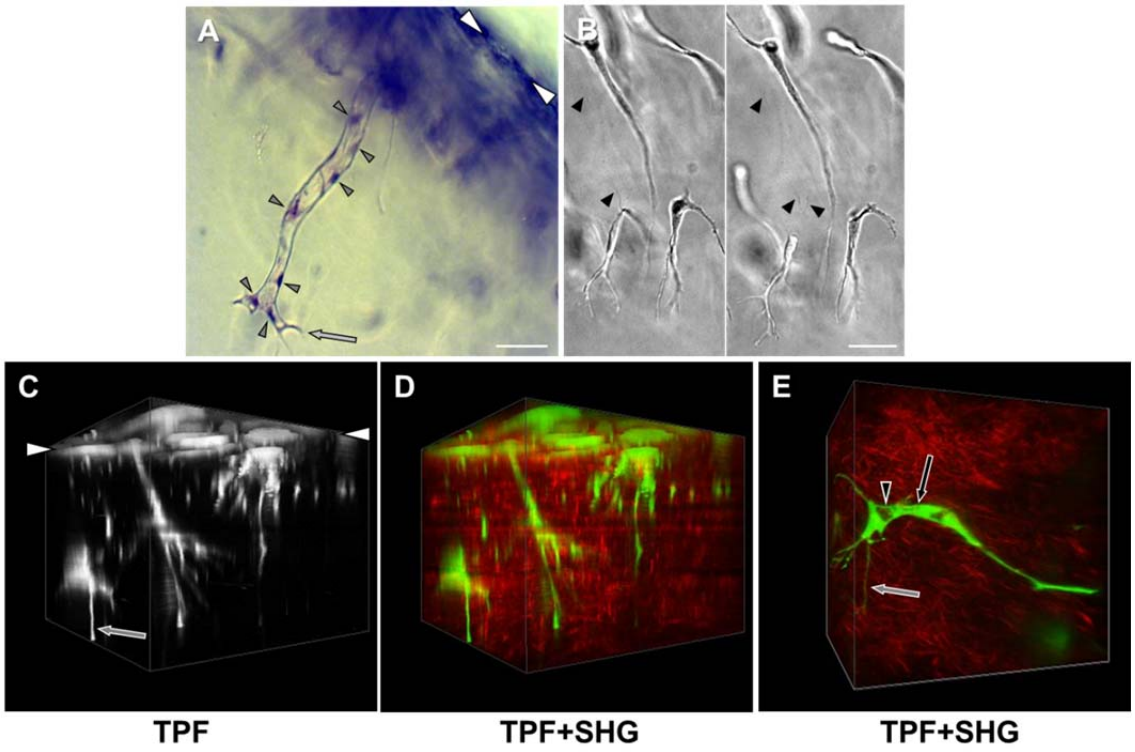

Figure 2- 1. Analysis of 3D EC invasion assays using light microscopy and NLOM. (A) ECs were seeded on the upper surface of a collagen matrix as a monolayer (white arrowheads) and allowed to invade into underlying matrix over time. Four-day cultures were fixed with 4% paraformaldehyde and stained with toluidine blue gels were cut perpendicular to the monolayer to obtain several thin gel slices which were photographed using light microscopy. (B) Time-lapse analysis of live invading EC movement through collagen matrices starting at 30 (left panel) and 31 (right panel) hours. Collagen matrix alterations are indicated by black arrowheads. (C-E) TPF and SHG gathered using NLOM were compiled into 3D images at 18 (C, D) and 48 hours (E). (D, E) False color was applied to show invading EC structures (green) within collagen matrix (red). Extended peripheral sprout processes were observed to form along the leading edge of invading structures (gray arrows) as well as vacuolar structures (black arrow in E) initiating lumenal structures (dark open areas) indicated by black arrowhead. Scale bar is 50 μm.

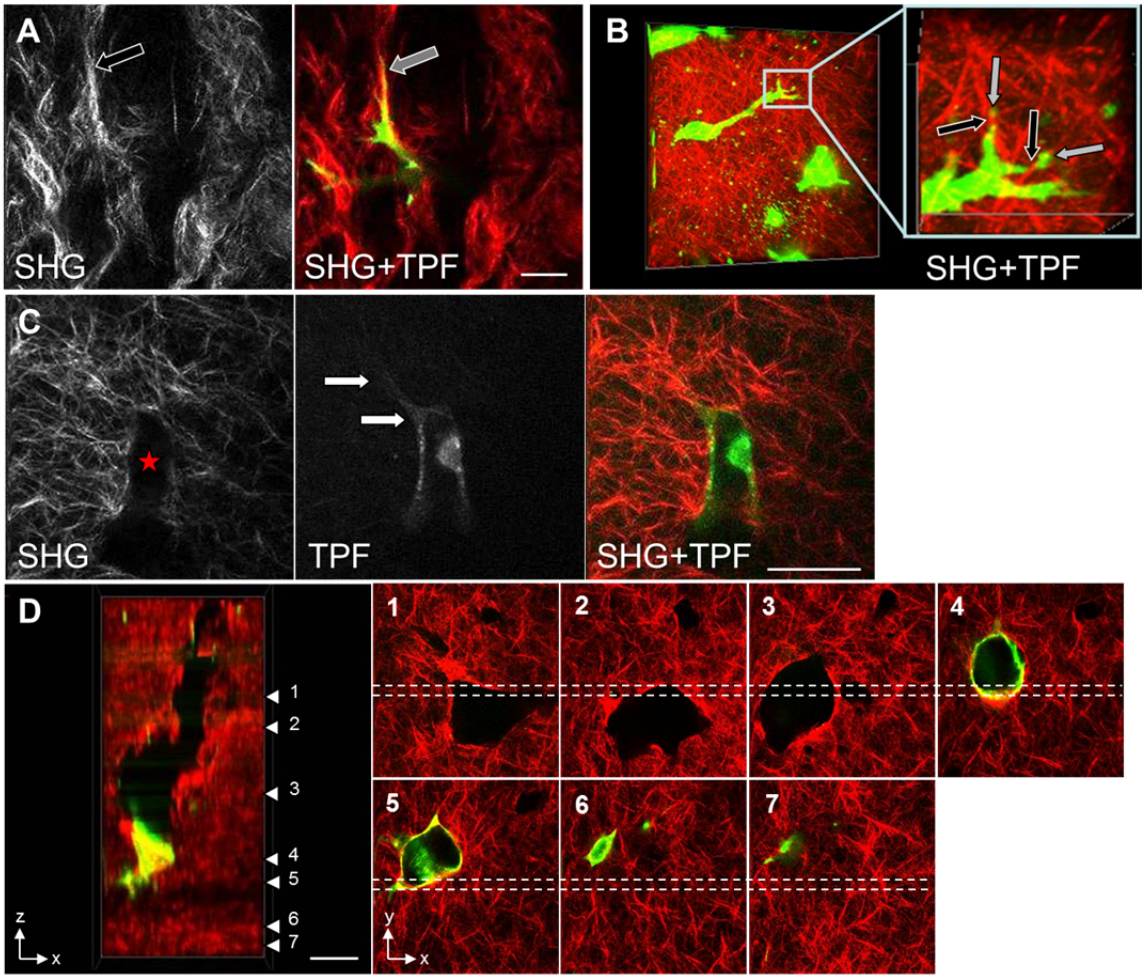

Figure 2- 2. Invading structures interact with collagen fibers and degrade collagen. (A) NLOM 2D images of collagen SHG and SHG + TPF overlay captured at 24 hours showed extended process (gray arrow) migrating along a fibrous collagen structure (black arrow). Scale bar is 20 μm. (B) NLOM 3D reconstruction captured at 48 hours revealed extended peripheral processes from an invading structure (green) intersected with individual collagen fibers (red). Magnified window shows fine EC processes (gray arrows) circumventing individual collagen fibrils (black arrows). (C) Individual NLOM sections of collagen SHG, TPF and their overlay (SHG+TPF) at 48 hours revealed a collagen-free space (red star) surrounded by an invading EC structure with an extended process (indicated by white arrows). (D) 3D reconstruction from 700 sections at 0.5 μm intervals showing a tunnel within the collagen matrix (red) behind an invading EC structure. Panels 1-7 on right illustrate samples of individual 2D data sections used to compile the 3D stacked image from the approximate area outlined by white dashed lines. Scale bar is 50 μm.

Dissolution of 3D Collagen Fibers Occurs During Invasion

As invasion proceeds and ECs continue to advance through 3D collagen matrices, lumen formation is initiated. The formation of these structures and cell advancement coincided with the disappearance of collagen SHG signal (Figure 2-2C). Single optical sections of collagen fibers (SHG), the corresponding EGFP-expressing EC (TPF) and the overlay image (SHG+TPF) are shown. These data revealed that establishment of an open lumen (dark area within TPF) resulted in dissolution or displacement of the collagen matrix as evidenced by a lack of SHG signal (red star). However, the cytoplasmic extension beyond the lumen (marked by white arrows) has not initiated dissolution or displacement of the collagen matrix. This is further illustrated in Figure 2-2D, where portions of individual optical overlays (SHG+TPF) were compiled into a 3D stacked image (Figure 2-2D, left panel). Samples of the single optical sections used to compile the image are marked as panels 1-7. Dashed white lines indicate the area utilized from each image to compile the stack image, which captured a degraded ECM tunnel behind an invading structure.

Collagen Matrices Are Reorganized During Cell Migration and Lumen Formation

In addition to collagen degradation or displacement, NLOM revealed that the composition and arrangement of collagen matrices was altered during invasion (Figure 2-3). NLOM analyses of polymerized collagen matrices prior to addition of ECs revealed homogenous distribution of SHG signal and fibrous collagen (data not shown). Simultaneous acquisition of SHG and TPF images of invading structures revealed

increased SHG signal intensity between branch points of invading structures (Figure 2-3A, white arrow). In addition to elevated collagen intensity that occurred between bifurcations of lumenal structures, we also observed increased collagen SHG intensity around the periphery of lumens (Figure 2-3B). Thus, NLOM provided evidence that as ECs invade into 3D collagen matrices, visible alterations occurred in the density and arrangement of fibrous collagen at the periphery of invading structures. Additionally, no collagen signal was detected inside the lumen, demonstrating that an ECM-free space exists within the lumenal compartment.

The elevated collagen SHG intensity observed may result from displacement or compaction of collagen fibers locally by the invading structure, or could be explained by collagen deposition. Analysis of ECs invading into 3D fibrin matrices at analogous times revealed no ability to detect deposition of fibrous collagen at bifurcations or at the periphery of invading structures (data not shown). These data suggest that increased collagen intensity at bifurcations and at the periphery of lumens is not the result of collagen deposition.

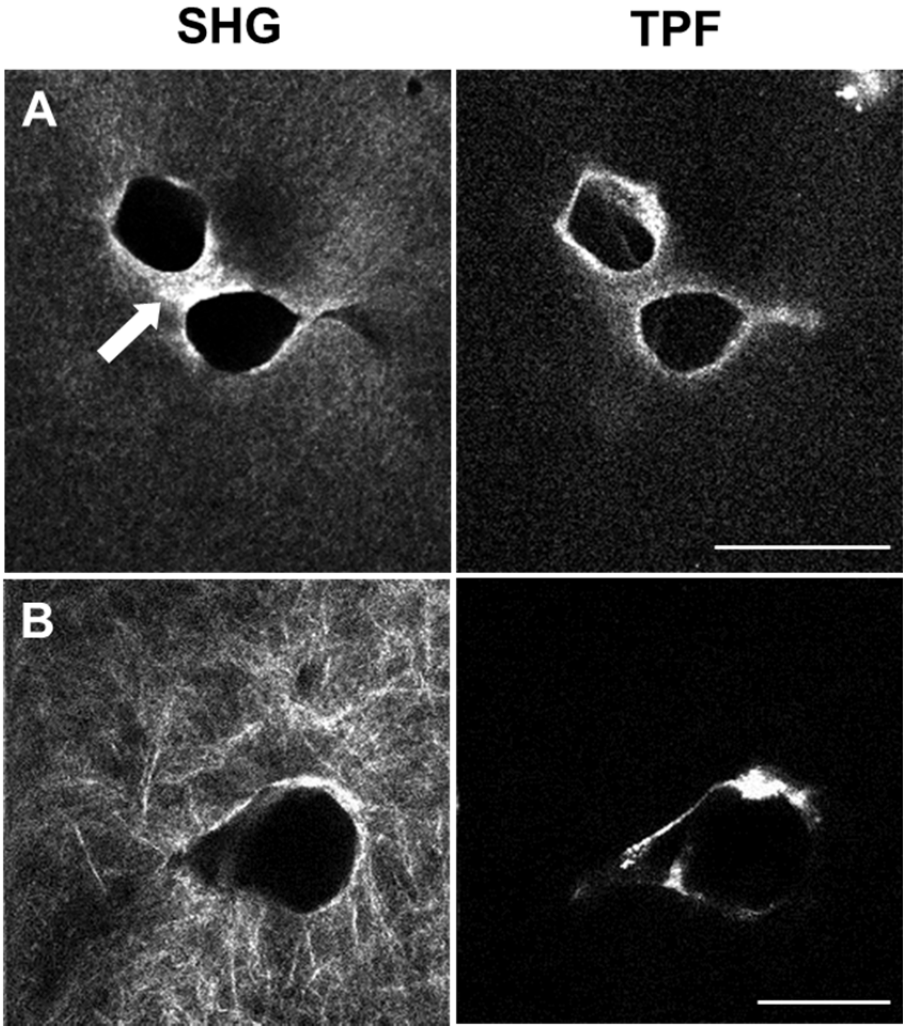

Figure 2- 3. Invading ECs alter collagen arrangement and increase collagen intensity at the periphery of lumens and at bifurcation points. (A) Single optical sections depicting increased collagen intensity near bifurcations of invading structures (white arrow). Lumens are the open dark areas in SHG lined by ECs (TPF). (B) Single optical sections depicting increased collagen intensity at the perimeter of an EC lumen. Images were taken after (A) 96 and (B) 108 hours of culture. Scale bar is 50 μm.

Quantification of Alterations in Collagen Matrix Density at Lumenal Branch Points

To ensure the observed alterations in collagen intensity were not due to heterogeneous distribution of fibrous collagen, we performed experiments comparing fibrous and homogenous 3D collagen matrices. Homogenous collagen matrices were useful in these experiments because SHG signals collected with NLOM were uniformly distributed and collagen fibers were not resolved. Fibrous and homogenous collagen matrices were prepared and analyzed to quantify and compare the increased collagen intensity observed near areas of lumenal branching. Single optical sections from invading structures in fibrous (Figure 2-4A) and homogeneous (Figure 2-4C) collagen environments illustrate that local increases in collagen matrix density coincide with lumenal bifurcation events in invading structures regardless of collagen structure. Quantification of the CIR values of collagen (SHG) signals (normalized to the average pixel intensity of the surrounding collagen matrix) and plotting these CIR values using 2D line scanned histographs revealed that the area with highest CIR coincided with the area between branching lumens for fibrous (Figure 2-4B) as well as homogeneous collagen matrices (Figure 2-4D). Scanning lines are depicted in Figures 2-4A and C. The data demonstrate that the area between lumens exhibited increased density compared to the surrounding regions within the field of view for both fibrous (Figure 2-4B) and homogeneous (Figure 2-4D) collagen matrices. Collectively, these data indicate that the NLOM signals are quantifiable and reveal increased CIR at areas of bifurcation between sprouting structures.

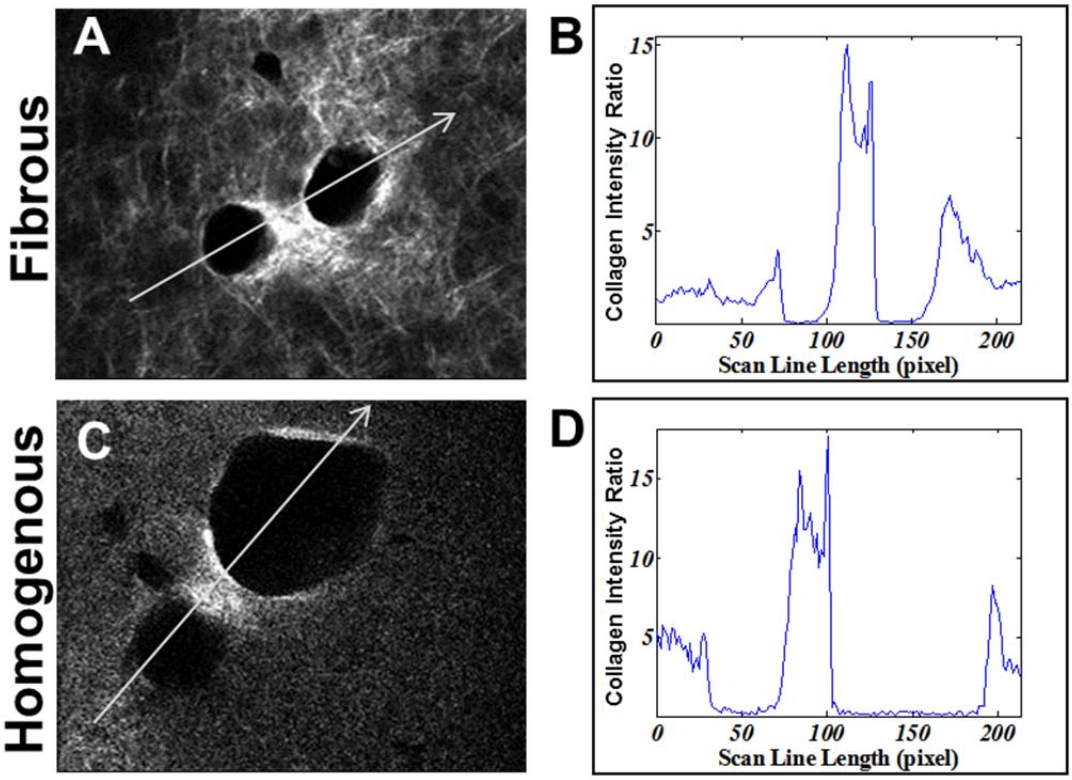

Figure 2- 4. Quantification of elevated Collagen Intensity Ratio (CIR) between bifurcations of invading structures revealed a 4-5 fold elevation within fibrous and homogenous collagen matrices compared with reference collagen intensity. (A, C) Single optical sections collected at bifurcation points between invading structures in (A) fibrous and (C) homogenous collagen matrices. (B, D) Line scans (see gray arrows in panels A&C) quantify CIR along a single line in (A) fibrous and (C) homogeneous matrices.

Extracellular Matrix Density Increased around Lumens of Invading Structures, but not Tips

In addition to bifurcation points, we consistently observed areas of elevated collagen intensity (increased SHG intensity) around the perimeter of open lumens (see Figure 2-3B). To more precisely define the nature of the increased collagen density, we utilized homogenous 3D collagen matrices. Data from seven independent invading structures were analyzed. In the first series of experiments, peripheral CIR values were compared between lumens and invading tips (Figure 2-5). Two individual optical sections from the lumen and tip portions were selected from an invading structure. For individual sections, a vertical axis (V) was assigned as the morphologic symmetric axis and a perpendicular horizontal axis (H) was located at maximum lumen width (Figures 2-5A and 2-5B). The CIR values of lumen ($Lumen_H$, $Lumen_V$) and tip (Tip_H, Tip_V) were calculated at the cell periphery along horizontal and vertical axes to compare peripheral collagen intensities. In Figure 2-5C, analysis of seven individual invading structures showed similar trends where the CIR values of the horizontal and vertical axes at the lumen site were significantly greater than those at the tip site (P values are shown in Table 2-1). Among the data, CIR values at the periphery of lumenal structures were increased compared to the tip, which remained at or near one relative to overall or background collagen intensity. These data indicate that no appreciable differences were observed in local collagen concentration at the periphery of invading tips compared with the surrounding matrix.

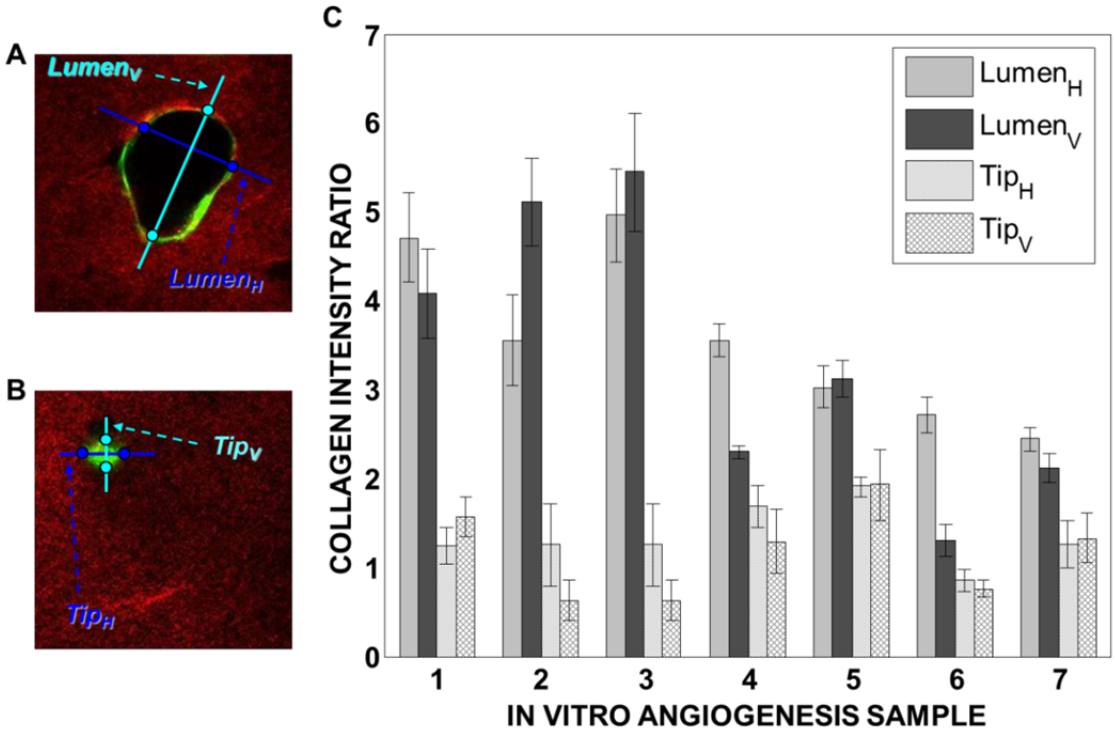

Figure 2- 5. Quantification of the CIR at the periphery of invading structures revealed a significant increase around lumens but not tips. Representative NLOM sections are used for CIR quantification at the periphery of (A) lumens and (B) tips. (C) Mean vertical (V) and horizontal (H) CIR based on average SHG values were calculated (see methods) and compared for seven individual samples. Data presented are average CIR values at 72 hours +/- s.d. Statistical significance values are provided in Table 2-1.

Further examination revealed that the increased CIR associated with the formation of lumenal structures does not occur uniformly around the perimeter of lumens. To quantify this effect, CIR values at four end points of vertical ($Lumen_{V1}$ and $Lumen_{V2}$) and horizontal ($Lumen_{H1}$ and $Lumen_{H2}$) axes were compared to test whether the increased collagen intensity phenomenon was isotropically distributed. Analysis of seven individual invading structures (Figure 2-6) showed that the CIR values of the four end points were not equal, indicating that the observed increase in local collagen

concentration was anisotropic. Statistically significant differences were observed for individual data points (Table 2-2). Anisotropic matrix remodeling suggests that the lumenal compartment does not fill passively (i.e. like a balloon) and that an axis of lumen expansion exists.

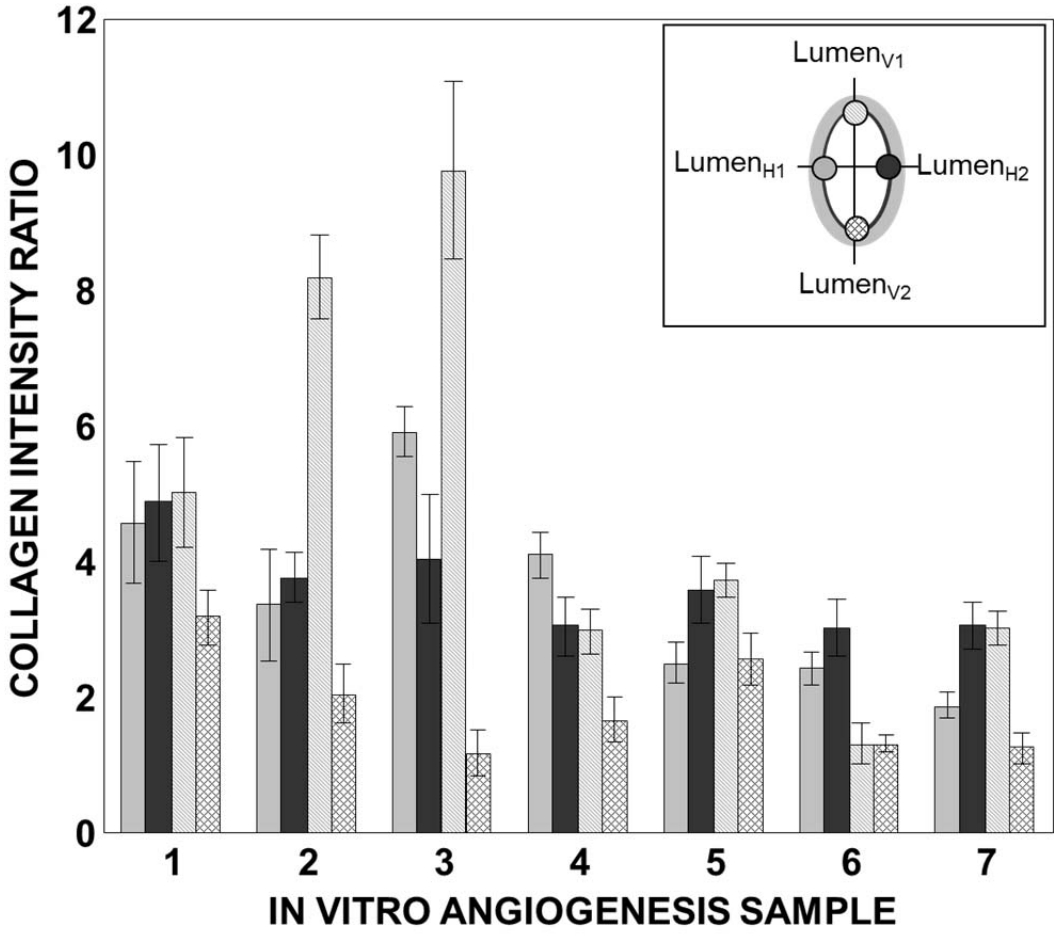

Figure 2- 6. Quantification of CIR at the periphery of lumens revealed an anisotropic distribution of collagen density. CIR values were calculated at four points (LumenH_1, H_2, V_1 and V_2), as shown in the legend and compared for seven individual samples (see methods). Data presented are average CIR values at 72 hours +/- s.d. Statistical significance values are provided in Table 2-2.

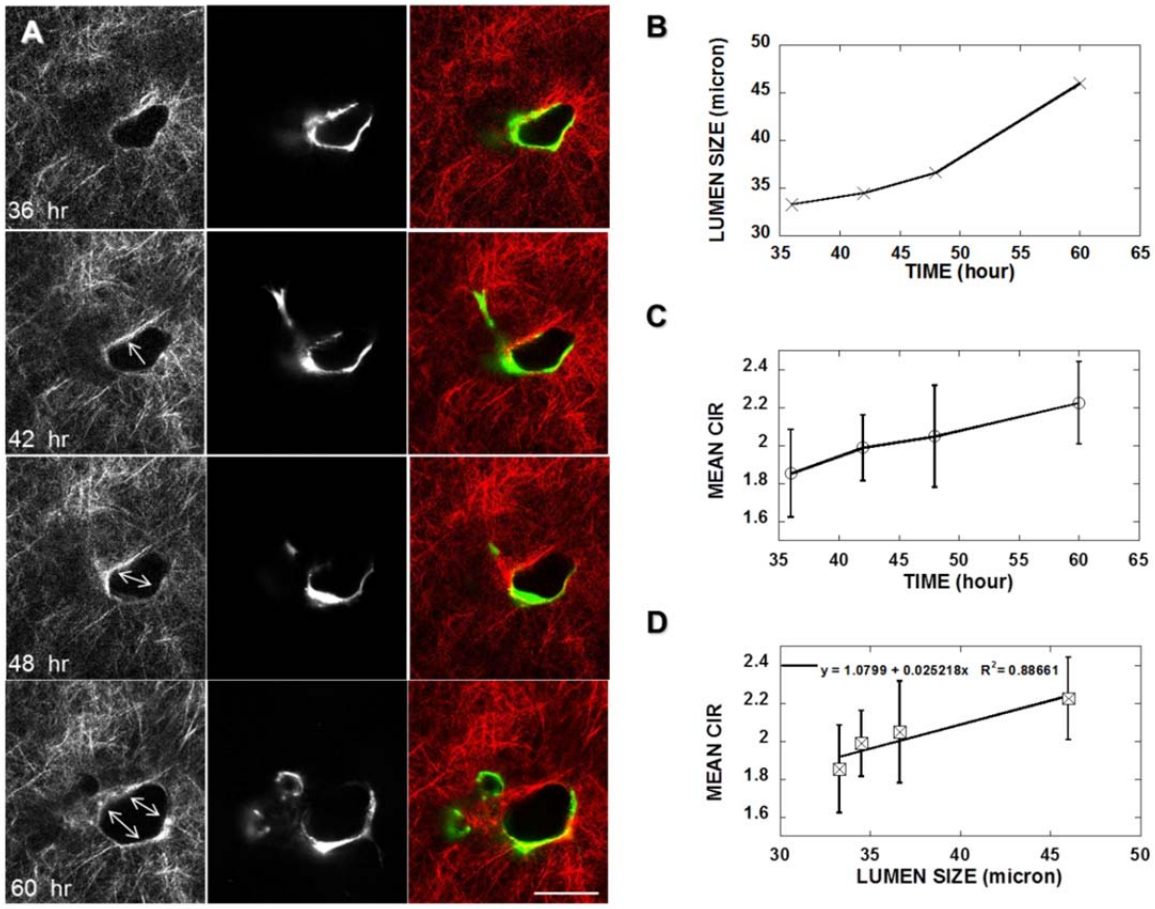

Figure 2- 7. Time-lapse analyses demonstrate that CIR is proportional to lumen diameter. (A) Single optical sections depicting SHG (left column), TPF (middle column) and overlay images (right column) at 36, 42, 48 and 60 hours. White arrows depict direction of lumen expansion. (B) Quantification of lumen size with time. (C) Quantification of the mean CIR around the lumen. Data values represent average CIR values at 4 points along the periphery of the lumen +/- s.d. as depicted in Figure 2-6. (D) Linear relationship between lumen size and mean CIR. Scale bar=50 µm.

Lumen Expansion is Associated with Elevated Collagen Intensity at Periphery

To investigate the relationship between lumen size and CIR at periphery of lumen, time-lapse analyses were performed. Invading structures were imaged with NLOM at the same focal plane at 36, 42, 48 and 60 hours as described in the methods. Lumen size was observed to expand, contract and/or maintain steady diameter. Elevated collagen intensities were observed in the direction of lumen expansion as indicated by arrows (Figure 2-7A). Lumen size and mean CIR at the periphery of lumens incrementally increased with time (Figures 2-7B and 2-7C, respectively). A linear relationship was established (R=0.88661) between lumen size and mean CIR (Figure 2-7D), indicating that mean CIR at the periphery of lumens was proportional to lumen size. The linear relationship between lumen size and mean CIR was observed for both expanding and contracting lumens.

Matrix Metalloproteinase Inhibition Increased Collagen Intensity Ratio at the Periphery of Lumens while Restricting Advancement of Invading Structures

To determine the role of the matrix metalloproteinases in modulating alterations in collagen matrix intensity at the periphery of lumen within advancing ECs, GM6001, a general matrix metalloproteinase inhibitor, was tested. Cultures were allowed to develop for 24 hours before being imaged with NLOM. Following image capture, cultures were treated with vehicle control (DMSO) or GM6001 and imaged again at the same focal depth at 48 hours (Figure 2-8). Images from pre-treatment (24 hr) and post-treatment

(48hr) revealed inhibited expansion of the lumen in GM6001-treated cultures, but not control (Figure 2-8A). The addition of GM6001 successfully inhibited EC proteolysis as evidenced by a small enlargement in lumen size (Figure 2-8B). In addition, GM6001-treated cultures demonstrated a reduced ability to invade (Figure 2-8C). Following GM6001 addition at 24 hours, the mean CIR increased significantly compared to controls at 48 hours (Figure 2-8D). Although an increase in mean CIR was observed in the control, the increase was more robust with GM6001 treatment. Quantification of the percent increase in lumen size and CIR is shown in Figure 2-8E. Lumen size increases were significantly greater in the control cultures compared to GM6001, while CIR was significantly higher following GM6001 treatment, compared to control. This indicated inhibition of proteolysis with GM6001 resulted in a small change in lumen diameter and a large change in CIR. This phenomenon is depicted by the collagen alteration index (CAI) value where change in CIR is normalized by change in lumen diameter (Figure 2-8F).

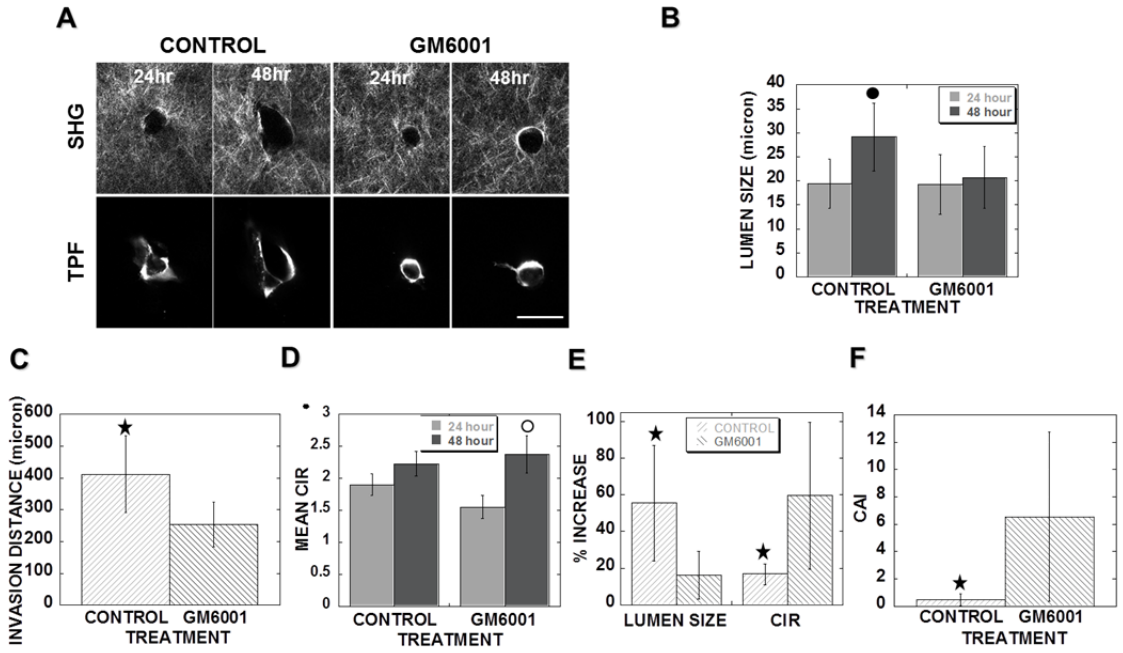

Figure 2- 8. Addition of a global metalloproteinase inhibitor, GM6001 significantly increased CIR. Invading cultures were allowed to proceed for 24 hours before imaging invading structures (24 hr). Following image capture, 2.5 μM GM6001 or Control (DMSO) was added. Cells were allowed to invade an additional 24 hours before the same structure was imaged (48 hr). (A) Single optical sections before and after GM6001 or control treatment. Scale bar=50 μm. (B) Change in lumen size observed from 24 to 48 hours and (C) average invasion distance of sprouting structures at 48 hours following GM6001 or control treatment. (D) Mean CIR observed at 24 and 48 hours. (E) Average percent increase in lumen size, and CIR. (F) Collagen alteration index, which is calculated as the percent increase in CIR divided by the percent increase in lumen size for control and GM6001 treatment. For data analyses, 6 structures were analyzed for control treatment and 8 for GM6001. Data presented are average values +/- s.d. Circles and stars indicate statistical significance observed when compared to 24 hour and GM6001 treatments, respectively. Filled symbols indicate p values < 0.05, open symbols indicate p <0.01, student's t-test assuming unequal variance was applied.

Membrane-Associated Metalloproteinases are Responsible for Regulating Collagen Intensity at the Periphery of Lumens

To determine which class of metalloproteinases is responsible for alterations in collagen intensity, endogenous inhibitors were applied. Tissue inhibitor of metalloproteinase (TIMP)-1 and TIMP-3 were selected because TIMP-1 is capable of inhibiting soluble MMPs while TIMP-3 inhibits membrane-associated forms as well as soluble MMPs [363]. Thus, the addition of TIMP-1 versus TIMP-3 can distinguish between the roles of soluble and membrane-associated MMPs in regulating collagen intensity at the periphery of lumens. Experiments were performed as described in Figure 2-8. While TIMP-1 allowed lumen expansion and appeared identical to control cultures, TIMP-3 prevented lumenal expansion (Figure 2-9A). In addition, invasion distance was significantly greater in control and TIMP-1-treated cultures compared to those treated with TIMP-3 after 48 hours (Figure 2-9B). These data are consistent with a previous report where TIMP-1 had no effect on EC invasion, but TIMP-3 completely inhibited [330]. The change in mean collagen intensity ratio (CIR) observed from 24 to 48 hours was similar in control and TIMP-1 treated cultures, while TIMP-3 treatment significantly increased the mean CIR (Figure 2-9C). The change of CIR level of TIMP-3 was higher than that observed in control or TIMP-1 treatment. Plotting the percent increase in lumen size and CIR revealed a similar trend in control and TIMP-1, which exhibited a significantly higher increase in lumen size compared to the TIMP-3 treated group (Figure 2-9D). In contrast, TIMP-1 and control structures showed a smaller increase in mean CIR compared to TIMP-3. As shown in Figure 2-9E, the CAI value for

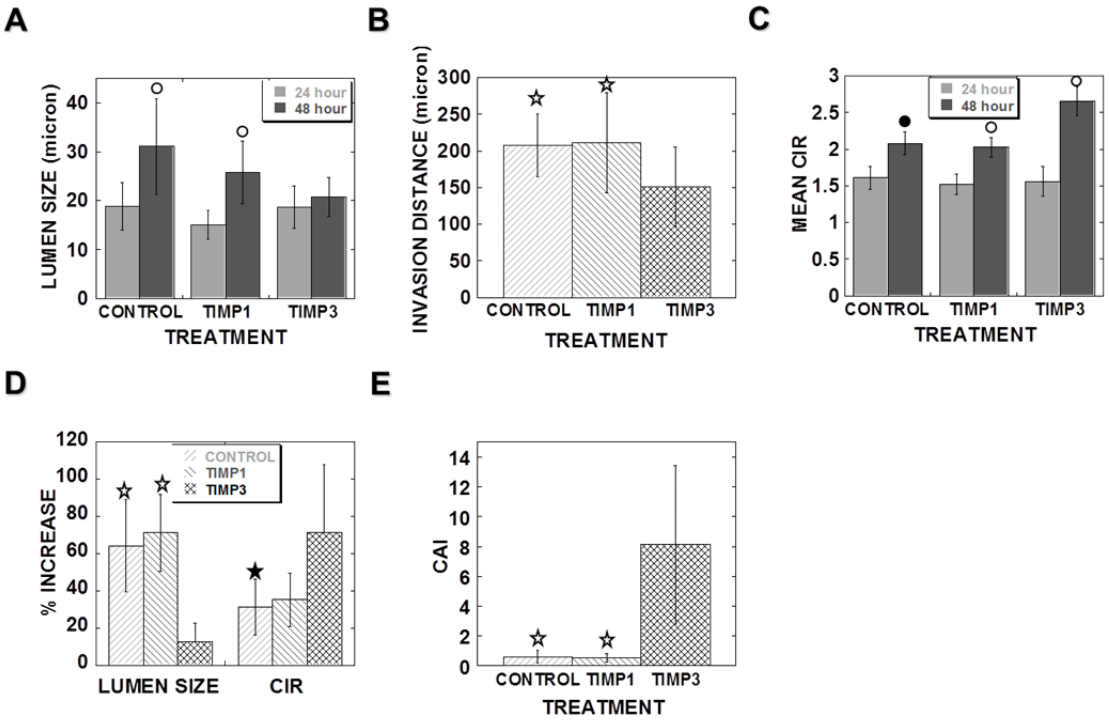

Figure 2- 9. Blocking membrane-associated, but not soluble, metalloproteinases increases CIR and CAI. Invading cultures were allowed to proceed for 24 hours before imaging invading structures. Following image capture, recombinant purified TIMP-1 or TIMP-3 was added, along with control buffer (M199). Cells were allowed to invade an additional 24 hours before the same structure was imaged (48hr). (A) Lumen size observed at 24 and 48 hours and (B) average invasion distance of sprouting structures at 48 hours following TIMP-3, TIMP-1 or control treatment. (C) Mean collagen intensity ratio (CIR) observed at 24 and 48 hours. (D) Average percent increase in lumen size, and CIR. (E) Collagen alteration index, which is calculated as the percent increase in lumen size divided by the CIR for control, TIMP-1 and TIMP-3 treatment. For data analyses, 9 structures were analyzed for control, 7 for TIMP-1 and 6 for TIMP-3 treatment. Data presentation and statistical analyses are identical to Figure 2-8.

TIMP-3 was significantly greater than control or TIMP-1, which were comparable. These data reveal that treatment with TIMP-3 was consistent with GM6001 treatment, and indicate membrane-associated MMPs but not soluble MMPs are responsible for regulating collagen intensities at the periphery of invading ECs.

Endothelial Cell Traction Force Contributes to Collagen Matrix Alterations at the Periphery of Lumens

To determine whether cell traction forces are responsible for collagen matrix alterations around lumens, the Rho associated kinase (p160ROCK) inhibitor, H1152 was applied. The small GTPase Rho has previously been shown to mediate the generation of traction forces in endothelial cells through ROCK [24]. Cultures were allowed to develop for 48 hours before being imaged with NLOM. Following image capture, cultures were treated with vehicle control or H1152 (30 μM) and imaged again at the same focal depth at 72 hours (Figure 2-10). Lumen expansion observed in control cultures was reduced with H1152 treatment (Figures 2-10A&B). Interestingly, H1152 treatment decreased the CIR from 48 to 72 hours (Figure 2-10C), despite a slight lumen expansion. CIR increase was observed in control cultures. Plotting the percent increase in lumen size and CIR (Figure 2-10D), revealed an increase in lumen diameter and CIR for control cultures, consistent with data in Figures 2-8&9. However, inhibition of ROCK resulted in a marginal increase in lumen size coupled with a decrease in CIR. As a result, the CAI differed dramatically between control and H1152 treatment (Figure 2-10E). These data indicate that inhibition of ROCK decreased collagen matrix alterations at the periphery of lumens and that EC traction is responsible for regulating collagen intensity at the periphery of invading structures.

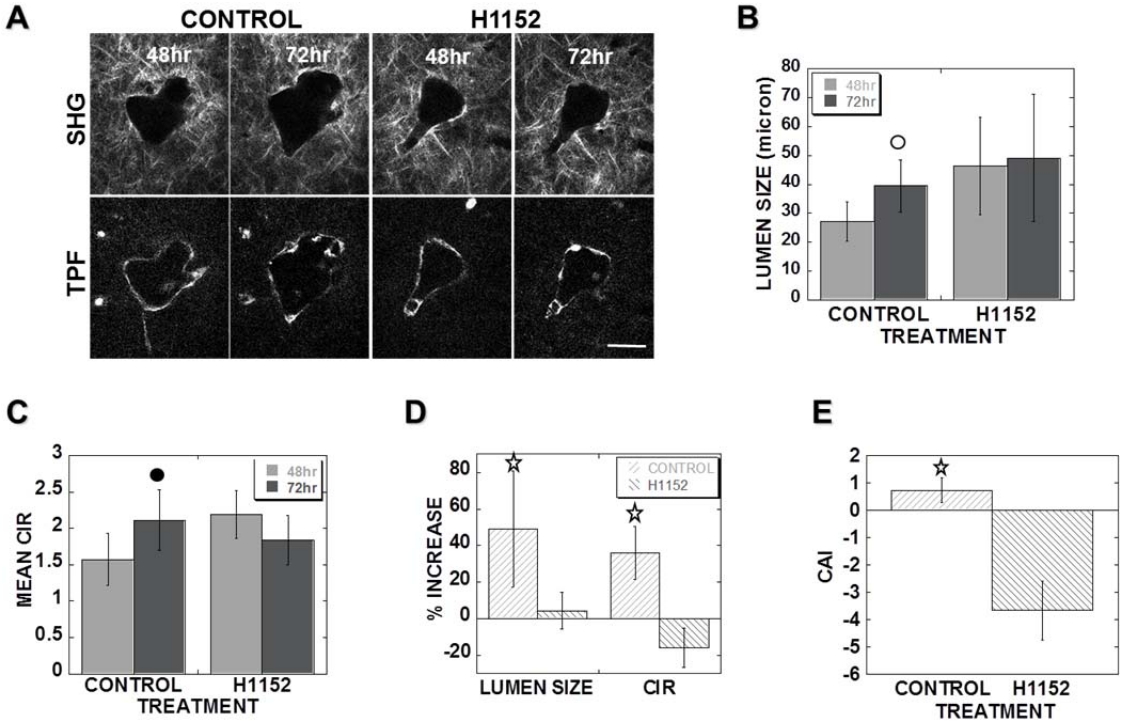

Figure 2- 10. p160ROCK inhibition with H1152 decreases CIR and CAI. Invading cultures were allowed to proceed for 48 hours before imaging invading structures. Following image capture, 30 μM H1152 or control (water) was added. Cells were allowed to invade an additional 24 hours before the same structure was imaged (72 hr). (A) Single optical sections before and after H1152 or control treatment. Scale bar=50 μm. (B) Lumen size observed at 48 and 72 hours. (C) Mean CIR observed at 48 and 72 hours. (D) Average percent increase in lumen size and CIR. (E) Collagen alteration index (CAI), which is calculated as the percent increase in CIR divided by the percent increase in lumen size for control and H1152 treatment. For data analyses, 10 structures were analyzed for control H1152 treatment. Circles and stars indicate statistical significance observed when compared to 48hour and H1152 treatments, respectively. Filled symbols indicate p values < 0.05, open symbols indicate p <0.01, student's t-test assuming equal variance was applied.

To determine whether the enhanced collagen matrix alterations observed as a result of MMP inhibition were modulated by p160ROCK blockade, H1152 was applied to cultures pretreated with GM6001. In these experiments, cultures were allowed to develop for 24 hours before being imaged with NLOM. Following image capture, cultures were treated for another 24 hours with GM6001 and imaged at the same focal depth at 48 hours. The cultures were next treated with vehicle control or H1152 (30 μM) and imaged again at 72 hours (Figure 2-11). Following GM6001 treatment, from 24 to 48 hours, a 20% increase in lumen size and 50% increase in CIR was observed, consistent with previous data (Figure 2-8). Treatment with H1152 from 48-72 hours decreased lumen expansion somewhat (Figures 2-11B), but significantly reduced the CIR (Figure 2-11C) compared to GM6001 treatment alone. Plotting the percent increase in lumen size and CIR from 48 to 72 hours (Figure 2-11D), revealed an increase in lumen diameter and CIR for GM6001-treated cultures. Inhibition of ROCK from 48 to 72 hours resulted in a negligible increase in lumen size and a decrease in CIR. Thus, the CAI values differed dramatically between control and H1152 treatment, with H1152 increasing the ratio dramatically. This result demonstrates that ECs engage both membrane-associated MMPs and traction to ensure matrix accommodation and lumen expansion.

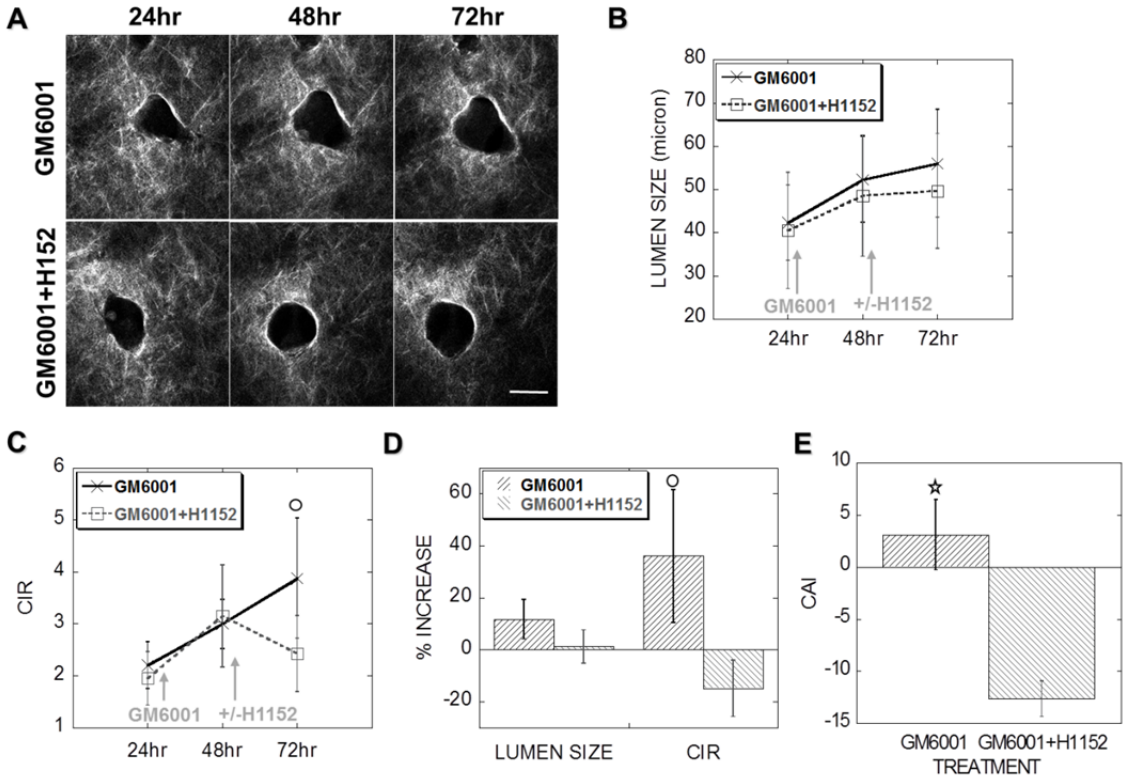

Figure 2- 11. p160ROCK inhibition relaxes CIR and CAI observed with proteinase inhibition. 3D cultures were established for 24 hours before invading structures were imaged. 2.5 μM GM6001 was then added and incubated from 24-48 hours. Cultures were imaged with NLOM at the same focal depth at 48 hours before adding H1152 (30 μM) or control (water). Cells were allowed to invade until 72hr when the same structures were imaged for the final time. (A) Single SHG optical sections at 24, 48 and 72 hours. Scale bar=50 μm. (B) Lumen sizes observed from 24 to 72 hours. (C) Mean CIR observed from 24 to 72 hours. (D) Average percent increase in lumen size and CIR from 48 to 72 hours. (E) Collagen alteration index (CAI), which is calculated as the percent increase in CIR divided by the percent increase in lumen size for control and H1152 treatment from 48 to 72 hours. Data presented are average values +/- s.d. For data analyses, 9 structures were analyzed for GM6001 treatment and 9 for GM6001+H1152. Circles and stars indicate statistical significance observed when compared to 48hour and H1152 treatments, respectively. Filled symbols indicate p values < 0.05, open symbols indicate p <0.01, student's t-test assuming equal variance was applied.

Discussion

In this study, we utilized NLOM to more closely define interactions between invading ECs and 3D collagen matrices. Our data demonstrated that extended peripheral processes of invading ECs migrated along intact collagen fibers, frequently circumventing them to continue migrating through the matrix. In addition, the presence of lumenal structures coincided with collagen dissolution or displacement as evidenced by the disappearance of SHG signal. Finally, invading EC structures leave behind tracks or tunnels that are devoid of ECM. Interestingly, the density of collagen is significantly anisotropically altered in surrounding areas of lumen formation, suggesting collagen matrix displacement or compaction. Furthermore, elevated collagen intensity was observed at areas associated with branching of lumenal structures. The high sensitivity and specificity of NLOM indicating the collagen matrix revealed a non-homogeneous environment within which invading ECs navigated and remodeled. These findings open the possibility that the heterogeneous matrix may influence and even guide or direct invasion. Time-lapse data from NLOM demonstrated lumen expansion was associated with elevated local collagen concentration. Global matrix metalloproteinase inhibition with GM6001 resulted in a significant increase in collagen intensity at the periphery of lumens that was reproduced with TIMP-3, but not TIMP-1 treatment. These data indicate that collagen intensity alterations are determined by membrane-associated, but not soluble MMPs. Inhibiting p160ROCK, which mediates the generation of traction

forces by endothelial [24] and other cells [364], decreased lumen expansion and collagen intensity ratios compared to control treatment. Pretreatment with metalloproteinases elevated CIR that could be reduced by p160ROCK inhibition, revealing that a balance between proteolysis and force generation dictates ECM organization at the periphery of invading structures.

We observed a strong correlation between collagen fiber orientation and sprout outgrowth. ECs tracked along existing fibrous collagen (Figure 2-2A) as well as intersecting with and extending processes beyond collagen bundles (Figure 2-2B*).* These data are consistent with a previous report demonstrating radiating collagen fibers at the periphery of tumors and local cell invasion that predominantly occurred along aligned collagen fibers *in vivo* [340], that was confirmed by manipulating collagen fiber orientation [343]. Further, cultured tumor explants can realign collagen fibers, allowing individual tumor cells to migrate radially along aligned fibers [340]. Bud formation in the mammary gland may occur in a similar manner, with long bundles of collagen fibers that radiate from terminal buds to influence ductal outgrowth and patterning [344]. These observations are consistent with findings by Utzinger and colleagues who observed angiogenic sprout outgrowth from microvessel fragments embedded in 3D collagen matrices [346]. Collagen fibril architecture was observed to be aligned along the direction of sprout outgrowth, suggesting that sprouting angiogenic structures may also exert tension on and reorganize the matrix as they advance [346]. Although we do not observe overt collagen alterations at the tips of outgrowing ECs, the possibility remains that the arrangement of collagen fibers may be altered by ECs protrusions as

invasion proceeds. Time lapse imaging is currently underway to definitively determine whether sprouts simply sense or rearrange collagen fibers as invasion proceeds. Regardless, these EC-ECM interactions cannot be appreciated in traditional 2D culture systems.

Increased matrix stiffness can modulate EC morphogenesis, where cells tested with increased matrix rigidity formed larger lumens [20, 133, 253, 271, 365, 366] demonstrating that ECs, much like fibroblasts [318, 367, 368] respond to alterations in matrix tension. Unlike fibroblasts, which respond by increasing contractile properties and can differentiate into myofibroblasts [369], ECs respond to increase in matrix tension by increasing lumen diameter [271], a process that is mediated through membrane-associated metalloproteinase activity [333]. Our data reveal that advancement of invading structures resulted in cell-mediated anisotropic increases in collagen matrix intensity at the periphery of lumens. This may generate specific mechanical cues for continual remodeling of the advancing sprout via localized proteolysis required for continual expansion of the lumen. Experiments employing metalloproteinase inhibition resulted in increased collagen intensity around the lumen and limited sprout advancement. Thus, the balance between generation of matrix tension and initiation of proteolytic events must be exquisitely controlled to ensure sprout development. We speculate this balance serves to efficiently deliver nutrients to surrounding tissue, because increased collagen density can be a diffusive barrier for macromolecular transport.

ECs respond to biochemical cues such as matrix attachment sites, angiogenic growth factors and shear stress [370-372], but substantial evidence also demonstrates that mechanical signals within the matrix can affect cell behavior and morphogenic responses. Our data demonstrate that collagen matrices are anisotropically altered at the periphery of lumens, indicating that the cell-mediated forces that are applied to the periphery of the invading structure are not uniform and these alterations may affect subsequent development of the advancing structure. Because vacuole formation, fusion and coalescence are prerequisites for lumen formation in endothelial and epithelial systems [373, 374], vacuolar trafficking during lumen formation may be directed by matrix alterations observed at the periphery. ECM remodeling is a dynamic process involving integrins and proteases. Integrins, the primary ECM receptors mediating ECM remodeling [375], act as mechanotransducers and can transfer mechanical force from the cell to ECM or vice versa [376], and likewise control vacuole formation events [261]. In addition to vacuolar trafficking, cell-derived tension within the collagen matrix could also control vascular compliance. Cells are capable of exerting tension to realign collagen fibers while migrating through 3D ECM [364, 377-379]. The elevated collagen intensity at the bifurcation area of lumens (Figure 2-4) is indicative of increased collagen density and hence increased rigidity. This could be a contributing factor as to why atherosclerotic plaques tend to occur at the bifurcation of aorta, carotid and coronary arteries [380] since arterial compliance, a diagnostic marker for plaque [381], is associated with ECM rigidity [382]. At the present time, the functional significance of collagen matrix alterations remains undefined.

Endothelial sprouting requires proteinases. Our data demonstrate that soluble MMPs do not play a role in sprouting events because TIMP-1-treated cultures invade similarly to control, while the addition of TIMP-3 limits lumenal expansion and invasion in established invading structures. It is well-established that MT1-MMP is required for endothelial sprouting responses and lumen formation [80, 96, 332, 333]. In addition, MT1-MMP is utilized by tumor cells for outgrowth in three dimensions [383]. Thus, MT1-MMP is a key enzyme that degrades type I collagen and mediates cell movement in three dimensions. Friedl and colleagues have demonstrated that proteolytic activity localizes to the middle portion of a tumor cell migrating in 3D. This scenario is consistent with our observations, where increased collagen intensity is observed at the periphery of lumens, analogous to what has been described as the 'stalk' of a newly-forming angiogenic vessel [384]. The time-lapse data presented demonstrated that increased CIR was directly proportional to lumenal expansion, an event that is dependent on MT1-MMP activity [333]. By inhibiting membrane-associated MMPs using TIMP-3 or GM6001, we observed elevated CIR at the periphery of lumens compared to non-treated and TIMP-1 controls. These data argue that the elevated CIR resulting from decreased collagen proteolysis was due to increased interactions between ECs and the surrounding collagen matrix and tension exerted on the web of ECM by the invading ECs. In the absence of proteolysis, cell-matrix interactive forces act on the surrounding collagen matrix to increase force generation, traction and tension, visualized at the cell periphery as an increase in collagen intensity. These forces are likely generated circumferentially via integrin receptors and the cytoskeleton. Consistent with this idea,

SHG imaging of mammary glands *in vivo* revealed increased collagen intensity at the periphery of glandular structures compared to the surrounding ECM [340]. In addition, our observations were consistent with data collected from neovessel outgrowth from microvessel explants in collagen matrices, as well as undigested microvessels [346], where collagen aligned asymmetrically along the base of invading sprouts, but was less apparent and not different from surrounding matrix at the leading edge. Our studies utilizing Rho kinase inhibition support this contention, where blocking Rho kinase and the subsequent ability to generate tension resulted in a significant decrease in collagen intensity ratio, and thus, a change in the distribution and organization of collagen fibers. A similar phenomenon has recently been reported to be required for outgrowth of tumor explants [343]. Further investigation of the specific nature of these regions of compacted or compressed collagen is warranted.

CHAPTER III

ANGIOGENIC RESPONSES TO MECHANICALLY AND MICROSCOPICALLY CHARACTERIZED, MICROBIAL TRANSGLUTAMINASE CROSS-LINKED COLLAGEN MATRICES

Overview

Sprouting endothelial cells (ECs) use both soluble and insoluble cues to guide migration and expand the existing vascular network to meet changing trophic needs of the tissue during angiogenesis. Fundamental to this expansion are physical interactions between ECs and extracellular matrix (ECM) that influence sprout migration, lumen formation and stabilization. These physical interactions suggest that ECM mechanical properties may influence sprouting ECs and, therefore, angiogenic responses. In a 3D model of angiogenesis in which a monolayer of ECs is induced to invade an underlying collagen matrix, we measure angiogenic responses as a function of collagen matrix stiffness by inducing collagen cross-linking with microbial transglutaminase (mTG). With biaxial mechanical testing, we show that collagen matrices stiffen with both mTG treatment and incubation time. Using two-photon excited fluorescence (TPF) and second harmonic generation (SHG), we show collagen TPF intensity increases with mTG treatment and that the ratio of TPF/SHG correlates with biaxial tested mechanical stiffness. SHG and optical coherence microscopy (OCM) are further used to show that other physical properties of the matrix such as porosity and pore size do not change with

mTG treatment, thus providing the same density but different stiffness with which to measure angiogenic responses. Our results showed that stiffer matrices promote angiogenesis, measured by more invading sprouts that invade deeper. No differences in lumen size were observed between control and mTG stiffened 3D cultures, but there was evidence of greater matrix remodeling in stiffer gels using NLOM. Results of this study show angiogenic responses are enhanced with increasing stiffness and suggest that these properties may be used in tissue engineering and regenerative medicine applications to engineer angiogenesis.

Introduction

Angiogenesis, new blood vessel formation from existing structures, is necessary for normal physiological growth and developmental processes ranging from embryogenesis to wound healing, and pathologic processes ranging from psoriasis, cancer, rheumatoid arthritis, ischemia, inflammation and various cardiovascular diseases [323, 324, 385]. Cell migration, proliferation, intracellular alignment, adhesion, and lumen formation are coordinated cellular actions that enable ECs of existing vessels to detach from the vascular wall, degrade and penetrate the underlying basal lamina while invading the surrounding 3D interstitial ECM during angiogenesis [325-327]. These processes are regulated by biochemical and biophysical cues. The ECM is a scaffold that provides mechanical support and adhesive contact sites, along with mechanical signals, that combine with biochemical cues to promote angiogenesis.

Cell movement through 3D matrices is a precisely coordinated process. Growth factors and lipids, such as sphingosine-1-phosphate, deliver potent pro-angiogenic signals [270, 328, 329, 386] that stimulate endothelial outgrowth and invasion events and require membrane-associated (but not soluble) matrix metalloproteinases (MMPs) [330]. In particular, these events require MT1-MMP [331, 332, 387], which selectively and locally degrades ECM proteins at the cell surface-ECM interface without affecting the integrity of the ECM scaffold. Thus, newly-sprouting endothelial cells integrate signals from pro-angiogenic stimuli to initiate successful outgrowth in 3D matrices.

ECM stiffness influences various pathological diseases, such as cancer and atherosclerosis [283, 388]. How ECM stiffness influences cell behavior [309, 389] has been investigated *in vitro* among different cell types, including ECs [271, 318, 390, 391], smooth muscle cells [135, 392, 393], fibroblasts [113, 134, 318, 394], macrophages [395], leukocytes [391, 396], tumor cells [397-399] and stem cells [117, 400]. Substrate stiffness controls cell characteristics including, the size of focal adhesions, cell stiffness [397, 401] and traction forces generated by the cell [394, 397, 401]. The influence of ECM stiffness on angiogenesis has been investigated in several 2D [138] and 3D [133, 136, 137, 162, 195, 271, 273, 366, 402-405] *in vitro* studies. Among them, most 3D studies tuned ECM stiffness by changing protein concentration of various ECM including collagen [162, 271, 404, 405] and fibrinogen [136, 137, 273, 366, 403]. However, changing ECM protein concentration will not only change bulk mechanical properties (i.e. stiffness) but also change its topographical properties (i.e.

porosity, pore size, and fiber thickness). Therefore, decoupling ECM mechanical properties from its topographical properties remains a challenge.

3D ECM scaffolds can be created with synthetic polymers, such as polyethylene glycol (PEG) [132] or natural polymeric materials, such as collagen, fibrin, hyaluronan. The advantages of natural materials over synthetic materials are that natural materials are viscoelastic, biodegradable and contain natural ligands [406]. Type I collagen, the major collagen found in skin and bones, dominates 90% of total collagen present in the body and is the natural material most often used for creating 3D scaffolds. Collagen is also a strong promoter of EC morphogenesis [195]. The microstructure, biophysical properties and gelation kinematics of collagen can be tuned by controlling concentration [158-161], temperature [159, 163-165], ionic strength [161], phosphate content and pH [133, 159, 163, 166] during collagen fibrillogenesis. In order to decouple stiffness from topographical properties, tuning stiffness via concentration is not an option. Without changing collagen concentration, collagen scaffold stiffness can be strengthened via crosslinking collagen physically [174-176], chemically (glutaraldehyde [163, 177, 178] and carbodiimide [181-183]), enzymatically (tissue transglutaminase tTG [67, 68][186, 187], microbial transglutaminase [185, 188], lysyl oxidase [189]) and non-enzymatically (glycation [190-194]). Even tissue transglutaminase and lysyl oxidase are physiologic, more merits [199, 200] of using mTG over tTG are Ca^{2+} independent, higher reaction rate and broader substrate specificity. How the topographical properties of the ECM microstructure influenced by mTG can be characterized with our NLOM-OCM combined system.

Nonlinear optical microscopy (NLOM) provides spatial and temporal information of ECs-matrix interactions during angiogenesis noninvasively and nondestructively [407] with evidence of its 3D high resolution imaging with no out-of-focus scattering, minimal photo-bleaching, reduced light scattering and deeper tissue penetration when compared with confocal microscopy [209]. Owing to lack of cetrosymmetric center, collagen has appreciable nonlinear susceptibility for second harmonic generation (SHG) [243, 334-339], a nonabsorptive process, and that property enables application of NLOM in collagen scaffold microstructure without using exogenous stains or dyes [165, 166, 229-233, 338]. The fluorescence from collagen depends on organization of collagen fibrils, the amount of cross-linked fibers [165, 230-232] and polymerization time [229]. NLOM has been applied to characterize optical properties of collagen treated with various cross-linkers including glutaraldehyde [165, 230], glycation [232] and genipin [231]. The effects of mTG-induced collagen cross-linking in the optical properties of collagen matrices have not been investigated to date.

Here, we utilized an *in vitro* model [330] that mimics the sprouting step of angiogenesis where ECs are allowed to invade in 3D collagen matrices. We used a NLOM-OCM combined system to investigate the mechanical and optical properties as well as the microstructure (topographical properties) of mTG-treated collagen and successfully decoupled stiffness from topographical properties. Our experiment results revealed that ECM stiffness induced by mTG treatment enhanced angiogenic responses.

Materials and Methods

Reagents and Chemicals

Type I rat-tail Collagen was obtained from BD Biosciences (San Jose, CA). Recombinant human vascular endothelial growth factor (VEGF) and fibroblast growth factor-2 (FGF-2) were purchased from R&D Systems (Minneapolis, MN). Medium 199 (M199) and fetal bovine serum (FBS) were purchased from Invitrogen (Grand Island, NY). Tumor promoting antigen (TPA, Phorbol 12-myristate 13-acetate) (what was TPA used for?) and ascorbic acid (AA) were purchased from Sigma (St. Louis, MO). Sphingosine-1-phosphate (S1P) was purchased from Avanti Polar Lipids (Alabaster, AL). ACTIVA WM, a gift from Ajinomoto (Japan), was derived from Sreptoverticilium mobaraense and mTG (39 kDa) was obtained with further purification of ACTIVA WM to remove maltodextrin (2.3-3 kDa). mTG has a higher specific activity to crosslink collagen over a wider range of temperature and pH and its activity is Ca^{2+} independent. ACTIVA WM was dissolved in ice-cold 50 mM sodium phosphate buffer (pH 6.0) and then dialyzed against 20 mM sodium acetate (pH 5.5) three times at 3 hour intervals before centrifugation at 3000 G for 30 min to collect the supernatant. Supernatant was loaded to a 50 ml SP Sepharose (Sigma) column with a continuous flow rate of 5 ml/min. Column was washed and protein eluted at the same flow rate with NaCl gradient from 0 mM to 500 mM in 20 mM sodium acetate buffer (pH 5.5). Fractions containing mTG were determined from Coormassie Stain, pooled together and dialyzed against distilled autoclaved water three times at 3 hour intervals. Dialyzed product was

lyophilized, weighted, dissolved with M199 with final concentration determined with BCA protein assay and stored at -70ºC for long term storage.

Cell Culture

Primary human umbilical vein endothelial cells (HUVECs) were purchased from Cambrex and used at passage 2-6. ECs were grown on gelatin-coated tissue culture flasks (1 mg/ml) in culture media of M199 containing 15% FBS, 400 μg/ml bovine hypothalamic extract [359], 100 μg/ml heparin (Sigma), 0.1% gentamycin and 1% penicillin/streptomycin (Invitrogen). Cells were passaged once a week. EC lines stably expressing enhanced green fluorescent protein (EGFP) were generated using a recombinant lentivirus system (Invitrogen) [407].

Collagen Gel for Optical and Mechanical Properties Measurement and Angiogenic Evaluation

Fibrous collagen gels were formed with rat-tail type I collagen, 5X DMEM, reconstitution buffer, neutralized with 1M NaOH [339] and mTG to create 3.5 mg/ml collagen matrices with final mTG concentrations of 0, 100 and 500 μg/ml. Cruciform shaped acellular collagen gels, used for optical and mechanical properties measurements, were formed within a cruciform shaped mold. Ice-cold collagen-mTG mixture mixed with beads was placed within the mold inside incubator for 12 hours for polymerization. The acellular gels were covered with 200 ml M199 until imaging with NLOM-OCM combined system and mechanical testing with biaxial bioreactor. For EC invasion studies, the collagen-mTG mixture containing 1 μM S1P 80 μl per well, used for 3D angiogenesis assay, was polymerized in 96-well plate in 37 ºC and 5% CO_2 incubator for

12 hours. After washing three times with sterile 160 µl M199 at 10 min intervals, 3D angiogenesis invasion assays were generated by seeding an EC monolayer on the 3D collagen surface with cell density of $7x10^4$ per well of 96 well plate in serum-free M199 containing reduced serum supplement II (RSII) [360], recombinant VEGF (40 ng/ml), recombinant FGF (40 ng/ml), AA (50 µg/ml) and TPA (50 ng/ml). Cultures were allowed to proceed for the times indicated before fixing in 4% paraformaldehyde in PBS prior to imaging.

Nonlinear Optical Microscopy-Optical Coherence Microscopy (NLOM-OCM) Combined System

System setup

Our custom-built NLOM-OCM combined system has been described previously [408]. Briefly, dispersion-compensated sub-10-fs pulses (800 nm, FWHM=133 nm) from a Ti:Al_2O_3 oscillator (Femtosource, Femtolasers) pumped by a Nd:YVO4 solid state laser (Verdi, Coherent) were split by 10/90 beam splitter. One beam (sample arm) was coupled into the epi-fluorescence port of an upright microscope (Axioskop2 MAT, Carl Zeiss GmBH) via dual-axis galvanometer driven mirrors (Model 6220, Cambridge Technology) mounted on an elevated breadboard and the other beam was used as reference arm. The beam in sample arm was directed to the microscope objective by a short pass dichroic mirror (635dcspxruv3p, Chroma). Nonlinear optical signals were collected by the 40x focusing objective (NA=0.8) and directed to a custom built two channel detector unit mounted on one of the dual accessory ports of the binocular head. The detector unit housed two dichroic mirrors and bandpass filters (Chroma), focusing

lenses (PCX, focal length: 50 mm, 31 2321, Linos Photonics), and a pair of photon-counting photomultiplier tubes (R7400P, Hamamatsu). Appropriate long pass dichroic mirrors and bandpass filters were used for SHG (430dcxru and HQ405/40, respectively; Chroma) and TPF detection (580dcxr and HQ480/40, respectively; Chroma). In imaging mode each photomultiplier tube was connected to a preamplifier/discriminator (F-100T, Advanced Research Technologies) that thresholds signal current and converts to TTL pulses for photon counting. Image intensities were displayed in photon counts on a PC (Optiplex GX280, Dell). For OCM, simultaneous backscatter laser light in sample arm was combined with return light from reference arm and focused into single mode optical fiber which directed into a home-made spectrometer for Fourier domain detection. Throughout this experiment, less than 40mW of laser power was incident on the scanning mirrors, approximately 10 mW at the sample.

Image acquisition and analysis

Samples of cruciform shaped acellular collagen gels or of 3D angiogenesis assays were imaged without stains using NLOM-OCM combined system rendering en face, 2D images with integrated intensities of 4 scans at each focal depth. A stack of images was generated by incrementally changing the depth of focus. For acellular matrices, five image stacks were acquired at least 1 mm distance apart and each stack contained 10 images at depth from 10 μm to 100 μm below gel surface. For 3D angiogenesis assay, image stacks with 5 μm increment were acquired from structures containing lumens from monolayer to sprout tip. SHG, TPF and backscatterred OCM signals were collected simultaneously with NLOM-OCM combined system. Image files acquired from NLOM

were converted from 16-bit to 8-bit files via MATLAB by scaling the maximum pixel value to 255.

Optical properties and topographical properties of acellular matrices

Fuzzy thresholding algorithm written with MATLAB code was applied on SHG images to create binary masks of collagen fibers. The automated custom MATLAB algorithm includes steps of increasing dynamic range of image with intensity transformation, smoothing image with fuzzy transformation and finally based on histogram of smoothing image to create binary mask which corresponds to collagen fibers [409]. With binary mask of SHG (collagen fibers), porosity, pore size and pore number could be quantified with MATLAB software. Negative binary mask was used to highlight the void region or pore locations and porosity was calculated by void region pixel number to total pixel number of 256x256 in a value between 0 and 1. Number of void regions was reported as pore number. Pore size was acquired from converting pixel number of average void region area into actual area size with unit of μm^2. Segmented SHG and TPF for optical properties quantification of acellular matrix could be created with SHG and TPF images multiplied by collagen fiber binary mask, therefore, only SHG, TPF intensities from collagen fibers will be used for quantification. Normalized segmented SHG and TPF were created with normalizing pixel intensities in segmented SHG and TPF to its corresponding background noise after obtaining background noise of SHG and TPF from averaging the signal intensities of SHG and TPF among all void region (pore) from negative collagen binary mask. Optical properties, such as SHG mean, TPF mean and SHG/TPF ratio, could be calculated after obtaining pixel

intensities of normalized segmented SHG and TPF. SHG mean and TPF mean are defined with total pixel intensities in normalized segmented SHG and TPF divided by total pixels of collagen fibers respectively. TPF/SHG ratio is calculated with averaging pixel-wise TPF/SHG ratio of normalized segmented TPF over SHG on area with collagen fibers.

Lumen area and collagen intensity ratio

Binary masks of TPF images to reveal lumen boundary were created with the same algorithms used for SHG binary mask creation. The combination of binary masks of SHG and TPF was used for selecting the lumen of interest to create binary lumen mask. Lumen area in μm^2 was calculated by converting total pixel numbers of lumen into actual lumen size with known value of actual area per pixel. Collagen intensity ratio (CIR) from SHG (or OCM) was calculated from averaging the normalized segmented SHG (or OCM) intensities inside the ring area with inner circumference equaled to lumen area and ring thickness equaled to lumen wall thickness.

Biaxial Bioreactor for Mechanical Properties Measurements

After imaging with NLOM-OCM combined system, the cruciform shaped gel was coupled to loading carriage of biaxial bioreactor filled with 1x phosphate buffer saline (Sigma). The bioreactor was transferred onto a testing platform containing two force transducers for force recording, four computer controlled step motors and one CCD camera on top for strain measurement based on tracing beads movement ([410], Bai et al.[in submission]). The data of load-stretch ratio curve was reported after 3rd cycle since the preconditioning condition could be achieved after 3rd cycle (data not shown).

Transmitted Light Image Acquisition and Quantification

3D angiogenesis cultures were fixed in 3% glutaraldehyde in PBS and stained with toluidine blue as previously described [330]. Invading structure number per field of view was acquired under 10X objective. To quantify invasion distance, photographs of invading cells were taken from a side view with an Olympus CKX41 microscope equipped with a Q color 3 Olympus camera. Invasion distance and lumen diameter measurement were measured digitally using Image Pro Analyzer software.

Statistics

Student's T-tests were applied in statistics evaluation among studies of optical properties, topographical properties and angiogenic responses and significant differences were labeled or tabulated in Figure 3-2, Figure 3-6, Figure 3-8, Figure 3-9, Figure 3-12 and Figure 3-13. P-value < 0.05 was considered a significant difference.

Results

Nonlinear Mechanical and Optical Properties of mTG Cross-linked Collagen Matrices

In this study, we sought to characterize angiogenic responses as a function of 3D collagen matrix stiffness while keeping density constant. To accomplish this, we crosslinked 3.5 mg/ml collagen gels with mTG and reasoned, (and later confirmed,) that by holding density constant, other microstructural properties such as porosity would not change. Cruciform-shaped collagen gels (3.5 mg/ml) were mechanically tested in our custom biaxial bioreactor. Graphs of load (g) as a function of strain are shown in Figure 3-1 for collagen gels treated with mTG (control, 100, 500 μg/ml) and incubated for 1 (Figure 3-1A), 2 (Figure 3-1B) and 7 days (Figure 3-1C). The mechanical testing curves exhibited nonlinear and viscoelastic responses characteristic of soft tissues. For each day, load (g) to stretch gel 5% increased with mTG dose, and load magnitude increased with each day of measurement. Collagen gels treated with 500 μg/ml mTG were consistently stiffer than all other treatment groups. On Day 1, loads at 5% stretch were 1.87, 2.44, and 3.69 g for control, 100, and 500 μg/ml mTG treated collagen gels, respectively (see Figure 3-1A). On Day 2 (Figure 3-1B), loads at 5% stretch were 2.07, 2.29, and 4.66 g for control, 100, and 500 μg/ml mTG, respectively, indicating an increase in load for control as well as mTG treated gels. On Day 7, these trends continued with loads at 5% stretch of 2.70 and 10.18 g for control and 500 μg/ml mTG treated gels, respectively.

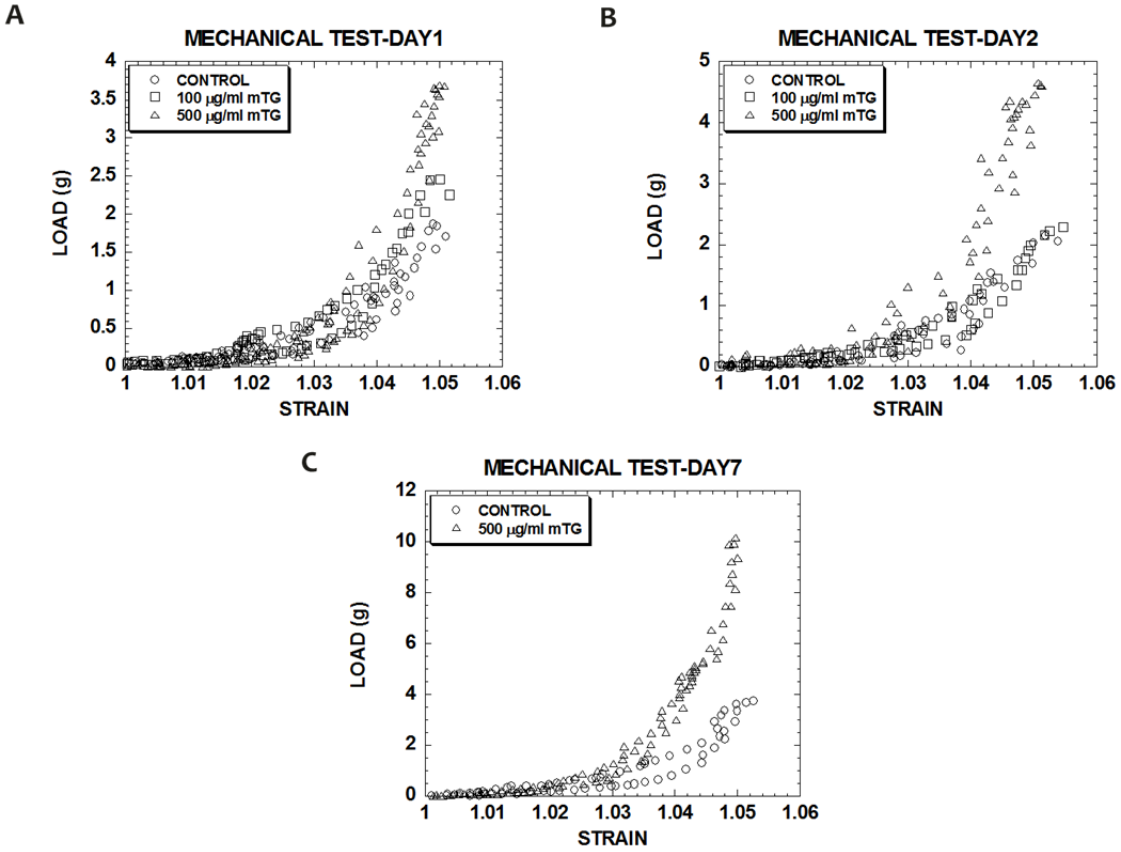

Figure 3- 1. Biaxial mechanical tests of acellular cruciform-shaped collagen gels revealed nonlinear viscous response curves with larger loads for higher mTG doses and incubation times. Load (g)-strain curves of control and mTG-treated collagen gels tested on Day 1 (A) and Day 2 (B), and Day 7 (C). Note changes in scale of Load (g) axes.

Our NLOM-OCM combined system is sensitive to endogenous collagen signals, two-photon excited fluorescence (TPF) and second harmonic generation (SHG), enabling simultaneous visualization of both to better characterize collagen nonlinear optical properties. Collagen TPF has previously been shown to correlate with cross-linking [229], of which one fluorescent cross-link is reportedly pyridinoline [411]. Collagen SHG results from the mixing of light within its quasicrystalline structure and is thus sensitive to molecular order and collagen higher order structures [243, 339].

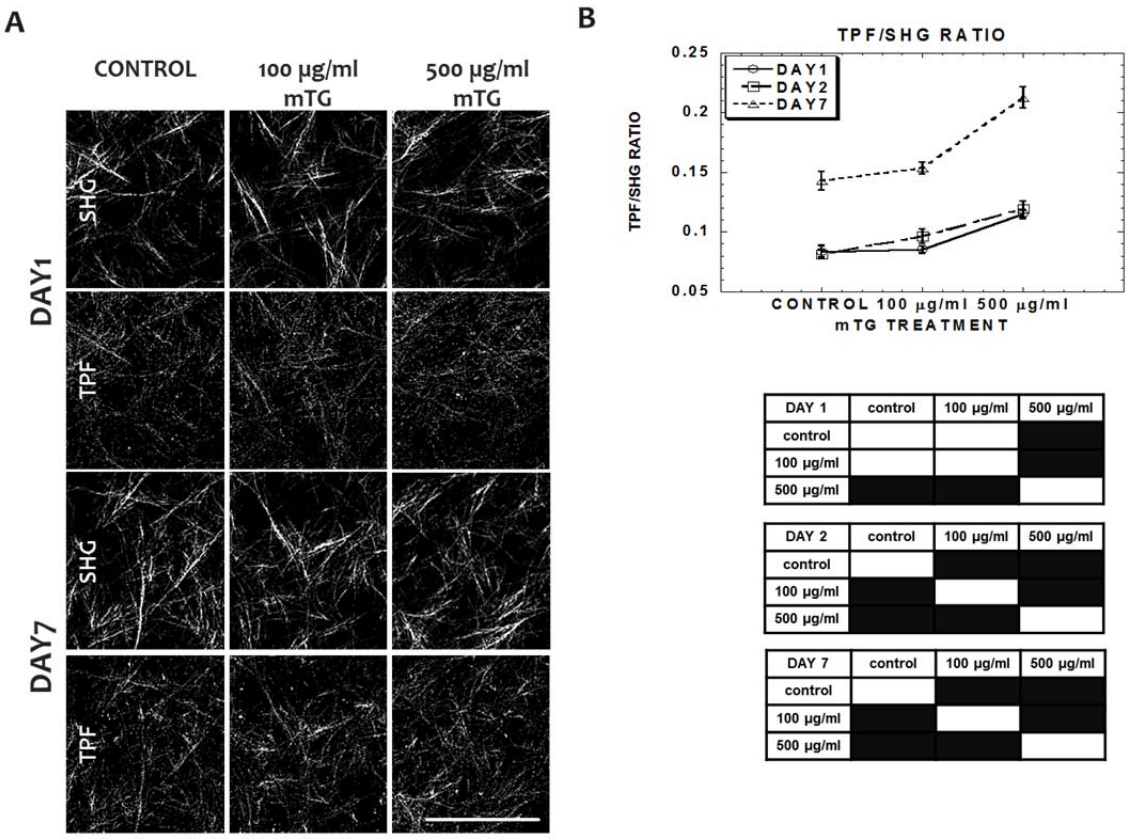

Figure 3- 2. TPF/SHG ratio correlates with mTG dose and incubation time. (A) Representative TPF and SHG images of control and mTG-treated acellular collagen ECM at Day 1 and Day 7. Plots of TPF/SHG ratio (B) of collagen as a function of mTG dose treatment and incubation time. In statistics table, region highlighted with black color represents for significant difference with $p<0.05$. Error bars represent mean +/- STD. Scale bar is 50 µm.

SHG and TPF images of acellular collagen matrices were collected at Day 1 and 7 of control and mTG treated gels (Figure 3-2A). Under each condition, collagen TPF intensity was noticeably higher on Day 7 than on Day 1. Quantification of SHG and TPF images revealed that TPF and TPF/SHG in mTG treated gels was enhanced with dose up to 500 µg/ml but not SHG, see Figure 3-2B (TPF, SHG data not shown). Consistent with mechanical testing results, measurements of TPF to SHG ratio increased from Day 1 to

Day 7. On each day (Day 1, Day 2, and Day 7), TPF/SHG ratio increased with mTG dose and peaked at 500 μg/ml mTG treatment (Figure 3-2B) with significant difference compared to control. On Day 1, TPF/SHG of acellular collagen increased from 0.083±0.004 for control to 0.085±0.003 and 0.115±0.003 when treated with 100 and 500 μg/ml mTG, respectively. On Day 2, TPF/SHG exhibited a similar trend as Day 1 with values of 0.081±0.003 for control and 0.096±0.005 and 0.119±0.006 for 100 and 500 μg/ml mTG treated gels, respectively. The most prominent difference in collagen TPF/SHG ratio was observed at Day 7, where TPF/SHG values nearly doubled from Day 1. Collagen TPF/SHG ratios measured on Day 7 were 0.142±0.007, 0.153±0.005 and 0.212±0.008 for control, 100, and 500 μg/ml mTG treated gels, respectively.

If collagen TPF/SHG ratio did correlate with collagen cross-linking level, then the optical measurement should correlate with the mechanical response measurement. As an indicator of collagen mechanical properties, we used load (g) at 5% stretch. Correlative plots were shown in Figure 3-3 of load (g) at 5% stretch with SHG (Figure 3-3A), TPF (Figure 3-3B), and TPF/SHG (Figure 3-3C). Consistent with previous work [229], SHG was observed not to depend on collagen cross-linking and, thus, did not show a correlation with load at 5% stretch. Collagen TPF did show increased intensity with mTG treatment and mechanical properties, though its correlation coefficient with load at 5% stretch was weak ($r = 0.666$). Collagen TPF/SHG exhibited the highest correlation with load at 5% stretch with a correlation coefficient, $r = 0.918$.

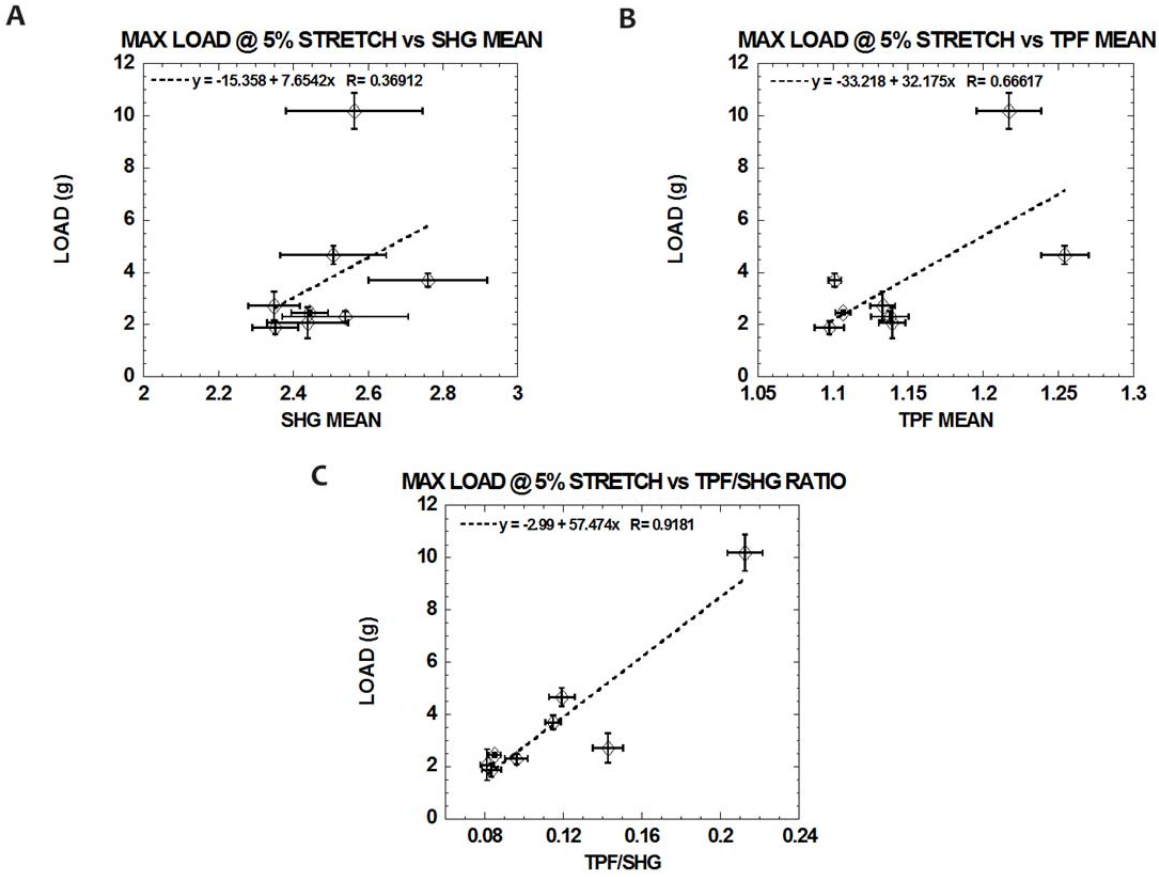

Figure 3- 3. Load (g) at 5% stretch correlates well with TPF/SHG ratio compared with SHG mean or TPF mean. Plots of load (g) at 5% stretch as function of SHG mean (A), TPF mean (B) and TPF/SHG ratio (C).

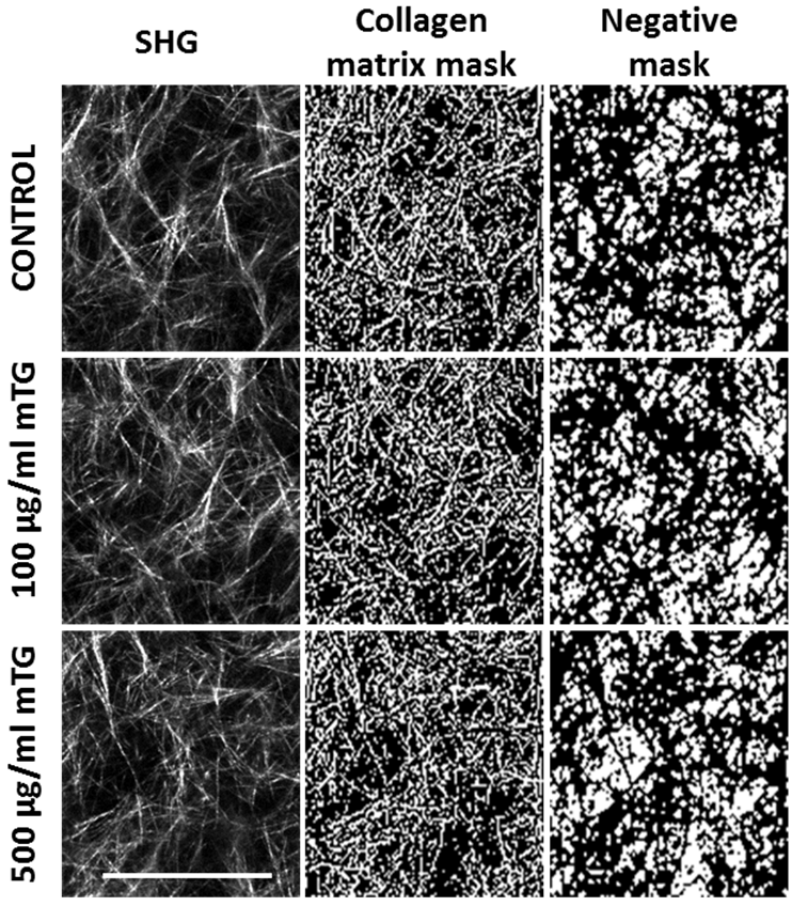

Figure 3- 4. Representative SHG images of control and mTG-treated collagen ECM used to create collagen matrix mask which can be inverted to highlight matrix porosity (negative mask). Scale bar is 50 µm.

Microstructural Properties of Collagen Matrices Remained Unchanged with mTG Treatment

Mechanical testing and NLOM experiments demonstrated that collagen nonlinear mechanical and optical properties were modulated with mTG treatment. We next characterized gel microstructural properties with SHG. Representative and processed SHG images were shown in Figure 3-4 of control and 100 and 500 µg/ml mTG treated collagen gels. Binary masks of collagen fibrous structures were obtained by applying

fuzzy thresholding algorithms non-discriminately to all images (see Methods). The negative of these masks were used to highlight gel porosity. These negative binary masks were used to further quantify the physical properties of porosity, pore size, and pore number per unit area (see Figure 3-5). Porosity is defined as the ratio of void to total area. Porosity was quantified for control and mTG treated collagen gels and shown in Figure 3-5A. The bar graph reveals no significant difference in porosity compared with control with values of 0.765±0.050, 0.760±0.034, and 0.764±0.032 for control, 100, and 500 μg/ml mTG treated gels, respectively. Pore sizes of control and 100 and 500 μg/ml mTG treated collagen gels were quantified and were shown in boxplot in Figure 3-5B. Median pore sizes measured 14 μm^2 and there was no difference between each group. Pore number per field of view was quantified under the same field of view (80μmx80μm), see Figure 3-5C. For control and 100 and 500 μg/ml mTG treated collagen gels, pore numbers were 253.7±57.9, 258.8±50.7 and 254.6±47.5 respectively, with no significant difference from control.

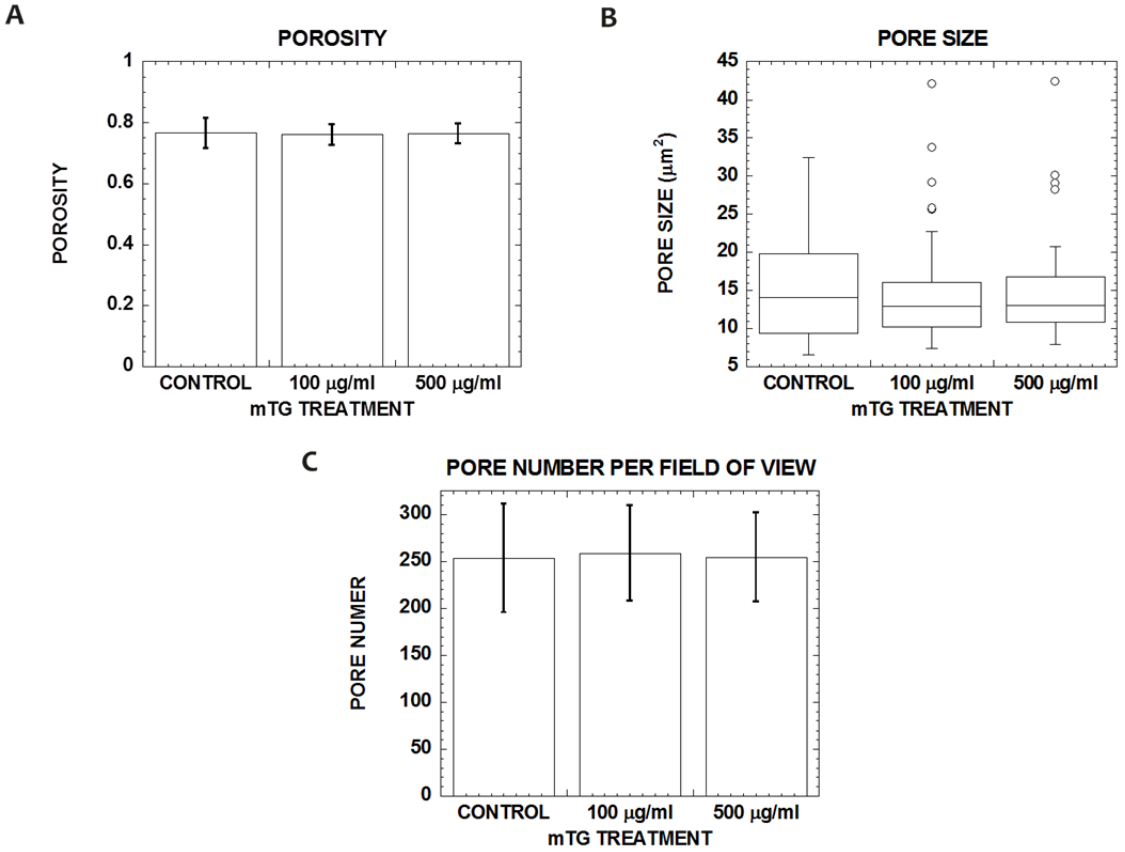

Figure 3- 5. Porosity, pore size and pore number per field of view of collagen ECM don't change with mTG treatment. Bar graph of porosity (void fraction) (A), boxplot of pore size (B) and bar graph of pore number per field of view (C) in control and mTG treated collagen ECM. 50 SHG images were analyzed. Error bars in (A) and (C) represent mean+/-STD.

Matrix Stiffness Promoted Angiogenic Responses

With mTG treatment, collagen gels (3.5 mg/ml) bore higher loads without concurrent changes in microstructural properties. Thus, we measured angiogenic responses to changes in stiffness of control and mTG treated 3D collagen gels. Monolayer of human umbilical vein endothelial cells (ECs) was induced to undergo angiogenic morphogenesis, i.e., invade the underlying collagen gel and form lumens. After 48

hours, cultures were fixed, stained with toluidine blue, and sectioned transversely for cross-sectional views. Representative photographs of sectioned cultures from control and 500 μg/ml mTG treated collagen gels were shown in Figure 3-6A and illustrate that stiffer matrices promoted angiogenic responses including more invading structures and deeper invasion distances. The number of invading angiogenic structures was quantified using a 4x objective (~1 mm^2) and shown in bar graph in Figure 3-6B. The highest number of invading structures was observed in collagen gels stiffened with 500 μg/ml mTG (76.7±3.2) which was significantly (statistically) greater than the number measured in control (59±8.9) and 100 μg/ml mTG treated collagen gels (68±6.1). Also, angiogenic sprouts invaded deeper in collagen gels stiffened with 500 μg/ml mTG (266.4±94.2 μm) than controls (173.2±66.5 μm) as shown in Figure 3-6C. However, collagen gel stiffness did not appear to affect diameters of the formed lumens. There was no significant difference between lumen diameters formed in control (20.4±12.1 μm) and 500 μg/ml mTG treated collagen gels (24.5±14.4 μm) as shown in Figure 3-6D.

Lumenogenesis in Stiffer Matrices Resulted in More Collagen Matrix Remodeling

We have previously shown that NLOM is capable of observing and quantifying EC-ECM interactions noninvasively without using stains or dyes [407]. In our previous study, we observed collagen remodeling as a result of lumenogenesis and higher perilumenal collagen density than of the surrounding collagen matrix. This perilumenal collagen density was quantified as collagen intensity ratio (CIR) and varied proportionally with lumen size. CIR was calculated by normalizing perilumenal collagen SHG intensity by that of the surrounding collagen matrix. Thus, CIR may be used as a

measure of local collagen density (as a multiplicative factor of the surrounding matrix density) assuming no changes in collagen fiber diameters. In this study, we measured CIR as a function of matrix stiffness and used recently integrated OCM [408] to validate local measures of collagen density.

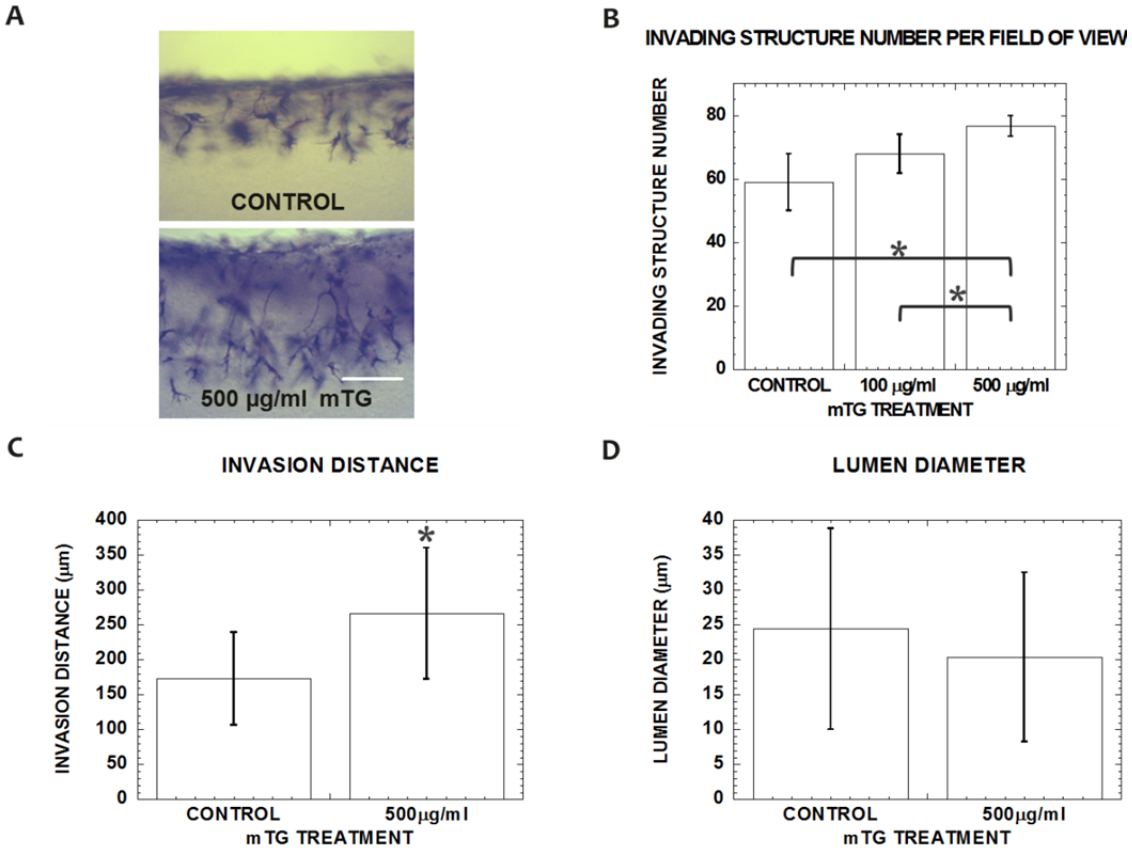

Figure 3- 6. Stiffer matrix promotes angiogenic invasion with more structures invading deeper into collagen gel. Cross-sectional images of control and 500 µg/ml mTG-treated cultures stained with toluidine blue at 48 hours (A). Scale bar is 250 µm. Quantification of invading structure number (B), invasion distance (C), and lumen diameter (D) in control and 500 µg/ml mTG-treated collagen gels at 48 hours. Symbol * represents $p<0.05$.

Angiogenic 3D cultures were imaged with NLOM-OCM after 72 hours. Representative SHG, TPF, and OCM images were shown in Figure 3-7 of lumen cross

section formed within control and 100 and 500 μg/ml mTG treated collagen gels. SHG was used to specifically image collagen and its spatial distribution around a lumen forming sprout. TPF was used to specifically image green fluorescent protein expressing ECs lining the formed lumen. In contrast, OCM was non-specific and derives contrast from both ECs and collagen matrix.

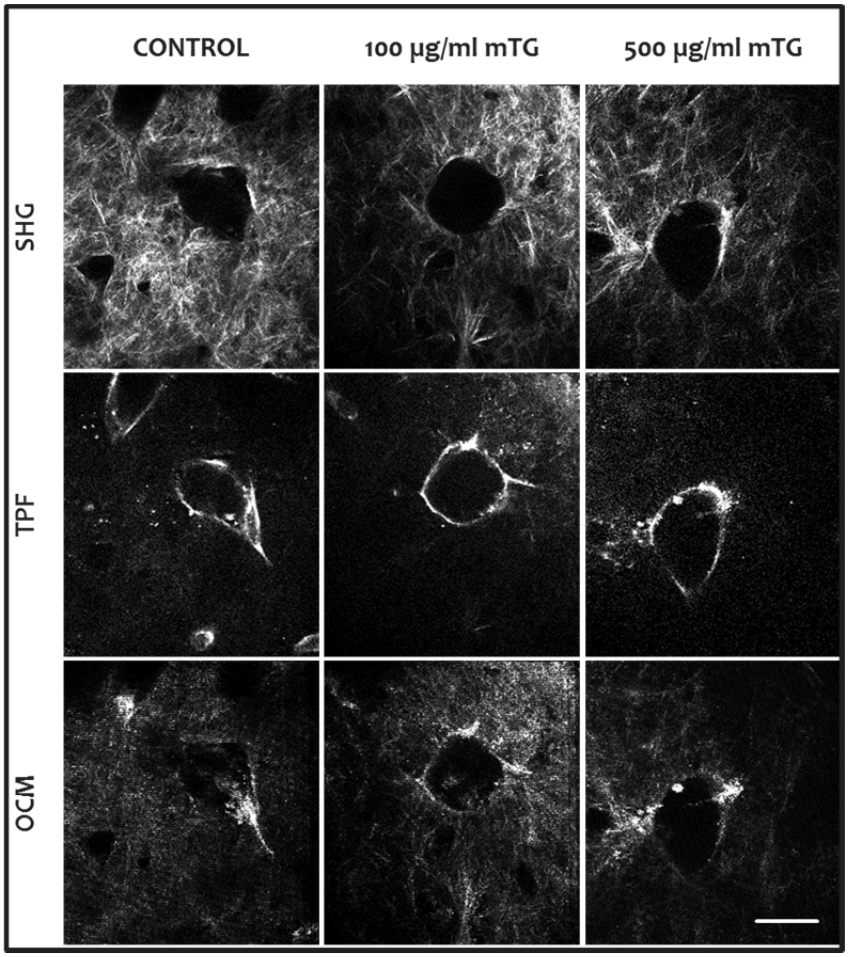

Figure 3- 7. Representative images of simultaneously acquired collagen SHG, cellular TPF, and non-specific OCM from within control and mTG-treated 3D cultures. Cultures were fixed at 72 hours. Scale bar is 50 μm.

When visualized with NLOM-OCM en face images, lumen areas may be measured in contrast to lumen diameters when using transverse sections of 3D cultures (as in Figure 3-6). Consistent with lumen diameters quantified with transverse sections, no significant difference in lumen area was measured in mTG treated collagen matrices (5414.5±500.9 and 5752.2±404.8 μm^2 in 100 and 500 μg/ml mTG, respectively) compared with controls (5872.2±651.0 μm^2) as shown in Figure 3-8A. However, the amount of collagen remodeling as quantified by CIR around lumens was higher in stiffer matrices. CIR around lumens formed in 500 μg/ml mTG treated collagen gels measured 2.2±0.1 times higher density than surrounding matrix compared with 1.9±0.1 and 1.8±0.1 for control and 100 μg/ml mTG treated gels, respectively (see Figure 3-8B). Furthermore, if we normalized each CIR measurement to lumen area, matrix remodeling (as measured by CIR/lumen area) during lumenogenesis increased in stiffer matrices (Figure 3-8C).

Finally, we validated SHG measures of CIR with OCM. A complicating factor when quantifying collagen density with SHG is that its intensity has a quadratic relationship with pathlength. In other words, SHG will vary quadratically with path length in nonlinear medium, in this case, the collagen fiber. OCM contrast, however, depends on backscattered light. Thus, using the same image regions we calculate CIR with simultaneously acquired SHG and OCM and plot their correlation in Figure 3-8D. A dotted line is shown for exact correspondence, i.e., CIR(SHG) = CIR(OCM). The correlative plot measured a correlation coefficient R = 0.8247.

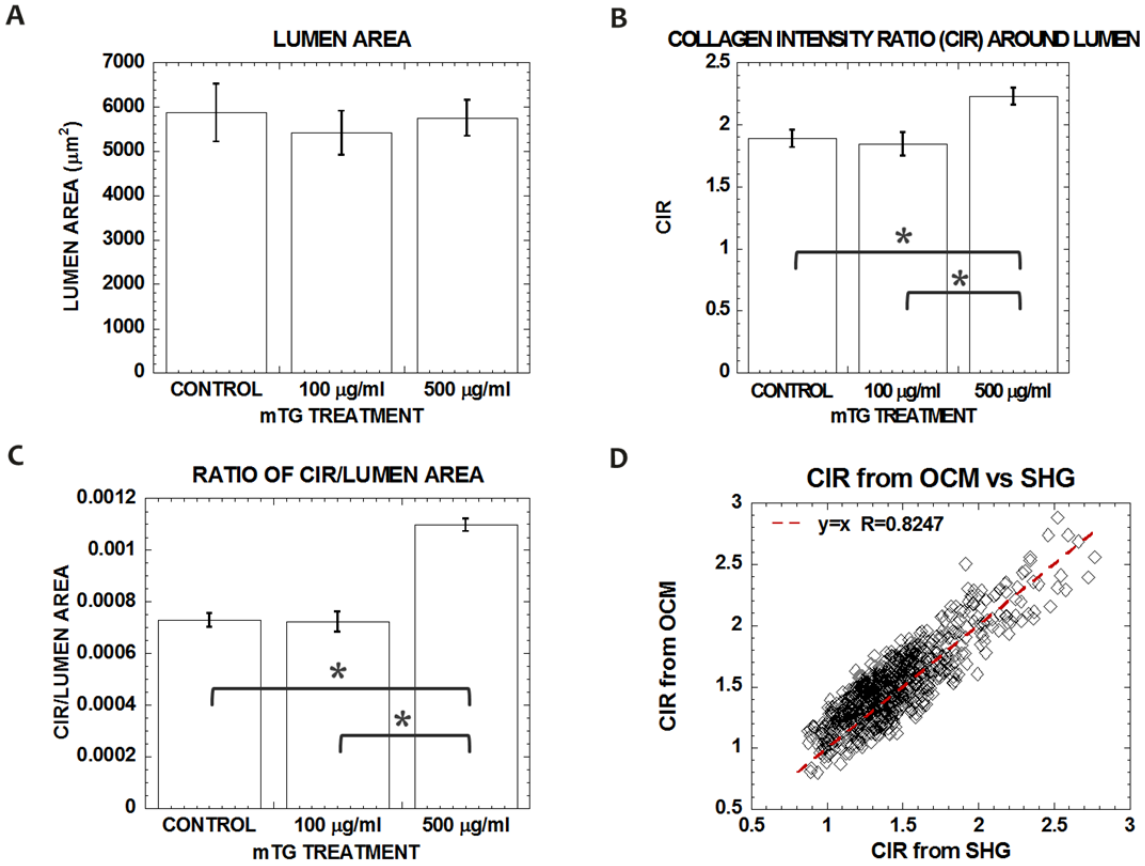

Figure 3- 8. Greater matrix remodeling is observed during lumenogenesis in stiffer matrices. Bar graph of lumen area (A), luminal collagen intensity ratio (CIR) (B), and CIR normalized by lumen area in control and mTG-treated cultures (C). Correlative plot of OCM and SHG derived CIR showing correspondence between linear and nonlinear signals (D). Error bars represent mean +/- SE. Sampling number n=35, 25, 50 in (A-B) and n=304, 218, 503 in (C) for control, 100 μg/ml mTG and 500 μg/ml mTG respectively. Symbol ***** represents $p<0.05$.

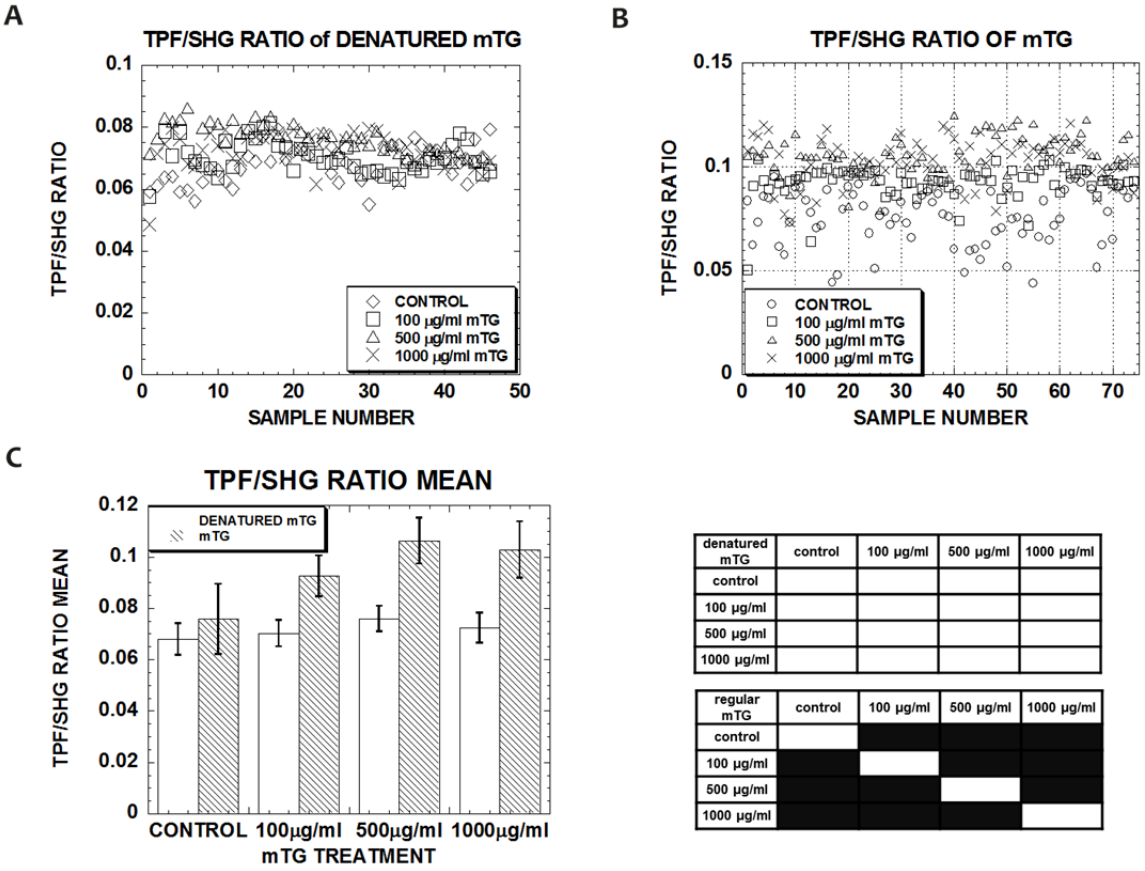

Figure-3- 9. Scatter plot of TPF/SHG ratio from 45 images in acellular regular mTG and denatured mTG-treated collagen gels (A). Scatter plot of TPF/SHG ratio from 75 images in acellular regular mTG-treated collagen gels (B). Bar graph of mean SHG/TPF ratio in regular mTG-treated and denatured mTG-treated acellular collagen gels (C). In statistics table, region highlighted with black color represents for significant difference with $p<0.05$. Error bars stand for mean+/- STD.

Discussion

Here, we evaluated biochemical state of mTG-treated collagen with SHG and TPF signals from NLOM, validated the effectiveness of mTG in enhance collagen stiffness, correlated optical property with mechanical property and characterized the microstructure. mTG induced the change in optical properties since denatured mTG showed no effect in changing TPF/SHG ratio at all (Figure 3-9). Among topographical properties in microstructure, we also characterized spectroscopically whether mTG treatment resulted in changes in collagen fiber diameters (explain this procedure. It's not trivial). The corresponding scatter graphs of quantification results of porosity, pore size, pore numbers per field of view were shown in ECM (Figure 3-10). The intrinsic properties of linearity and nonlinearity from OCM and SHG could be used to identify if matrix fiber thickness changed with mTG treatment. The representative SHG, OCM images of acellular matrices for each condition were shown in Figure 3-11A. In the result of fiber thickness quantification, the OCM/SHG ratios were 2.446±0.331, 2.485±0.229 and 2.412±0.242 for control, 100 μg/ml mTG and 500 μg/ml mTG respectively (Figure 3-11C) with no significant difference between conditions. Therefore, cross-linking with mTG stiffened collagen matrices with evidence of optical and mechanical properties while remaining their topographical properties unchanged.

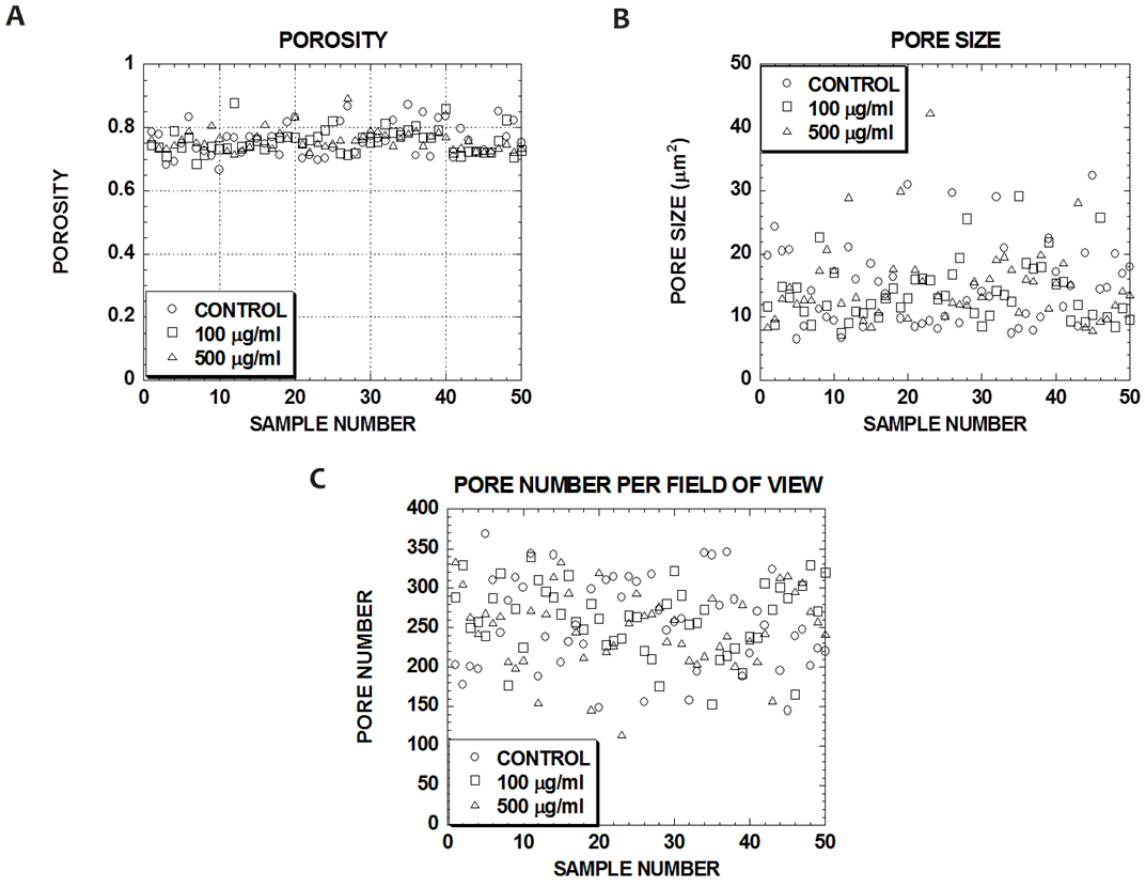

Figure-3- 10. Scatter plots of porosity (A), pore size (B) and pore number (C) in acellular collagen ECM in control and mTG-treated collagen gels. Sample number n=50.

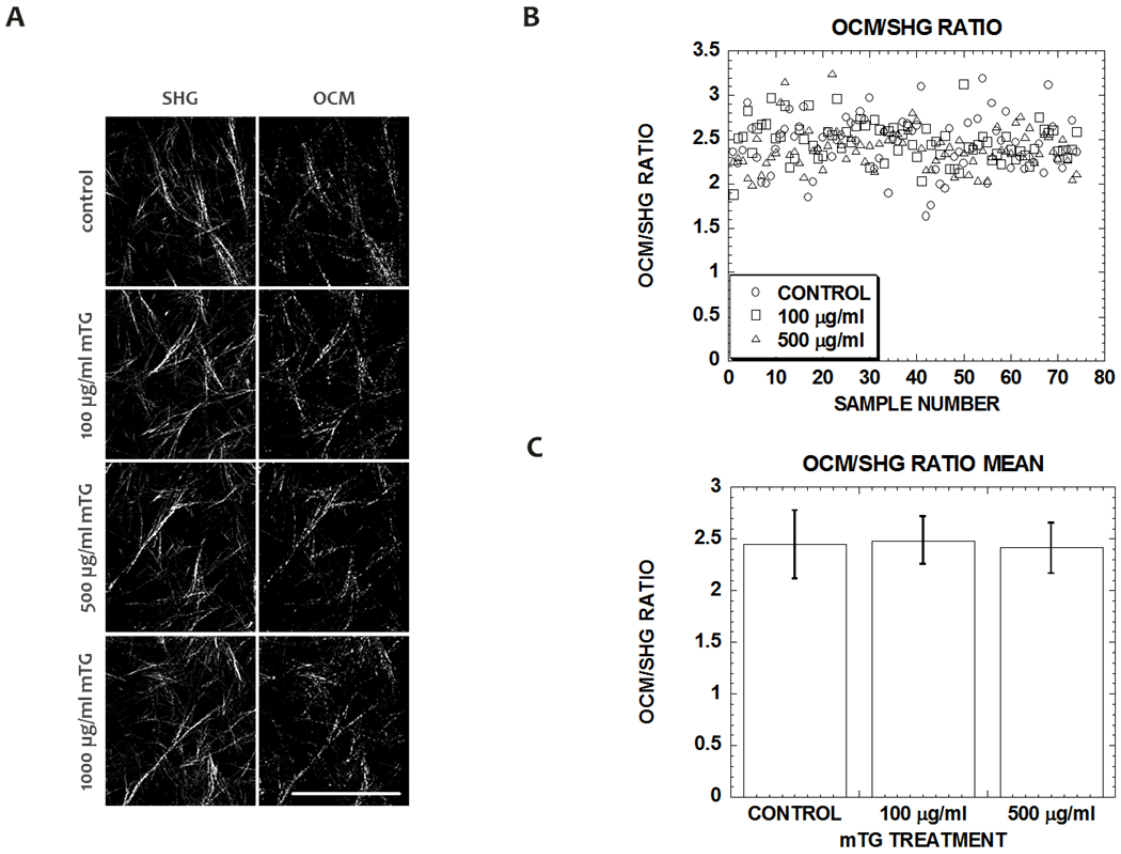

Figure-3- 11. Representative SHG and OCM images of acellular control and mTG-treated collagen gels (A). Scatter plot of OCM/SHG ratio from 75 images in acellular control and mTG-treated collagen gels (B). Bar graph of mean OCM/SHG ratio in acellular control and mTG-treated collagen gels (C). Error bars stands for mean +/- STD.

There are various groups report optical properties of type I collagen [166, 229, 233] or crosslinked type I collagen [165, 230-232] with NLOM. The fluorescence emission spectrum and fluorescence maxima of collagen [229] or collagen treated with crosslinker [231] is excitation wavelength dependent and is crosslinker/crosslinker concentration dependent [231, 232] for cosslinked collagen. Our result showed similar trend that TPF (but not SHG) increase with mTG dose and same trend is also shown in TPF/SHG ratio (Figure 3-2B). For collagen or crosslinker-treated collagen, the fluorescence intensity of

collagen increases with incubation time [229, 231, 232]. After collagen polymerization, Pyridinium-type crosslink (pyridinoline) will produce fluorescence have been proven experimentally [411-413] but whether mTG induced fluorescence in the same manner still needs to be addressed. SHG of collagen, the reflectance of the microstructure morphology, will not change with incubation time [229] but SHG of crosslinked collagen might change with time, which depends on crosslinker. For example, SHG of glycated crosslinked collagen [232] increased with incubation time but not SHG of genipin crosslinked collagen [231]. In our result, SHG showed little variance with time from Day 1, Day 2 to Day 7 but TPF signal increased with incubation time (data not shown) as evidenced with Figure 3-2A and that corresponds to another result that TPF/SHG ratio increased with incubation time Figure 3-2B.

Raub et al. [165] showed that TPF signal of collagen increased with glutaraldehyde treatment but not SHG signal and glutaraldehyde also enhanced collagen storage modulus from rheology measurement. Compared with glutaraldehyde, mTG crosslinked collagen enzymatically, not chemically and nontoxic at all. Here, mTG also enhanced collagen stiffness and increased TPF signal and TPF/SHG ratio but not SHG dependent on dose and incubation time (Figure 3-1 and 3-2). Compared with other group correlates mechanical property with TPF alone [165], our result showed TPF/SHG ($r=0.91$, Figure 3-3C) linearly correlates with acellular scaffold stiffness better than SHG ($r=0.36$, Figure 3-3A) or TPF ($r=0.66$, Figure 3-3B).

Collagen microstructures could be modulated with pH, temperature and concentration during collagen entropy-driven self-assembly fibrillogenesis processes

[159, 172, 203] and have been characterized using confocal [201, 202] or nonlinear optical microscopy [165, 166, 230, 233]. Increasing pH decreases fiber diameter and pore size but increases pore density and finally results in increasing storage modulus [166]. Increasing temperature decreases fiber diameter and pore size and results in increasing storage modulus [165]. With confocal microscopy, Yang et al. [201, 202] showed that increasing collagen concentration decreases fiber diameter, fiber length and pore size but increases fiber number and finally results in increasing storage modulus. Here, we investigated mTG influence on collagen microstructure and we noticed that there is no change with porosity, pore size and pore number per field of view (Figure 3-5 and Figure 3-10). The pore size average value in our study using MATLAB algorithm was around 14 μm^2 for 3.5 mg/ml, which was comparable with Yang's study (mesh size around 4 μm for 3.5 mg/ml) [201] or Raub's study (10 μm^2 for 4 mg/ml) [166] and they both used particle feature of image J for the pore size quantification. Instead of directly measuring fiber diameter from SHG images, we took advantage of properties difference (nonlinear vs. linear) of SHG and OCM and used OCM/SHG ratio to evaluate influence of mTG on fiber thickness variation. Our result showed that OCM/SHG ratio doesn't change with mTG dose with value =2.4 but that ratio will change with collagen concentration (data not shown) which agrees with other studies [201, 202, 233].

Researchers tried to address how ECM stiffness or compliance influences angiogenesis and most of them modulated ECM stiffness via changing ECM protein concentration, such as collagen [162, 271] or fibrin [136-138, 273], and concluded angiogenesis prefers compliant ECM. However, varying densities would change ligand

densities, mechanical properties and topographical properties at the same time [201, 202, 233]. Study done by Critser et al. [162] revealed that via controlling matrix concentration, there were more cord like network formation in stiffer gel (3.5 mg/ml) compared with compliant gel (0.5 mg/ml) but after *in vivo* subcutaneous implantation, significant increased vessel sizes occurred in stiffer matrix (3.5 mg/ml) after 14 days of transplantation. Yamamura et al. [133] modulated pH to vary collagen gel stiffness and concluded that thicker and deeper capillary networks were formed in rigid gel other than compliant gel. Even though changing pH will also change collagen microstructure [166] but the extent of microstructure changing was less than varying collagen concentration [166, 174] with remaining ligand densities. mTG enhanced ECM stiffness (Figure 3-1) without changing topographical properties (Figure 3-4 & 3-5 and Figure 3-10 & 3-11) and our 3D angiogenesis assay showed that in 3.5 mg/ml collagen gel, more capillary structures formation in stiffer ECM with deeper invasion distance but no difference in lumen diameter (Figure 3-6). Even though mTG crosslinked collagen gel has been extensively washed with M199, the possibility of residue mTG influencing EC invasion behavior cannot be ruled out. We setup another control experiment via adding mTG into media after HUVEC monolayer formation, therefore the underneath collagen stiffness would be the same and the result revealed less invasion structures and shorter invasion distance in topical mTG well compared with control (Figure 3-12 & Figure 3-13). The retardation of EC invasion in topical mTG well might owe to mTG's ability to crosslink cell junctions [414].

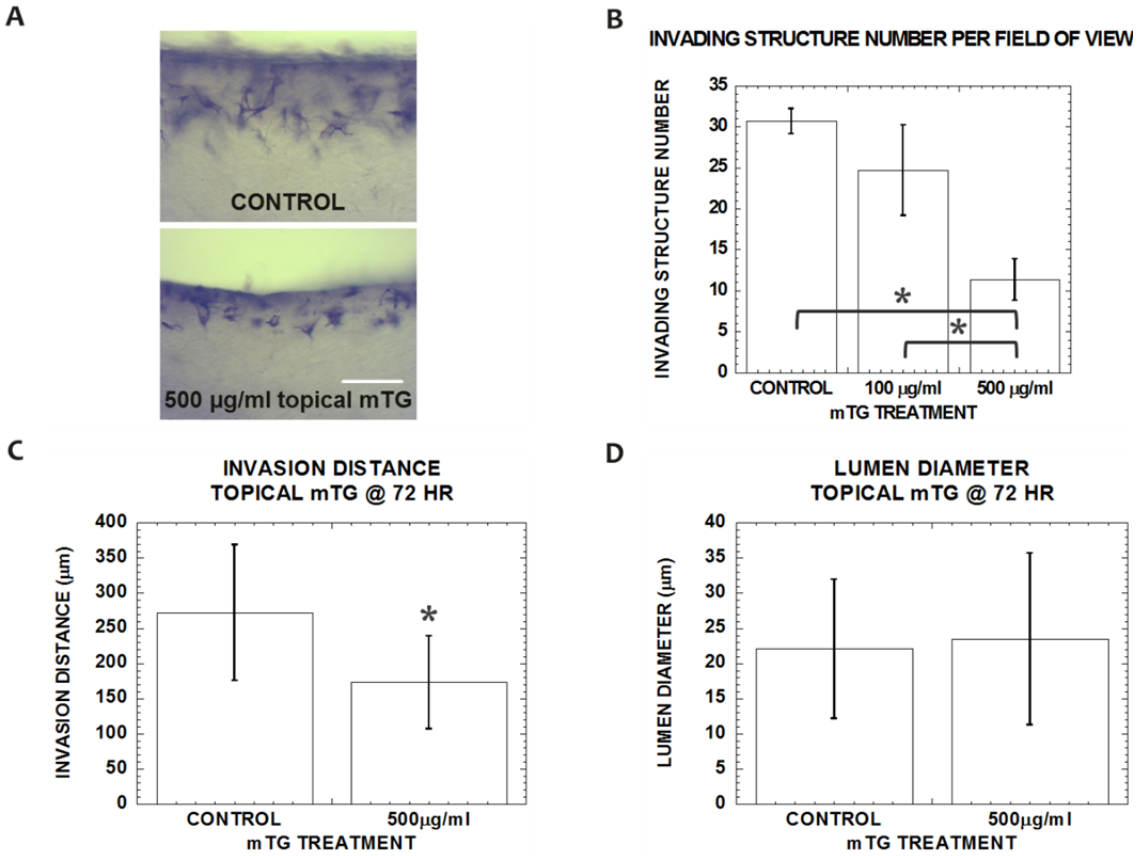

Figure-3- 12. Cross-sectional images of sectioned cultures stained with toluidine blue in control and cultures with topically applied mTG in media above monolayer at 72 hour (A). Scale bar is 250 µm. Invading structure number (B), invasion distance (C) and lumen diameter (D) in control and cultures with topically applied mTG in media above monolayer. Sample number n=4 gels in (A) and n=127, 111 in (C) and n=57, 44 in (D) for control and 500 µg/ml mTG-treated gels respectively. Symbol ***** represents $p<0.05$.

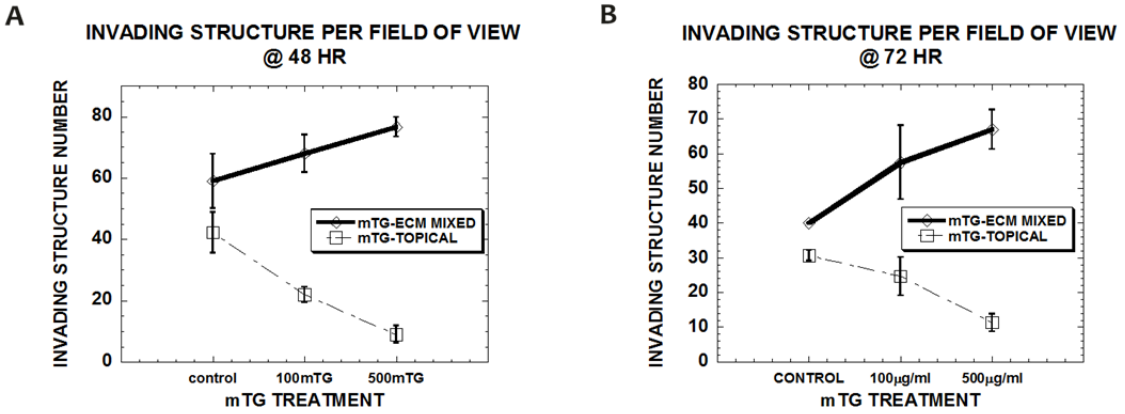

MIXED	control	100 µg/ml	500 µg/ml
control			
100 µg/ml			
500 µg/ml			

TOPICAL	control	100 µg/ml	500 µg/ml
control			
100 µg/ml			
500 µg/ml			

MIXED	control	100 µg/ml	500 µg/ml
control			
100 µg/ml			
500 µg/ml			

TOPICAL	control	100 µg/ml	500 µg/ml
control			
100 µg/ml			
500 µg/ml			

Figure-3- 13. Number of invading angiogenic invading structure number is enhanced in mTG-treated collagen ECM but is suppressed in 3D cultures with topically applied mTG in media above monolayer. Invading structure number at 48 hours (A) and 72 hours (B) in control, mTG-treated collagen and topically applied 3D cultures. In statistics table, region highlighted with black color represents for significant difference with $p<0.05$.

Lumen expansion during angiogenesis required synergistic of cell traction and membrane-associated metalloproteinase and cell-matrices interaction during lumenogenesis could be observed with NLOM as evidence of collagen intensity ratio (CIR) increasing with lumen expansion [407]. With NLOM, we observed that CIR increased with increasing stiffness (Figure 3-7 & 3-8) with CIR=1.88±0.06 for control and 2.23±0.06 for 500 µg/ml but average lumen size didn't change (5872.2±650.9 μm^2 for control and 5752.1±404.8 μm^2 for 500 µg/ml). To rule out lumen size effect, the normalized CIR still showed the same trend, i.e. higher normalized CIR in stiffer matrices than control. With NLOM-OCM combined system, we further concluded that

higher collagen density around the lumen in stiff matrices (Figure 3-8D). The amount of cell traction and the size of focal adhesion depend on resistance (stiffness) of ECM [275] and cell traction is necessary for focal adhesion growth and maintenance [297-302, 415] and cell-cell adherens junctions mediation [298, 320]. Cell-ECM traction modulates the tension in cell-cell contact [322] and the size of cell-cell junctions [321]. Cell mobility could be regulated by the crosstalk between cell-cell junction and integrin adhesions [416]. The higher CIR value in stiffer matrices implies higher traction generated by ECs and that higher traction might be necessary to maintain vessel integrity and control vessel permeability [105].

In conclusion, we were the first to report optical properties of mTG treated collagen, correlated optical properties with mechanical properties measuring with biaxial bioreactor and successfully decoupled matrix stiffness with concentration for angiogenesis response investigation. Our result revealed matrix stiffness promotes angiogenesis in 3.5 mg/ml collagen concentration.

CHAPTER IV

CONCLUSION AND FUTURE WORK

Conclusion

The interactions between endothelial cells (ECs) and the extracellular matrix (ECM) are fundamental in mediating various steps of angiogenesis. Here, EC-ECM interactions have been characterized using a noninvasive and non-destructive nonlinear optical microscopy (NLOM) technique to optically image endothelial sprouting morphogenesis in 3D collagen matrices using second harmonic generation (SHG) and two-photon excited fluorescence (TPF), respectively. Lumenogenesis associated with increasing collagen density around its periphery is the synergistic result of membrane-associated matrix metalloproteinase activity and the generation of cell tension, as evidenced with proteinase inhibition and Rho-associated kinase (p160ROCK) inhibition studies. Collagen microstructure plays a pivotal role in regulating angiogenesis and also determines its mechanical stiffness. With a combined NLOM-OCM system, probing microstructure, optical and mechanical properties noninvasively is feasible. A linear relationship between optical properties (TPF/SHG) and mechanical properties could enable us to probe local mechanical properties of tissues noninvasively; However, this area of study will need further investigation, such as incorporating other topographical

properties to predict ECM stiffness. We successfully decoupled ECM stiffness from ligand concentration by applying mTG to strengthen collagen scaffold stiffness and were able to demonstrate that increasing ECM stiffness enhanced angiogenic responses *in vitro*. The result of mTG modulated collagen stiffness while maintaining its topographical properties might aid the tissue engineering and regenerative medicine fields. For example, generating a collagen scaffold with gradient stiffness using mTG would allow testing whether durataxis regulates the speed of wound healing and cell migration in three-dimensional matrices. The results from the mTG topical control experiment were also encouraging; mTG successfully retarded EC migration, which may be important for cancer research. Further investigation into presentation of altered matrix stiffness and how it affects EC migration in three dimensions is needed.

Future Work

Together the work presented here studies endothelial cell interactions with the extracellular matrix in angiogenesis. The data show the effectiveness of mTG in enhancing collagen scaffold stiffness and the powerful ability of NLOM-OCM combined system in probing optical, mechanical and topographical properties noninvasively. With these abilities, we could further investigate cell-matrix interactions in a wound healing model, the influence of collagen microstructure on angiogenesis, and

the effects of altering the stiffness gradient on angiogenic patterning. Future works include:

1. Cell/Matrix Interactions during Angiogenesis in Fibrin and Fibrin/Collagen Mixture

2. Influence of Collagen Microstructure on Angiogenesis

3. Influence of Stiffness Gradient on Angiogenesis

Cell/Matrix Interactions during Angiogenesis in Fibrin and Fibrin/Collagen Mixture

Motivation

Wound healing, an integration of dynamic interactive processes, consists of four overlapping stages: hemostasis, inflammation, proliferation (re-epithelialization and granulation tissue formation), and tissue remodeling [417, 418]. Wound healing is an integration of dynamic interactive processes involving soluble mediators [417, 419], formed blood elements, ECM [420], and parenchymal cells [421]. Successful hemostasis is dependent on fibrin clot formation, platelet adhesion, and aggregation [421]. Granulation tissue forms via combination of fibroplasia and neovascularization and consists of neovessels, macrophages, fibroblasts, and loose connective tissue. Once the wound is filled with granulation tissue and covered with neoepidermis, fibroblasts transform into myofibroblasts, which contract the wound [420]. ECM remodeling, cell maturation, and cell apoptosis create the third phase of wound repair, which overlaps

with tissue formation. The dynamic reciprocity of complex interaction and feedback control of cells-cytokines-enzyme-matrix control the dynamics of provisional matrix in wound healing and transition from an initial fibrin-fibronectin-rich ECM, to an intermediate fibrin-collagen mixture, and in the end a collagen rich scar tissue [420]. Angiogenic capillaries begin to invade fibrin rich clots, organize into capillary networks, and diminish gradually with collagen accumulation as the granulation tissues produce collagen-rich scar tissue [422]. The spatial and temporal dynamic cell-matrix interactions of angiogenesis in heterogeneous ECM proteins are still unclear, which makes the possibility of studying heterologous matrices compelling.

Preliminary result or method

In Figure 4-1 showed the preliminary result of using NLOM-OCM combined system in imaging 3D acellular fibrin/collagen mixture while protein concentration (4 mg/ml) was kept constant. Figure 4-1 also highlights the capability of OCM in capturing fibrin microstructure non-invasively. Fibrin microstructure is clearly modulated by thrombin concentration (0.01 U/mg created more fibrous fibrin microstructure, especially at fibrin/collagen ratio of 90:10 and 80:20). Therefore, noninvasively characterizing cell-matrix interactions spatially and temporally during angiogenesis in fibrin or fibrin/collagen mixture is feasible with our NLOM-OCM combined system. Similar to collagen, fibrin microstructure are also influenced by various factors [423-425], such as fibrinogen concentration, thrombin concentration, calcium concentration and ionic strength.

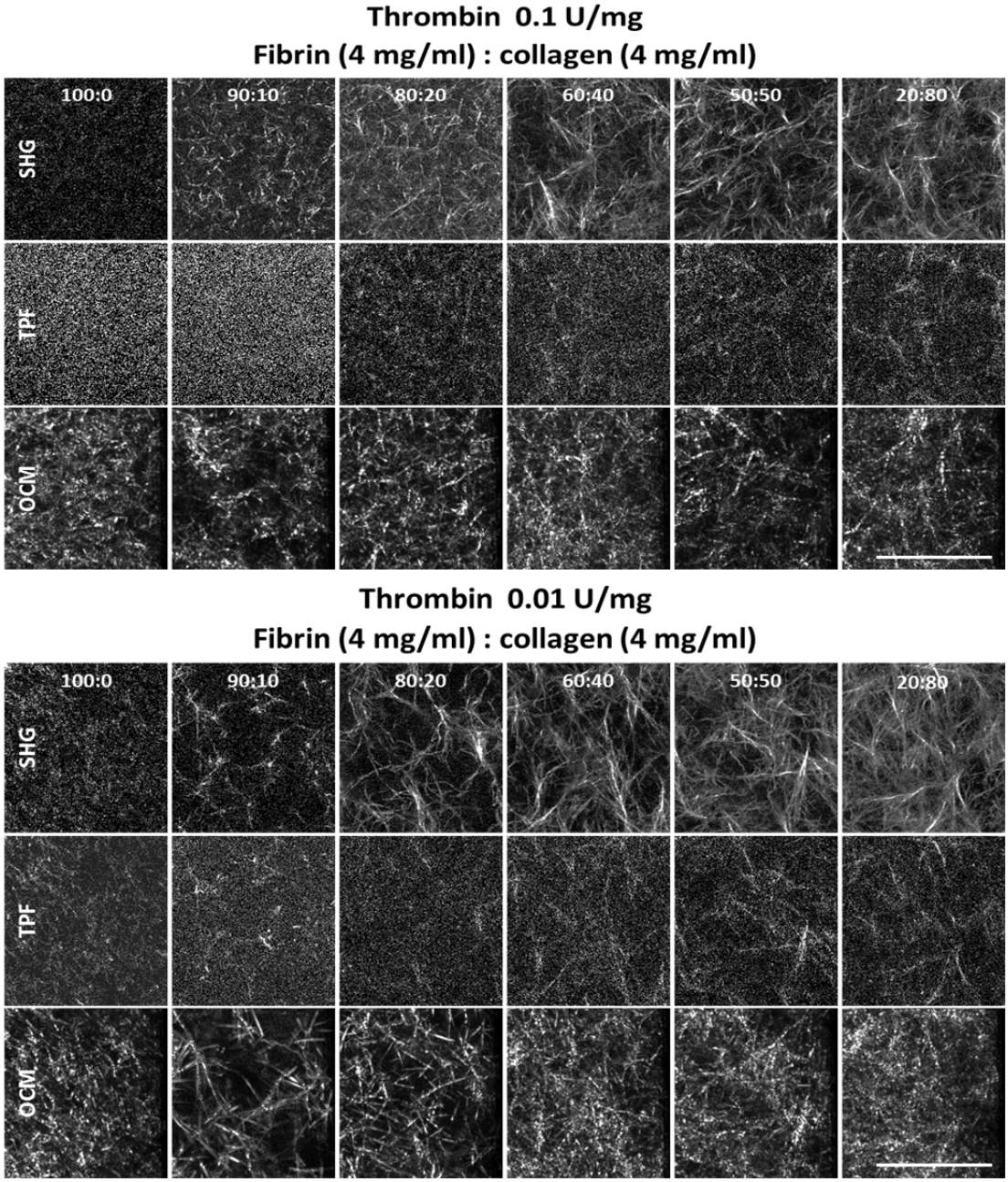

Figure 4- 1. Using NLOM-OCM combined system to image acellular fibrin and fibrin/collagen mixture 3D matrices modulated by thrombin concentration. Scale bar=50 μm

Influence of Collagen Microstructure on Angiogenesis

Motivation

Whether ECM stiffness or microstructure or both of them plays a pivotal in angiogenesis has been debated for a while. Our results revealed that collagen stiffness tuned by mTG enhanced more cell-matrix interaction, induced deeper capillary structure invasion but had no influence on lumen size (see Chapter III). So will ECM microstructure influence lumen size during angiogenesis? In order to address that question, we have to modulate ECM microstructure while keeping stiffness constant.

Preliminary result or method

In chapter I, our review of previous works revealed collagen microstructure could be tuned with concentration, pH, temperature and ionic strength during fibrillogenesis. In chapter III, we showed that mTG could modulate collagen ECM stiffness with mTG dose and incubation time. Therefore, study of microstructure influence on angiogenesis could be performed with using gels with same stiffness but different collagen density. In preliminary study (Figure 4-2), we modulated collagen microstructure via collagen concentration (1, 2.5 and 3.5 mg/ml), and treated with mTG of different dose and incubation time, and evaluated mechanical properties. We noticed that we could get the same mechanical response in two groups (listed in Table 4-1). Therefore, it's feasible to study microstructure influence on angiogenesis. Also, intense TPF images correspond to the groups with longer incubation time (Figure 4-2B). mTG can crosslink fibrin [426], gelatin [427, 428], collagen [188, 429-432] and matrigel [433] but no report about heterogeneous ECM protein crosslinking with mTG. If we could crosslink fibrin in our

3D model and even crosslink collagen/fibrin mixture, we could push this study further into how heterogeneous microstructure influence on angiogenesis.

Table 4- 1. Groups with same mechanical testing result from gels with different concentration, mTG dose treatment and incubation.

group	concentration	mTG dose	Incubation time
1	1 mg/ml	500 μg/ml	7 days
	3.5 mg/ml	0 μg/ml	2 days
2	2.5 mg/ml	500 μg/ml	7 days
	3.5 mg/ml	400 μg/ml	2 days

Influence of Stiffness Gradient on Angiogenesis

Motivation

During tissue development, inflammation and wound healing, cells experience gradients of physical and chemical cues, which influence their migration, proliferation and differentiation [434]. ECM with gradient properties can connect mechanically mismatched tissues [435, 436]. Interface tissue engineering (ITE), the new emerging field in regenerative medicine, aims to generate functional biological tissue to repair or replace the diseased or damaged tissue at interfaces of different tissue types. It is potentially important for controlled angiogenesis for implantation of tissue-engineered devices and will provide new ideas to vascular remodeling and angiogenesis [437-440]. Human body's interface tissues consist of complex structures and gradient physical properties which cannot be regenerated using conventional isotropic or monophasic scaffolds [440]. Gradient biomaterials are materials with anisotropy in composition, structure, mechanics and biomolecular level. Gradients in biology include chemical and

physical gradients. Chemical gradients [441] include gradients of morphogens, such as transcription factors [442, 443], chemokines [444], and cytokines [445-448]. Physical gradients include gradual changes in physical properties, such as stiffness [113, 449, 450], porosity, pore size [450-452] and other topographical properties. The challenge in ITE is to vascularize interface tissue and improve the efficiency of 3D cell culture. Gradient materials influence cell behaviors, such as cell migration [453], osteoblast differentiation [442] etc., but how gradients influence angiogenesis and cell-matrix interactions still need further investigation.

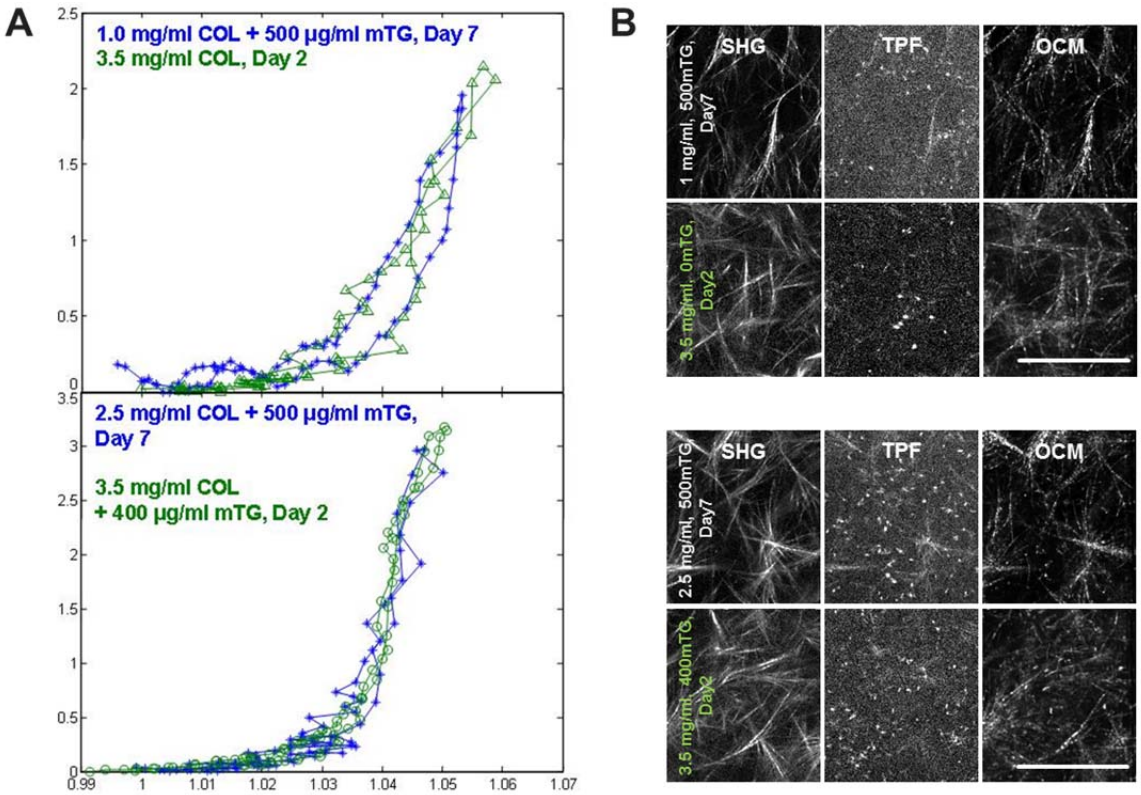

Figure 4- 2. Mechanical characterizing results by biaxial bioreactor in collagen with different concentration, different mTG dose treatment and different incubation time. (A) mechanical characterization results. (B) microstructural characterization with NLOM-OCM combined system. COL: collagen, mTG: microbial transglutaminase, scale bar =50 µm

Preliminary result or method

Collagen has been applied in ITE in creating multiphase [454] and gradient tissues [455]. We showed our capability to noninvasively investigate cell-matrix interactions during angiogenesis (chapter II), enhance collagen matrix stiffness with mTG while keeping microstructural properties constant and probe stiffness of collagen scaffold noninvasively (chapter III). Therefore, it's feasible for us to create either two-phase or gradient scaffolds to study stiffness influence on angiogenesis without transition region (two-phase) or with transition region while keeping microstructural properties and ligand density unchanged. To create biphasic collagen scaffold, we could adapt the method from Gillette et al. [454] to polymerize one layer over the other at different times. To create gradient stiffness matrices, we could adapt the method of diffusion [434, 437, 456-458] which employed molecular diffusion between two chemical sources in two sinks at 37 ºC. Another possible method was proposed by Nam et al. [455] which create 3D collagen with stiffness gradient through dialysis at 4 ºC for 48 hours.

REFERENCES

1. Folkman, J., *Angiogenesis and angiogenesis inhibition: an overview.* EXS, 1997. **79**: p. 1-8.
2. Griffioen, A.W. and G. Molema, *Angiogenesis: potentials for pharmacologic intervention in the treatment of cancer, cardiovascular diseases, and chronic inflammation.* Pharmacol Rev, 2000. **52**(2): p. 237-68.
3. Papetti, M. and I.M. Herman, *Mechanisms of normal and tumor-derived angiogenesis.* Am J Physiol Cell Physiol, 2002. **282**(5): p. C947-70.
4. Carmeliet, P., *Manipulating angiogenesis in medicine.* J Intern Med, 2004. **255**(5): p. 538-61.
5. Langer, R. and J.P. Vacanti, *Tissue engineering.* Science, 1993. **260**(5110): p. 920-926.
6. Cassell, O.C., et al., *Vascularisation of tissue-engineered grafts: the regulation of angiogenesis in reconstructive surgery and in disease states.* Br J Plast Surg, 2002. **55**(8): p. 603-10.
7. Eiselt, P., et al., *Development of technologies aiding large-tissue engineering.* Biotechnol Prog, 1998. **14**(1): p. 134-40.
8. Nomi, M., et al., *Principals of neovascularization for tissue engineering.* Mol Aspects Med, 2002. **23**(6): p. 463-83.
9. Secomb, T.W. and A.R. Pries, *Information transfer in microvascular networks.* Microcirculation, 2002. **9**(5): p. 377-87.

10. Frerich, B., et al., *In vitro model of a vascular stroma for the engineering of vascularized tissues.* Int J Oral Maxillofac Surg, 2001. **30**(5): p. 414-20.

11. Okano, T. and T. Matsuda, *Muscular tissue engineering: capillary-incorporated hybrid muscular tissues in vivo tissue culture.* Cell Transplant, 1998. **7**(5): p. 435-42.

12. Sheridan, M.H., et al., *Bioabsorbable polymer scaffolds for tissue engineering capable of sustained growth factor delivery.* J Control Release, 2000. **64**(1-3): p. 91-102.

13. Ko, H.C., B.K. Milthorpe, and C.D. McFarland, *Engineering thick tissues--the vascularisation problem.* Eur Cell Mater, 2007. **14**: p. 1-18; discussion 18-9.

14. Downs, K.M., *Florence Sabin and the mechanism of blood vessel lumenization during vasculogenesis.* Microcirculation, 2003. **10**(1): p. 5-25.

15. Egginton, S. and M. Gerritsen, *Lumen formation - In vivo versus in vitro observations.* Microcirculation, 2003. **10**(1): p. 45-61.

16. Jain, R.K., et al., *Quantitative angiogenesis assays: progress and problems.* Nat Med, 1997. **3**(11): p. 1203-8.

17. Norrby, K., *Angiogenesis: new aspects relating to its initiation and control.* APMIS, 1997. **105**(6): p. 417-37.

18. Norrby, K., *In vivo models of angiogenesis.* J Cell Mol Med, 2006. **10**(3): p. 588-612.

19. Vailhe, B., D. Vittet, and J.J. Feige, *In vitro models of vasculogenesis and angiogenesis.* Lab Invest, 2001. **81**(4): p. 439-52.

20. Korff, T. and H.G. Augustin, *Tensional forces in fibrillar extracellular matrices control directional capillary sprouting.* J Cell Sci, 1999. **112 (Pt 19)**: p. 3249-58.

21. Egginton, S., et al., *Unorthodox angiogenesis in skeletal muscle.* Cardiovasc Res, 2001. **49**(3): p. 634-46.

22. Rivilis, I., et al., *Differential involvement of MMP-2 and VEGF during muscle stretch- versus shear stress-induced angiogenesis.* Am J Physiol Heart Circ Physiol, 2002. **283**(4): p. H1430-8.

23. Haas, T.L., et al., *Matrix metalloproteinase activity is required for activity-induced angiogenesis in rat skeletal muscle.* Am J Physiol Heart Circ Physiol, 2000. **279**(4): p. H1540-7.

24. Shiu, Y.T., et al., *Rho mediates the shear-enhancement of endothelial cell migration and traction force generation.* Biophys J, 2004. **86**(4): p. 2558-65.

25. Ueda, A., et al., *Effect of shear stress on microvessel network formation of endothelial cells with in vitro three-dimensional model.* Am J Physiol Heart Circ Physiol, 2004. **287**(3): p. H994-1002.

26. Houck, K.A., et al., *Dual regulation of vascular endothelial growth factor bioavailability by genetic and proteolytic mechanisms.* J Biol Chem, 1992. **267**(36): p. 26031-7.

27. Robinson, C.J. and S.E. Stringer, *The splice variants of vascular endothelial growth factor (VEGF) and their receptors.* J Cell Sci, 2001. **114**(Pt 5): p. 853-65.

28. Dvorak, H.F., et al., *Vascular permeability factor/vascular endothelial growth factor, microvascular hyperpermeability, and angiogenesis.* Am J Pathol, 1995. **146**(5): p. 1029-39.

29. Roskoski, R., Jr., *VEGF receptor protein-tyrosine kinases: structure and regulation.* Biochem Biophys Res Commun, 2008. **375**(3): p. 287-91.

30. Olsson, A.K., et al., *VEGF receptor signalling - in control of vascular function.* Nat Rev Mol Cell Biol, 2006. **7**(5): p. 359-71.

31. Ferrara, N., H.P. Gerber, and J. LeCouter, *The biology of VEGF and its receptors.* Nat Med, 2003. **9**(6): p. 669-76.

32. Esser, S., et al., *Vascular endothelial growth factor induces VE-cadherin tyrosine phosphorylation in endothelial cells.* J Cell Sci, 1998. **111 (Pt 13)**: p. 1853-65.

33. Kevil, C.G., et al., *Vascular permeability factor/vascular endothelial cell growth factor-mediated permeability occurs through disorganization of endothelial junctional proteins.* J Biol Chem, 1998. **273**(24): p. 15099-103.

34. Gerber, H.P., et al., *Vascular endothelial growth factor regulates endothelial cell survival through the phosphatidylinositol 3'-kinase/Akt signal transduction pathway. Requirement for Flk-1/KDR activation.* J Biol Chem, 1998. **273**(46): p. 30336-43.

35. Connolly, D.T., et al., *Tumor vascular permeability factor stimulates endothelial cell growth and angiogenesis.* J Clin Invest, 1989. **84**(5): p. 1470-8.

36. Dimmeler, S., E. Dernbach, and A.M. Zeiher, *Phosphorylation of the endothelial nitric oxide synthase at ser-1177 is required for VEGF-induced endothelial cell migration.* FEBS Lett, 2000. **477**(3): p. 258-62.

37. Pepper, M.S., et al., *Vascular endothelial growth factor (VEGF) induces plasminogen activators and plasminogen activator inhibitor-1 in microvascular endothelial cells.* Biochem Biophys Res Commun, 1991. **181**(2): p. 902-6.

38. Ziche, M., et al., *Nitric oxide synthase lies downstream from vascular endothelial growth factor-induced but not basic fibroblast growth factor-induced angiogenesis.* J Clin Invest, 1997. **99**(11): p. 2625-34.

39. Takagi, H., et al., *Hypoxia regulates vascular endothelial growth factor receptor KDR/Flk gene expression through adenosine A2 receptors in retinal capillary endothelial cells.* Invest Ophthalmol Vis Sci, 1996. **37**(7): p. 1311-21.

40. Moscatelli, D., et al., *Both normal and tumor cells produce basic fibroblast growth factor.* J Cell Physiol, 1986. **129**(2): p. 273-6.

41. Presta, M., et al., *Purification from a human hepatoma cell line of a basic fibroblast growth factor-like molecule that stimulates capillary endothelial cell plasminogen activator production, DNA synthesis, and migration.* Mol Cell Biol, 1986. **6**(11): p. 4060-6.

42. Klein, S., M. Roghani, and D.B. Rifkin, *Fibroblast growth factors as angiogenesis factors: new insights into their mechanism of action.* EXS, 1997. **79**: p. 159-92.

43. Johnson, D.E. and L.T. Williams, *Structural and functional diversity in the FGF receptor multigene family.* Adv Cancer Res, 1993. **60**: p. 1-41.

44. Thomas, K.A., *Fibroblast growth factors.* FASEB J, 1987. **1**(6): p. 434-40.

45. Montesano, R., et al., *Basic fibroblast growth factor induces angiogenesis in vitro.* Proc Natl Acad Sci U S A, 1986. **83**(19): p. 7297-301.

46. Gospodarowicz, D., et al., *Structural characterization and biological functions of fibroblast growth factor.* Endocr Rev, 1987. **8**(2): p. 95-114.

47. Terranova, V.P., et al., *Human endothelial cells are chemotactic to endothelial cell growth factor and heparin.* J Cell Biol, 1985. **101**(6): p. 2330-4.

48. Mignatti, P., et al., *In vitro angiogenesis on the human amniotic membrane: requirement for basic fibroblast growth factor-induced proteinases.* J Cell Biol, 1989. **108**(2): p. 671-82.

49. Battegay, E.J., et al., *PDGF-BB modulates endothelial proliferation and angiogenesis in vitro via PDGF beta-receptors.* J Cell Biol, 1994. **125**(4): p. 917-28.

50. Bar, R.S., et al., *The effects of platelet-derived growth factor in cultured microvessel endothelial cells.* Endocrinology, 1989. **124**(4): p. 1841-8.

51. Nicosia, R.F., S.V. Nicosia, and M. Smith, *Vascular endothelial growth factor, platelet-derived growth factor, and insulin-like growth factor-1 promote rat aortic angiogenesis in vitro.* Am J Pathol, 1994. **145**(5): p. 1023-9.

52. D'Amore, P.A. and S.R. Smith, *Growth factor effects on cells of the vascular wall: a survey.* Growth Factors, 1993. **8**(1): p. 61-75.

53. Heldin, C.H. and B. Westermark, *Mechanism of action and in vivo role of platelet-derived growth factor.* Physiol Rev, 1999. **79**(4): p. 1283-316.

54. Leveen, P., et al., *Mice deficient for PDGF B show renal, cardiovascular, and hematological abnormalities.* Genes Dev, 1994. **8**(16): p. 1875-87.

55. Lindahl, P., et al., *Pericyte loss and microaneurysm formation in PDGF-B-deficient mice.* Science, 1997. **277**(5323): p. 242-5.

56. Hellstrom, M., et al., *Role of PDGF-B and PDGFR-beta in recruitment of vascular smooth muscle cells and pericytes during embryonic blood vessel formation in the mouse.* Development, 1999. **126**(14): p. 3047-55.

57. Soriano, P., *Abnormal kidney development and hematological disorders in PDGF beta-receptor mutant mice.* Genes Dev, 1994. **8**(16): p. 1888-96.

58. Derynck, R., et al., *Human transforming growth factor-beta complementary DNA sequence and expression in normal and transformed cells.* Nature, 1985. **316**(6030): p. 701-5.

59. Massague, J., *The transforming growth factor-beta family.* Annu Rev Cell Biol, 1990. **6**: p. 597-641.

60. Antonelli-Orlidge, A., et al., *An activated form of transforming growth factor beta is produced by cocultures of endothelial cells and pericytes.* Proc Natl Acad Sci U S A, 1989. **86**(12): p. 4544-8.

61. Yang, E.Y. and H.L. Moses, *Transforming growth factor beta 1-induced changes in cell migration, proliferation, and angiogenesis in the chicken chorioallantoic membrane.* J Cell Biol, 1990. **111**(2): p. 731-41.

62. Roberts, A.B., et al., *Transforming growth factor type beta: rapid induction of fibrosis and angiogenesis in vivo and stimulation of collagen formation in vitro.* Proc Natl Acad Sci U S A, 1986. **83**(12): p. 4167-71.

63. Phillips, G.D., R.A. Whitehead, and D.R. Knighton, *Inhibition by methylprednisolone acetate suggests an indirect mechanism for TGF-B induced angiogenesis.* Growth Factors, 1992. **6**(1): p. 77-84.

64. Pepper, M.S., *Transforming growth factor-beta: vasculogenesis, angiogenesis, and vessel wall integrity.* Cytokine Growth Factor Rev, 1997. **8**(1): p. 21-43.

65. Pierce, G.F., et al., *Platelet-derived growth factor (BB homodimer), transforming growth factor-beta 1, and basic fibroblast growth factor in dermal wound healing. Neovessel and matrix formation and cessation of repair.* Am J Pathol, 1992. **140**(6): p. 1375-88.

66. Egeblad, M. and Z. Werb, *New functions for the matrix metalloproteinases in cancer progression.* Nat Rev Cancer, 2002. **2**(3): p. 161-74.

67. Woessner, J.F., Jr., *The family of matrix metalloproteinases.* Ann N Y Acad Sci, 1994. **732**: p. 11-21.

68. Haas, T.L., *Endothelial cell regulation of matrix metalloproteinases.* Can J Physiol Pharmacol, 2005. **83**(1): p. 1-7.

69. Lauer-Fields, J.L., D. Juska, and G.B. Fields, *Matrix metalloproteinases and collagen catabolism.* Biopolymers, 2002. **66**(1): p. 19-32.

70. Lauer-Fields, J.L. and G.B. Fields, *Triple-helical peptide analysis of collagenolytic protease activity.* Biol Chem, 2002. **383**(7-8): p. 1095-105.

71. Cawston, T.E. and D.A. Young, *Proteinases involved in matrix turnover during cartilage and bone breakdown.* Cell Tissue Res, 2010. **339**(1): p. 221-35.

72. Sternlicht, M.D. and Z. Werb, *How matrix metalloproteinases regulate cell behavior.* Annual Review of Cell and Developmental Biology, 2001. **17**: p. 463-516.

73. Sato, H., et al., *A matrix metalloproteinase expressed on the surface of invasive tumour cells.* Nature, 1994. **370**(6484): p. 61-5.

74. Takino, T., et al., *Identification of the second membrane-type matrix metalloproteinase (MT-MMP-2) gene from a human placenta cDNA library. MT-MMPs form a unique membrane-type subclass in the MMP family.* J Biol Chem, 1995. **270**(39): p. 23013-20.

75. Velasco, G., et al., *Human MT6-matrix metalloproteinase: identification, progelatinase A activation, and expression in brain tumors.* Cancer Res, 2000. **60**(4): p. 877-82.

76. English, W.R., et al., *Membrane type 4 matrix metalloproteinase (MMP17) has tumor necrosis factor-alpha convertase activity but does not activate pro-MMP2.* J Biol Chem, 2000. **275**(19): p. 14046-55.

77. Haas, T.L., S.J. Davis, and J.A. Madri, *Three-dimensional type I collagen lattices induce coordinate expression of matrix metalloproteinases MT1-MMP and MMP-2 in microvascular endothelial cells.* Journal of Biological Chemistry, 1998. **273**(6): p. 3604-3610.

78. Galvez, B.G., et al., *Membrane type 1-matrix metalloproteinase is activated during migration of human endothelial cells and modulates endothelial motility and matrix remodeling.* J Biol Chem, 2001. **276**(40): p. 37491-500.

79. Oh, J., et al., *Mutations in two matrix metalloproteinase genes, MMP-2 and MT1-MMP, are synthetic lethal in mice.* Oncogene, 2004. **23**(29): p. 5041-8.

80. Chun, T.H., et al., *MT1-MMP-dependent neovessel formation within the confines of the three-dimensional extracellular matrix.* Journal of Cell Biology, 2004. **167**(4): p. 757-767.

81. Nagase, H., *Cell surface activation of progelatinase A (proMMP-2) and cell migration.* Cell Res, 1998. **8**(3): p. 179-86.

82. Strongin, A.Y., et al., *Mechanism of cell surface activation of 72-kDa type IV collagenase. Isolation of the activated form of the membrane metalloprotease.* J Biol Chem, 1995. **270**(10): p. 5331-8.

83. Seals, D.F. and S.A. Courtneidge, *The ADAMs family of metalloproteases: multidomain proteins with multiple functions.* Genes Dev, 2003. **17**(1): p. 7-30.

84. Porter, S., et al., *The ADAMTS metalloproteinases.* Biochem J, 2005. **386**(Pt 1): p. 15-27.

85. Handsley, M.M. and D.R. Edwards, *Metalloproteinases and their inhibitors in tumor angiogenesis.* Int J Cancer, 2005. **115**(6): p. 849-60.

86. Murphy, G., *The ADAMs: signalling scissors in the tumour microenvironment.* Nat Rev Cancer, 2008. **8**(12): p. 929-41.

87. van Hinsbergh, V.W., M.A. Engelse, and P.H. Quax, *Pericellular proteases in angiogenesis and vasculogenesis.* Arterioscler Thromb Vasc Biol, 2006. **26**(4): p. 716-28.

88. Lu, P., et al., *Extracellular matrix degradation and remodeling in development and disease.* Cold Spring Harb Perspect Biol, 2011. **3**(12).

89. Vazquez, F., et al., *METH-1, a human ortholog of ADAMTS-1, and METH-2 are members of a new family of proteins with angio-inhibitory activity.* J Biol Chem, 1999. **274**(33): p. 23349-57.

90. Iruela-Arispe, M.L., A. Luque, and N. Lee, *Thrombospondin modules and angiogenesis.* Int J Biochem Cell Biol, 2004. **36**(6): p. 1070-8.

91. Kahn, J., et al., *Gene expression profiling in an in vitro model of angiogenesis.* Am J Pathol, 2000. **156**(6): p. 1887-900.

92. Andreasen, P.A., et al., *The urokinase-type plasminogen activator system in cancer metastasis: a review.* Int J Cancer, 1997. **72**(1): p. 1-22.

93. Smith, H.W. and C.J. Marshall, *Regulation of cell signalling by uPAR.* Nat Rev Mol Cell Biol, 2010. **11**(1): p. 23-36.

94. Blasi, F. and P. Carmeliet, *uPAR: a versatile signalling orchestrator.* Nat Rev Mol Cell Biol, 2002. **3**(12): p. 932-43.

95. Green, K.A. and L.R. Lund, *ECM degrading proteases and tissue remodelling in the mammary gland.* Bioessays, 2005. **27**(9): p. 894-903.

96. Pepper, M.S., *Role of the matrix metalloproteinase and plasminogen activator-plasmin systems in angiogenesis.* Arteriosclerosis Thrombosis and Vascular Biology, 2001. **21**(7): p. 1104-1117.

97. Heymans, S., et al., *Inhibition of plasminogen activators or matrix metalloproteinases prevents cardiac rupture but impairs therapeutic angiogenesis and causes cardiac failure.* Nat Med, 1999. **5**(10): p. 1135-42.

98. Chirco, R., et al., *Novel functions of TIMPs in cell signaling.* Cancer Metastasis Rev, 2006. **25**(1): p. 99-113.

99. Will, H., et al., *The soluble catalytic domain of membrane type 1 matrix metalloproteinase cleaves the propeptide of progelatinase A and initiates autoproteolytic activation. Regulation by TIMP-2 and TIMP-3.* J Biol Chem, 1996. **271**(29): p. 17119-23.

100. Brew, K. and H. Nagase, *The tissue inhibitors of metalloproteinases (TIMPs): an ancient family with structural and functional diversity.* Biochim Biophys Acta, 2010. **1803**(1): p. 55-71.

101. Fernandez, C.A., et al., *Structural and functional uncoupling of the enzymatic and angiogenic inhibitory activities of tissue inhibitor of metalloproteinase-2 (TIMP-2): loop 6 is a novel angiogenesis inhibitor.* J Biol Chem, 2003. **278**(42): p. 40989-95.

102. Qi, J.H., et al., *A novel function for tissue inhibitor of metalloproteinases-3 (TIMP3): inhibition of angiogenesis by blockage of VEGF binding to VEGF receptor-2.* Nat Med, 2003. **9**(4): p. 407-15.

103. Yu, W.H., et al., *TIMP-3 binds to sulfated glycosaminoglycans of the extracellular matrix.* J Biol Chem, 2000. **275**(40): p. 31226-32.

104. Fernandez, C.A. and M.A. Moses, *Modulation of angiogenesis by tissue inhibitor of metalloproteinase-4.* Biochem Biophys Res Commun, 2006. **345**(1): p. 523-9.

105. Peyton, S.R., et al., *The emergence of ECM mechanics and cytoskeletal tension as important regulators of cell function.* Cell Biochem Biophys, 2007. **47**(2): p. 300-20.

106. Pedersen, J.A. and M.A. Swartz, *Mechanobiology in the third dimension.* Ann Biomed Eng, 2005. **33**(11): p. 1469-90.

107. Fraley, S.I., et al., *A distinctive role for focal adhesion proteins in three-dimensional cell motility.* Nat Cell Biol, 2010. **12**(6): p. 598-604.

108. Pickl, M. and C.H. Ries, *Comparison of 3D and 2D tumor models reveals enhanced HER2 activation in 3D associated with an increased response to trastuzumab.* Oncogene, 2009. **28**(3): p. 461-8.

109. Wozniak, M.A., et al., *ROCK-generated contractility regulates breast epithelial cell differentiation in response to the physical properties of a three-dimensional collagen matrix.* J Cell Biol, 2003. **163**(3): p. 583-95.

110. Cukierman, E., et al., *Taking cell-matrix adhesions to the third dimension.* Science, 2001. **294**(5547): p. 1708-1712.

111. Huebsch, N. and D.J. Mooney, *Inspiration and application in the evolution of biomaterials.* Nature, 2009. **462**(7272): p. 426-32.

112. Kuntz, R.M. and W.M. Saltzman, *Neutrophil motility in extracellular matrix gels: mesh size and adhesion affect speed of migration.* Biophys J, 1997. **72**(3): p. 1472-80.

113. Lo, C.M., et al., *Cell movement is guided by the rigidity of the substrate.* Biophysical Journal, 2000. **79**(1): p. 144-152.

114. Bischofs, I.B. and U.S. Schwarz, *Cell organization in soft media due to active mechanosensing.* Proc Natl Acad Sci U S A, 2003. **100**(16): p. 9274-9.

115. Discher, D.E., P. Janmey, and Y.L. Wang, *Tissue cells feel and respond to the stiffness of their substrate.* Science, 2005. **310**(5751): p. 1139-43.

116. O'Brien, F.J., et al., *The effect of pore size on cell adhesion in collagen-GAG scaffolds.* Biomaterials, 2005. **26**(4): p. 433-41.

117. Engler, A.J., et al., *Matrix elasticity directs stem cell lineage specification.* Cell, 2006. **126**(4): p. 677-89.

118. Zaman, M.H., et al., *Migration of tumor cells in 3D matrices is governed by matrix stiffness along with cell-matrix adhesion and proteolysis.* Proc Natl Acad Sci U S A, 2006. **103**(29): p. 10889-94.

119. Dvir, T., et al., *Nanotechnological strategies for engineering complex tissues.* Nat Nanotechnol, 2011. **6**(1): p. 13-22.

120. Engler, A.J., et al., *Myotubes differentiate optimally on substrates with tissue-like stiffness: pathological implications for soft or stiff microenvironments.* J Cell Biol, 2004. **166**(6): p. 877-87.

121. Solon, J., et al., *Fibroblast adaptation and stiffness matching to soft elastic substrates.* Biophys J, 2007. **93**(12): p. 4453-61.

122. Charest, J.M., et al., *Fabrication of substrates with defined mechanical properties and topographical features for the study of cell migration.* Macromol Biosci, 2012. **12**(1): p. 12-20.

123. Thompson, M.T., et al., *Tuning compliance of nanoscale polyelectrolyte multilayers to modulate cell adhesion.* Biomaterials, 2005. **26**(34): p. 6836-45.

124. Thompson, M.T., et al., *Biochemical functionalization of polymeric cell substrata can alter mechanical compliance.* Biomacromolecules, 2006. **7**(6): p. 1990-5.

125. Chen, A.A., et al., *Modulation of hepatocyte phenotype in vitro via chemomechanical tuning of polyelectrolyte multilayers.* Biomaterials, 2009. **30**(6): p. 1113-20.

126. Chou, S.Y., C.M. Cheng, and P.R. LeDuc, *Composite polymer systems with control of local substrate elasticity and their effect on cytoskeletal and morphological characteristics of adherent cells.* Biomaterials, 2009. **30**(18): p. 3136-42.

127. Brown, X.Q., K. Ookawa, and J.Y. Wong, *Evaluation of polydimethylsiloxane scaffolds with physiologically-relevant elastic moduli: interplay of substrate mechanics and surface chemistry effects on vascular smooth muscle cell response.* Biomaterials, 2005. **26**(16): p. 3123-9.

128. Tzvetkova-Chevolleau, T., et al., *The motility of normal and cancer cells in response to the combined influence of the substrate rigidity and anisotropic microstructure.* Biomaterials, 2008. **29**(10): p. 1541-51.

129. Lutolf, M.P. and J.A. Hubbell, *Synthesis and physicochemical characterization of end-linked poly(ethylene glycol)-co-peptide hydrogels formed by Michael-type addition.* Biomacromolecules, 2003. **4**(3): p. 713-22.

130. Zisch, A.H., et al., *Cell-demanded release of VEGF from synthetic, biointeractive cell ingrowth matrices for vascularized tissue growth.* FASEB J, 2003. **17**(15): p. 2260-2.

131. Raeber, G.P., M.P. Lutolf, and J.A. Hubbell, *Molecularly engineered PEG hydrogels: a novel model system for proteolytically mediated cell migration.* Biophys J, 2005. **89**(2): p. 1374-88.

132. Moon, J.J., et al., *Biomimetic hydrogels with pro-angiogenic properties.* Biomaterials, 2010. **31**(14): p. 3840-7.

133. Yamamura, N., et al., *Effects of the mechanical properties of collagen gel on the in vitro formation of microvessel networks by endothelial cells.* Tissue Eng, 2007. **13**(7): p. 1443-53.

134. Miron-Mendoza, M., J. Seemann, and F. Grinnell, *The differential regulation of cell motile activity through matrix stiffness and porosity in three dimensional collagen matrices.* Biomaterials, 2010. **31**(25): p. 6425-35.

135. McDaniel, D.P., et al., *The stiffness of collagen fibrils influences vascular smooth muscle cell phenotype.* Biophys J, 2007. **92**(5): p. 1759-69.

136. Kniazeva, E., et al., *Quantification of local matrix deformations and mechanical properties during capillary morphogenesis in 3D.* Integr Biol (Camb), 2012. **4**(4): p. 431-9.

137. Kniazeva, E. and A.J. Putnam, *Endothelial cell traction and ECM density influence both capillary morphogenesis and maintenance in 3-D.* Am J Physiol Cell Physiol, 2009. **297**(1): p. C179-87.

138. Stephanou, A., et al., *The rigidity in fibrin gels as a contributing factor to the dynamics of in vitro vascular cord formation.* Microvasc Res, 2007. **73**(3): p. 182-90.

139. Zimmerman, E., B. Geiger, and L. Addadi, *Initial stages of cell-matrix adhesion can be mediated and modulated by cell-surface hyaluronan.* Biophys J, 2002. **82**(4): p. 1848-57.

140. Shu, X.Z., et al., *Disulfide cross-linked hyaluronan hydrogels.* Biomacromolecules, 2002. **3**(6): p. 1304-11.

141. Young, J.L. and A.J. Engler, *Hydrogels with time-dependent material properties enhance cardiomyocyte differentiation in vitro.* Biomaterials, 2011. **32**(4): p. 1002-9.

142. Augst, A.D., H.J. Kong, and D.J. Mooney, *Alginate hydrogels as biomaterials.* Macromol Biosci, 2006. **6**(8): p. 623-33.

143. Kong, H.J., M.K. Smith, and D.J. Mooney, *Designing alginate hydrogels to maintain viability of immobilized cells.* Biomaterials, 2003. **24**(22): p. 4023-9.

144. Rowley, J.A. and D.J. Mooney, *Alginate type and RGD density control myoblast phenotype.* J Biomed Mater Res, 2002. **60**(2): p. 217-23.

145. Genes, N.G., et al., *Effect of substrate mechanics on chondrocyte adhesion to modified alginate surfaces.* Arch Biochem Biophys, 2004. **422**(2): p. 161-7.

146. Huebsch, N., et al., *Harnessing traction-mediated manipulation of the cell/matrix interface to control stem-cell fate.* Nat Mater, 2010. **9**(6): p. 518-26.

147. Kolambkar, Y.M., et al., *An alginate-based hybrid system for growth factor delivery in the functional repair of large bone defects.* Biomaterials, 2011. **32**(1): p. 65-74.

148. van der Rest, M. and R. Garrone, *Collagen family of proteins.* FASEB J, 1991. **5**(13): p. 2814-23.

149. Prockop, D.J. and K.I. Kivirikko, *Collagens: molecular biology, diseases, and potentials for therapy.* Annu Rev Biochem, 1995. **64**: p. 403-34.

150. Silver, F.H., J.W. Freeman, and G.P. Seehra, *Collagen self-assembly and the development of tendon mechanical properties.* J Biomech, 2003. **36**(10): p. 1529-53.

151. Gordon, M.K. and R.A. Hahn, *Collagens.* Cell Tissue Res, 2010. **339**(1): p. 247-57.

152. Chapman, J.A., et al., *The collagen fibril--a model system for studying the staining and fixation of a protein.* Electron Microsc Rev, 1990. **3**(1): p. 143-82.

153. Kadler, K.E. and R.B. Watson, *Procollagen C-peptidase: procollagen C-proteinase.* Methods Enzymol, 1995. **248**: p. 771-81.

154. Kadler, K.E., S.J. Lightfoot, and R.B. Watson, *Procollagen N-peptidases: procollagen N-proteinases.* Methods Enzymol, 1995. **248**: p. 756-71.

155. Parkinson, J., K.E. Kadler, and A. Brass, *Simple physical model of collagen fibrillogenesis based on diffusion limited aggregation.* J Mol Biol, 1995. **247**(4): p. 823-31.

156. Wood, G.C. and M.K. Keech, *The formation of fibrils from collagen solutions. 1. The effect of experimental conditions: kinetic and electron-microscope studies.* Biochem J, 1960. **75**: p. 588-98.

157. Wood, G.C., *The formation of fibrils from collagen solutions. 2. A mechanism of collagen-fibril formation.* Biochem J, 1960. **75**: p. 598-605.

158. Pins, G.D., et al., *Self-assembly of collagen fibers. Influence of fibrillar alignment and decorin on mechanical properties.* Biophys J, 1997. **73**(4): p. 2164-72.

159. Christiansen, D.L., E.K. Huang, and F.H. Silver, *Assembly of type I collagen: fusion of fibril subunits and the influence of fibril diameter on mechanical properties.* Matrix Biol, 2000. **19**(5): p. 409-20.

160. Mosser, G., et al., *Dense tissue-like collagen matrices formed in cell-free conditions.* Matrix Biol, 2006. **25**(1): p. 3-13.

161. Gobeaux, F., et al., *Fibrillogenesis in dense collagen solutions: a physicochemical study.* J Mol Biol, 2008. **376**(5): p. 1509-22.

162. Critser, P.J., et al., *Collagen matrix physical properties modulate endothelial colony forming cell-derived vessels in vivo.* Microvasc Res, 2010. **80**(1): p. 23-30.

163. Johnson, T.D., S.Y. Lin, and K.L. Christman, *Tailoring material properties of a nanofibrous extracellular matrix derived hydrogel.* Nanotechnology, 2011. **22**(49): p. 494015.

164. Yang, Y.L., S. Motte, and L.J. Kaufman, *Pore size variable type I collagen gels and their interaction with glioma cells.* Biomaterials, 2010. **31**(21): p. 5678-88.

165. Raub, C.B., et al., *Noninvasive assessment of collagen gel microstructure and mechanics using multiphoton microscopy.* Biophys J, 2007. **92**(6): p. 2212-22.

166. Raub, C.B., et al., *Image correlation spectroscopy of multiphoton images correlates with collagen mechanical properties.* Biophys J, 2008. **94**(6): p. 2361-73.

167. Forgacs, G., et al., *Assembly of collagen matrices as a phase transition revealed by structural and rheologic studies.* Biophys J, 2003. **84**(2 Pt 1): p. 1272-80.

168. Comper, W.D. and A. Veis, *The mechanism of nucleation for in vitro collagen fibril formation.* Biopolymers, 1977. **16**(10): p. 2113-2131.

169. Williams, B.R., et al., *Collagen fibril formation. Optimal in vitro conditions and preliminary kinetic results.* J Biol Chem, 1978. **253**(18): p. 6578-85.

170. Rosenblatt, J., B. Devereux, and D.G. Wallace, *Injec collagen as a pH-sensitive hydrogel.* Biomaterials, 1994. **15**(12): p. 985-95.

171. Hayashi, T. and Y. Nagai, *Factors affecting the interactions of collagen molecules as observed by in vitro fibril formation. III. Non-helical regions of the collagen molecules.* J Biochem, 1974. **76**(1): p. 177-86.

172. Roeder, B.A., et al., *Tensile mechanical properties of three-dimensional type I collagen extracellular matrices with varied microstructure.* J Biomech Eng, 2002. **124**(2): p. 214-22.

173. Kadler, K.E., A. Hill, and E.G. Canty-Laird, *Collagen fibrillogenesis: fibronectin, integrins, and minor collagens as organizers and nucleators.* Curr Opin Cell Biol, 2008. **20**(5): p. 495-501.

174. Weadock, K.S., et al., *Physical crosslinking of collagen fibers: comparison of ultraviolet irradiation and dehydrothermal treatment.* J Biomed Mater Res, 1995. **29**(11): p. 1373-9.

175. Ohan, M.P., K.S. Weadock, and M.G. Dunn, *Synergistic effects of glucose and ultraviolet irradiation on the physical properties of collagen.* J Biomed Mater Res, 2002. **60**(3): p. 384-91.

176. Lai, E.S., C.M. Anderson, and G.G. Fuller, *Designing a tubular matrix of oriented collagen fibrils for tissue engineering.* Acta Biomater, 2011. **7**(6): p. 2448-56.

177. Wu, X., et al., *Preparation and assessment of glutaraldehyde-crosslinked collagen-chitosan hydrogels for adipose tissue engineering.* J Biomed Mater Res A, 2007. **81**(1): p. 59-65.

178. Harriger, M.D., et al., *Glutaraldehyde crosslinking of collagen substrates inhibits degradation in skin substitutes grafted to athymic mice.* J Biomed Mater Res, 1997. **35**(2): p. 137-45.

179. Chvapil, M., J.A. Owen, and D.S. Clark, *Effect of collagen crosslinking on the rate of resorption of implanted collagen tubing in rabbits.* J Biomed Mater Res, 1977. **11**(2): p. 297-314.

180. Yannas, I.V. and J.F. Burke, *Design of an artificial skin. I. Basic design principles.* J Biomed Mater Res, 1980. **14**(1): p. 65-81.

181. Osborne, C.S., et al., *Investigation into the tensile properties of collagen/chondroitin-6-sulphate gels: the effect of crosslinking agents and diamines.* Med Biol Eng Comput, 1998. **36**(1): p. 129-34.

182. Powell, H.M. and S.T. Boyce, *EDC cross-linking improves skin substitute strength and stability.* Biomaterials, 2006. **27**(34): p. 5821-7.

183. Powell, H.M. and S.T. Boyce, *Wound closure with EDC cross-linked cultured skin substitutes grafted to athymic mice.* Biomaterials, 2007. **28**(6): p. 1084-92.

184. Duan, X. and H. Sheardown, *Crosslinking of collagen with dendrimers.* J Biomed Mater Res A, 2005. **75**(3): p. 510-8.

185. Garcia, Y., et al., *In vitro characterization of a collagen scaffold enzymatically cross-linked with a tailored elastin-like polymer.* Tissue Eng Part A, 2009. **15**(4): p. 887-99.

186. Yung, C.W., et al., *Transglutaminase crosslinked gelatin as a tissue engineering scaffold.* J Biomed Mater Res A, 2007. **83**(4): p. 1039-46.

187. Khew, S.T., Q.J. Yang, and Y.W. Tong, *Enzymatically crosslinked collagen-mimetic dendrimers that promote integrin-targeted cell adhesion.* Biomaterials, 2008. **29**(20): p. 3034-45.

188. Chen, R.N., H.O. Ho, and M.T. Sheu, *Characterization of collagen matrices crosslinked using microbial transglutaminase.* Biomaterials, 2005. **26**(20): p. 4229-4235.

189. Elbjeirami, W.M., et al., *Enhancing mechanical properties of tissue-engineered constructs via lysyl oxidase crosslinking activity.* J Biomed Mater Res A, 2003. **66**(3): p. 513-21.

190. Girton, T.S., et al., *Mechanisms of stiffening and strengthening in media-equivalents fabricated using glycation.* J Biomech Eng, 2000. **122**(3): p. 216-23.

191. Avery, N.C. and A.J. Bailey, *Enzymic and non-enzymic cross-linking mechanisms in relation to turnover of collagen: relevance to aging and exercise.* Scand J Med Sci Sports, 2005. **15**(4): p. 231-40.

192. Girton, T.S., T.R. Oegema, and R.T. Tranquillo, *Exploiting glycation to stiffen and strengthen tissue equivalents for tissue engineering.* J Biomed Mater Res, 1999. **46**(1): p. 87-92.

193. Howard, E.W., et al., *Cellular contraction of collagen lattices is inhibited by nonenzymatic glycation.* Exp Cell Res, 1996. **228**(1): p. 132-7.

194. Roy, R., A. Boskey, and L.J. Bonassar, *Processing of type I collagen gels using nonenzymatic glycation.* J Biomed Mater Res A, 2010. **93**(3): p. 843-51.

195. Francis-Sedlak, M.E., et al., *Collagen glycation alters neovascularization in vitro and in vivo.* Microvasc Res, 2010. **80**(1): p. 3-9.

196. Elgawish, A., et al., *Involvement of hydrogen peroxide in collagen cross-linking by high glucose in vitro and in vivo.* J Biol Chem, 1996. **271**(22): p. 12964-71.

197. Aronson, D., *Cross-linking of glycated collagen in the pathogenesis of arterial and myocardial stiffening of aging and diabetes.* J Hypertens, 2003. **21**(1): p. 3-12.

198. Francis-Sedlak, M.E., et al., *Characterization of type I collagen gels modified by glycation.* Biomaterials, 2009. **30**(9): p. 1851-6.

199. Ciardelli, G., et al., *Enzymatically crosslinked porous composite matrices for bone tissue regeneration.* J Biomed Mater Res A, 2010. **92**(1): p. 137-51.

200. Macedo, J.A., L.D. Sette, and H.H. Sato, *A comparative biochemical characterization of microbial transglutaminases: commercial vs. a newly isolated enzyme from Streptomyces Sp.* Food Bioprocess Technol, 2010. **3**(2).

201. Yang, Y.L., L.M. Leone, and L.J. Kaufman, *Elastic moduli of collagen gels can be predicted from two-dimensional confocal microscopy.* Biophys J, 2009. **97**(7): p. 2051-60.

202. Yang, Y.L. and L.J. Kaufman, *Rheology and confocal reflectance microscopy as probes of mechanical properties and structure during collagen and collagen/hyaluronan self-assembly.* Biophys J, 2009. **96**(4): p. 1566-85.

203. Roeder, B.A., K. Kokini, and S.L. Voytik-Harbin, *Fibril microstructure affects strain transmission within collagen extracellular matrices.* J Biomech Eng, 2009. **131**(3): p. 031004.

204. Vader, D., et al., *Strain-induced alignment in collagen gels.* PLoS One, 2009. **4**(6): p. e5902.

205. Xu, B., M.J. Chow, and Y. Zhang, *Experimental and modeling study of collagen scaffolds with the effects of crosslinking and fiber alignment.* Int J Biomater, 2011. **2011**: p. 172389.

206. Knezevic, V., et al., *Isotonic biaxial loading of fibroblast-populated collagen gels: a versatile, low-cost system for the study of mechanobiology.* Biomech Model Mechanobiol, 2002. **1**(1): p. 59-67.

207. Jhun, C.S., et al., *Planar biaxial mechanical behavior of bioartificial tissues possessing prescribed fiber alignment.* J Biomech Eng, 2009. **131**(8): p. 081006.

208. Hu, J.J., J.D. Humphrey, and A.T. Yeh, *Characterization of engineered tissue development under biaxial stretch using nonlinear optical microscopy.* Tissue Eng Part A, 2009. **15**(7): p. 1553-64.

209. Zipfel, W.R., R.M. Williams, and W.W. Webb, *Nonlinear magic: multiphoton microscopy in the biosciences.* Nat Biotechnol, 2003. **21**(11): p. 1369-77.

210. Paoli, J., M. Smedh, and M.B. Ericson, *Multiphoton laser scanning microscopy--a novel diagnostic method for superficial skin cancers.* Semin Cutan Med Surg, 2009. **28**(3): p. 190-5.

211. Oheim, M., et al., *Principles of two-photon excitation fluorescence microscopy and other nonlinear imaging approaches.* Adv Drug Deliv Rev, 2006. **58**(7): p. 788-808.

212. Imanishi, Y., K.H. Lodowski, and Y. Koutalos, *Two-photon microscopy: shedding light on the chemistry of vision.* Biochemistry, 2007. **46**(34): p. 9674-84.

213. Phan, T.G. and A. Bullen, *Practical intravital two-photon microscopy for immunological research: faster, brighter, deeper.* Immunol Cell Biol, 2010. **88**(4): p. 438-44.

214. Hanson, K.M. and C.J. Bardeen, *Application of nonlinear optical microscopy for imaging skin.* Photochem Photobiol, 2009. **85**(1): p. 33-44.

215. Zheng, W., et al., *Autofluorescence of epithelial tissue: single-photon versus two-photon excitation.* J Biomed Opt, 2008. **13**(5): p. 054010.

216. Li, C., et al., *Multiphoton microscopy of live tissues with ultraviolet autofluorescence.* IEEE Journal of selected topics in quantum electronics, 2010. **16**(3): p. 516-523.

217. Maiti, S., et al., *Measuring serotonin distribution in live cells with three-photon excitation.* Science, 1997. **275**(5299): p. 530-2.

218. Botchway, S.W., et al., *Real-time cellular uptake of serotonin using fluorescence lifetime imaging with two-photon excitation.* Microsc Res Tech, 2008. **71**(4): p. 267-73.

219. Williams, R.M., et al., *Mucosal mast cell secretion processes imaged using three-photon microscopy of 5-hydroxytryptamine autofluorescence.* Biophys J, 1999. **76**(4): p. 1835-46.

220. Pena, A., et al., *Spectroscopic analysis of keratin endogenous signal for skin multiphoton microscopy.* Opt Express, 2005. **13**(16): p. 6268-74.

221. Lin, S.J., et al., *Evaluating cutaneous photoaging by use of multiphoton fluorescence and second-harmonic generation microscopy.* Opt Lett, 2005. **30**(17): p. 2275-7.

222. Koehler, M.J., et al., *In vivo assessment of human skin aging by multiphoton laser scanning tomography.* Opt Lett, 2006. **31**(19): p. 2879-81.

223. Le, T.T., et al., *Label-free molecular imaging of atherosclerotic lesions using multimodal nonlinear optical microscopy.* J Biomed Opt, 2007. **12**(5): p. 054007.

224. Teuchner, K., et al., *Fluorescence studies of Melanin by stepwise two-photon femtosecond laser excitation.* J Fluorescence, 2000. **10**: p. 275-275.

225. Han, X., et al., *Near-infrared autofluorescence imaging of cutaneous melanins and human skin in vivo.* J Biomed Opt, 2009. **14**(2): p. 024017.

226. vandeVen, M., et al., *Pitfalls and their remedies in time-resolved fluorescence spectroscopy and microscopy.* J Fluoresc, 2005. **15**(3): p. 377-413.

227. Meerwaldt, R., et al., *Simple non-invasive assessment of advanced glycation endproduct accumulation.* Diabetologia, 2004. **47**(7): p. 1324-30.

228. Lutz, V., et al., *Characterization of fibrillar collagen types using multi-dimensional multiphoton laser scanning microscopy.* Int J Cosmet Sci, 2012. **34**(2): p. 209-15.

229. Kirkpatrick, N.D., et al., *In vitro model for endogenous optical signatures of collagen.* J Biomed Opt, 2006. **11**(5): p. 054021.

230. Raub, C.B., et al., *Predicting bulk mechanical properties of cellularized collagen gels using multiphoton microscopy.* Acta Biomater, 2010. **6**(12): p. 4657-65.

231. Hwang, Y.J., et al., *Effect of genipin crosslinking on the optical spectral properties and structures of collagen hydrogels.* ACS Appl Mater Interfaces, 2011. **3**(7): p. 2579-84.

232. Hwang, Y.J., J. Granelli, and J.G. Lyubovitsky, *Multiphoton optical image guided spectroscopy method for characterization of collagen-based materials modified by glycation.* Anal Chem, 2011. **83**(1): p. 200-6.

233. Hwang, Y.J. and J.G. Lyubovitsky, *Collagen hydrogel characterization: multi-scale and multi-modality approach.* Analytical Methods, 2011(3): p. 529-536.

234. Bailey, A.J., R.G. Paul, and L. Knott, *Mechanisms of maturation and ageing of collagen.* Mech Ageing Dev, 1998. **106**(1-2): p. 1-56.

235. Cox, G., et al., *3-dimensional imaging of collagen using second harmonic generation.* J Struct Biol, 2003. **141**(1): p. 53-62.

236. Stoller, P., et al., *Polarization-dependent optical second-harmonic imaging of a rat-tail tendon.* J Biomed Opt, 2002. **7**(2): p. 205-14.

237. Yasui, T., Y. Tohno, and T. Araki, *Determination of collagen fiber orientation in human tissue by use of polarization measurement of molecular second-harmonic-generation light.* Appl Opt, 2004. **43**(14): p. 2861-7.

238. Dombeck, D.A., et al., *Uniform polarity microtubule assemblies imaged in native brain tissue by second-harmonic generation microscopy.* Proc Natl Acad Sci U S A, 2003. **100**(12): p. 7081-6.

239. Both, M., et al., *Second harmonic imaging of intrinsic signals in muscle fibers in situ.* J Biomed Opt, 2004. **9**(5): p. 882-92.

240. Plotnikov, S.V., et al., *Characterization of the myosin-based source for second-harmonic generation from muscle sarcomeres.* Biophys J, 2006. **90**(2): p. 693-703.

241. Cox, G., N. Moreno, and J. Feijo, *Second-harmonic imaging of plant polysaccharides.* J Biomed Opt, 2005. **10**(2): p. 024013.

242. Gauderon, R., P.B. Lukins, and C.J. Sheppard, *Simultaneous multichannel nonlinear imaging: combined two-photon excited fluorescence and second-harmonic generation microscopy.* Micron, 2001. **32**(7): p. 685-9.

243. Yeh, A.T., et al., *Reversible dissociation of collagen in tissues.* Journal of Investigative Dermatology, 2003. **121**(6): p. 1332-1335.

244. Kim, B.M., et al., *Collagen structure and nonlinear susceptibility: effects of heat, glycation, and enzymatic cleavage on second harmonic signal intensity.* Lasers Surg Med, 2000. **27**(4): p. 329-35.

245. Teng, S.W., et al., *Multiphoton autofluorescence and second-harmonic generation imaging of the ex vivo porcine eye.* Invest Ophthalmol Vis Sci, 2006. **47**(3): p. 1216-24.

246. Wang, B.G. and K.J. Halbhuber, *Corneal multiphoton microscopy and intratissue optical nanosurgery by nanojoule femtosecond near-infrared pulsed lasers.* Ann Anat, 2006. **188**(5): p. 395-409.

247. Bank, R.A., et al., *Defective collagen crosslinking in bone, but not in ligament or cartilage, in Bruck syndrome: indications for a bone-specific telopeptide lysyl hydroxylase on chromosome 17.* Proc Natl Acad Sci U S A, 1999. **96**(3): p. 1054-8.

248. Eyre, D.R., T.J. Koob, and K.P. Van Ness, *Quantitation of hydroxypyridinium crosslinks in collagen by high-performance liquid chromatography.* Anal Biochem, 1984. **137**(2): p. 380-8.

249. Veraart, J.R., et al., *Capillary electrophoresis of the collagen crosslinks HP and LP utilizing absorbance, wavelength-resolved laser-induced fluorescence and conventional fluorescence detection.* Biomed Chromatogr, 1998. **12**(4): p. 226-31.

250. Theodossiou, T., et al., *Thermally induced irreversible conformational changes in collagen probed by optical second harmonic generation and laser-induced fluorescence.* Lasers Med Sci, 2002. **17**(1): p. 34-41.

251. Vernon, R.B., et al., *Organized Type-I Collagen Influences Endothelial Patterns during Spontaneous Angiogenesis in-Vitro - Planar Cultures as Models of*

Vascular Development. In Vitro Cellular & Developmental Biology-Animal, 1995. **31**(2): p. 120-131.

252. Vernon, R.B., et al., *Reorganization of basement membrane matrices by cellular traction promotes the formation of cellular networks in vitro.* Lab Invest, 1992. **66**(5): p. 536-47.

253. Deroanne, C.F., C.M. Lapiere, and B.V. Nusgens, *In vitro tubulogenesis of endothelial cells by relaxation of the coupling extracellular matrix-cytoskeleton.* Cardiovasc Res, 2001. **49**(3): p. 647-58.

254. Kuzuya, M., et al., *Inhibition of endothelial cell differentiation on a glycosylated reconstituted basement membrane complex.* Exp Cell Res, 1996. **226**(2): p. 336-45.

255. Chalupowicz, D.G., et al., *Fibrin II induces endothelial cell capillary tube formation.* J Cell Biol, 1995. **130**(1): p. 207-15.

256. Schor, A.M., S.L. Schor, and T.D. Allen, *Effects of culture conditions on the proliferation, morphology and migration of bovine aortic endothelial cells.* J Cell Sci, 1983. **62**: p. 267-85.

257. Montesano, R., L. Orci, and P. Vassalli, *In vitro rapid organization of endothelial cells into capillary-like networks is promoted by collagen matrices.* J Cell Biol, 1983. **97**(5 Pt 1): p. 1648-52.

258. Montesano, R. and L. Orci, *Tumor-Promoting Phorbol Esters Induce Angiogenesis Invitro.* Cell, 1985. **42**(2): p. 469-477.

259. Madri, J.A., B.M. Pratt, and A.M. Tucker, *Phenotypic modulation of endothelial cells by transforming growth factor-beta depends upon the composition and organization of the extracellular matrix.* J Cell Biol, 1988. **106**(4): p. 1375-84.

260. Bayless, K.J., R. Salazar, and G.E. Davis, *RGD-dependent vacuolation and lumen formation observed during endothelial cell morphogenesis in three-dimensional fibrin matrices involves the alpha(v)beta(3) and alpha(5)beta(1) integrins.* American Journal of Pathology, 2000. **156**(5): p. 1673-1683.

261. Davis, G.E. and C.W. Camarillo, *An alpha 2 beta 1 integrin-dependent pinocytic mechanism involving intracellular vacuole formation and coalescence regulates capillary lumen and tube formation in three-dimensional collagen matrix.* Experimental Cell Research, 1996. **224**(1): p. 39-51.

262. Nicosia, R.F., R. Tchao, and J. Leighton, *Interactions between newly formed endothelial channels and carcinoma cells in plasma clot culture.* Clin Exp Metastasis, 1986. **4**(2): p. 91-104.

263. Vernon, R.B. and E.H. Sage, *A novel, quantitative model for study of endothelial cell migration and sprout formation within three-dimensional collagen matrices.* Microvasc Res, 1999. **57**(2): p. 118-33.

264. Nehls, V. and D. Drenckhahn, *A microcarrier-based cocultivation system for the investigation of factors and cells involved in angiogenesis in three-dimensional fibrin matrices in vitro.* Histochem Cell Biol, 1995. **104**(6): p. 459-66.

265. Nehls, V. and D. Drenckhahn, *A novel, microcarrier-based in vitro assay for rapid and reliable quantification of three-dimensional cell migration and angiogenesis.* Microvasc Res, 1995. **50**(3): p. 311-22.

266. Nakatsu, M.N., et al., *Angiogenic sprouting and capillary lumen formation modeled by human umbilical vein endothelial cells (HUVEC) in fibrin gels: the role of fibroblasts and Angiopoietin-1.* Microvasc Res, 2003. **66**(2): p. 102-12.

267. English, D., et al., *Lipid mediators of angiogenesis and the signalling pathways they initiate.* Biochim Biophys Acta, 2002. **1582**(1-3): p. 228-39.

268. Hla, T., *Physiological and pathological actions of sphingosine 1-phosphate.* Semin Cell Dev Biol, 2004. **15**(5): p. 513-20.

269. Spiegel, S. and S. Milstien, *Sphingosine-1-phosphate: an enigmatic signalling lipid.* Nat Rev Mol Cell Biol, 2003. **4**(5): p. 397-407.

270. Lee, O.H., et al., *Sphingosine 1-phosphate induces angiogenesis: Its angiogenic action and signaling mechanism in human umbilical vein endothelial cells.* Biochemical and Biophysical Research Communications, 1999. **264**(3): p. 743-750.

271. Sieminski, A.L., R.P. Hebbel, and K.J. Gooch, *The relative magnitudes of endothelial force generation and matrix stiffness modulate capillary morphogenesis in vitro.* Experimental Cell Research, 2004. **297**(2): p. 574-584.

272. Califano, J.P. and C.A. Reinhart-King, *A Balance of Substrate Mechanics and Matrix Chemistry Regulates Endothelial Cell Network Assembly.* Cellular and Molecular Bioengineering, 2008. **1**: p. 122-132.

273. Ghajar, C.M., et al., *The effect of matrix density on the regulation of 3-D capillary morphogenesis.* Biophys J, 2008. **94**(5): p. 1930-41.

274. Kalluri, R., *Basement membranes: structure, assembly and role in tumour angiogenesis.* Nat Rev Cancer, 2003. **3**(6): p. 422-33.

275. Califano, J.P. and C.A. Reinhart-King, *Exogenous and endogenous force regulation of endothelial cell behavior.* J Biomech, 2010. **43**(1): p. 79-86.

276. von Tell, D., A. Armulik, and C. Betsholtz, *Pericytes and vascular stability.* Exp Cell Res, 2006. **312**(5): p. 623-9.

277. Gossl, M., et al., *Impact of coronary vasa vasorum functional structure on coronary vessel wall perfusion distribution.* Am J Physiol Heart Circ Physiol, 2003. **285**(5): p. H2019-26.

278. Sheriff, D., *Point: The muscle pump raises muscle blood flow during locomotion.* J Appl Physiol, 2005. **99**(1): p. 371-2; discussion 374-5.

279. Lemmon, C.A., C.S. Chen, and L.H. Romer, *Cell traction forces direct fibronectin matrix assembly.* Biophys J, 2009. **96**(2): p. 729-38.

280. Guo, W.H., et al., *Substrate rigidity regulates the formation and maintenance of tissues.* Biophys J, 2006. **90**(6): p. 2213-20.

281. Reinhart-King, C.A., *Endothelial cell adhesion and migration.* Methods Enzymol, 2008. **443**: p. 45-64.

282. Chen, C.S., *Mechanotransduction - a field pulling together?* J Cell Sci, 2008. **121**(Pt 20): p. 3285-92.

283. Paszek, M.J., et al., *Tensional homeostasis and the malignant phenotype.* Cancer Cell, 2005. **8**(3): p. 241-54.

284. Georges, P.C. and P.A. Janmey, *Cell type-specific response to growth on soft materials.* J Appl Physiol, 2005. **98**(4): p. 1547-53.

285. Lu, L., et al., *Mechanical properties of actin stress fibers in living cells.* Biophys J, 2008. **95**(12): p. 6060-71.

286. Arnold, M., et al., *Activation of integrin function by nanopatterned adhesive interfaces.* Chemphyschem, 2004. **5**(3): p. 383-8.

287. Cavalcanti-Adam, E.A., et al., *Lateral spacing of integrin ligands influences cell spreading and focal adhesion assembly.* Eur J Cell Biol, 2006. **85**(3-4): p. 219-24.

288. Zaidel-Bar, R., et al., *Early molecular events in the assembly of matrix adhesions at the leading edge of migrating cells.* J Cell Sci, 2003. **116**(Pt 22): p. 4605-13.

289. Yoshigi, M., et al., *Mechanical force mobilizes zyxin from focal adhesions to actin filaments and regulates cytoskeletal reinforcement.* J Cell Biol, 2005. **171**(2): p. 209-15.

290. Lele, T.P., et al., *Mechanical forces alter zyxin unbinding kinetics within focal adhesions of living cells.* J Cell Physiol, 2006. **207**(1): p. 187-94.

291. Reinhard, M., et al., *The proline-rich focal adhesion and microfilament protein VASP is a ligand for profilins.* EMBO J, 1995. **14**(8): p. 1583-9.

292. Frey, M.T., et al., *Cellular responses to substrate topography: role of myosin II and focal adhesion kinase.* Biophys J, 2006. **90**(10): p. 3774-82.

293. Wang, H.B., et al., *Focal adhesion kinase is involved in mechanosensing during fibroblast migration.* Proc Natl Acad Sci U S A, 2001. **98**(20): p. 11295-300.

294. Chen, B.H., et al., *Roles of Rho-associated kinase and myosin light chain kinase in morphological and migratory defects of focal adhesion kinase-null cells.* J Biol Chem, 2002. **277**(37): p. 33857-63.

295. Kostic, A. and M.P. Sheetz, *Fibronectin rigidity response through Fyn and p130Cas recruitment to the leading edge.* Mol Biol Cell, 2006. **17**(6): p. 2684-95.

296. Zaidel-Bar, R., Z. Kam, and B. Geiger, *Polarized downregulation of the paxillin-p130CAS-Rac1 pathway induced by shear flow.* J Cell Sci, 2005. **118**(Pt 17): p. 3997-4007.

297. Totsukawa, G., et al., *Distinct roles of MLCK and ROCK in the regulation of membrane protrusions and focal adhesion dynamics during cell migration of fibroblasts.* J Cell Biol, 2004. **164**(3): p. 427-39.

298. Grosheva, I., et al., *Caldesmon effects on the actin cytoskeleton and cell adhesion in cultured HTM cells.* Exp Eye Res, 2006. **82**(6): p. 945-58.

299. Helfman, D.M., et al., *Caldesmon inhibits nonmuscle cell contractility and interferes with the formation of focal adhesions.* Mol Biol Cell, 1999. **10**(10): p. 3097-112.

300. Leopoldt, D., H.F. Yee, Jr., and E. Rozengurt, *Calyculin-A induces focal adhesion assembly and tyrosine phosphorylation of p125(Fak), p130(Cas), and paxillin in Swiss 3T3 cells.* J Cell Physiol, 2001. **188**(1): p. 106-19.

301. Szczepanowska, J., E.D. Korn, and H. Brzeska, *Activation of myosin in HeLa cells causes redistribution of focal adhesions and F-actin from cell center to cell periphery.* Cell Motil Cytoskeleton, 2006. **63**(6): p. 356-74.

302. Xia, D., J.T. Stull, and K.E. Kamm, *Myosin phosphatase targeting subunit 1 affects cell migration by regulating myosin phosphorylation and actin assembly.* Exp Cell Res, 2005. **304**(2): p. 506-17.

303. Clark, E.A., et al., *Integrin-mediated signals regulated by members of the rho family of GTPases.* J Cell Biol, 1998. **142**(2): p. 573-86.

304. Ren, X.D., W.B. Kiosses, and M.A. Schwartz, *Regulation of the small GTP-binding protein Rho by cell adhesion and the cytoskeleton.* EMBO J, 1999. **18**(3): p. 578-85.

305. Schoenwaelder, S.M. and K. Burridge, *Bidirectional signaling between the cytoskeleton and integrins.* Curr Opin Cell Biol, 1999. **11**(2): p. 274-86.

306. Etienne-Manneville, S. and A. Hall, *Rho GTPases in cell biology.* Nature, 2002. **420**(6916): p. 629-35.

307. Hall, A., *Rho GTPases and the actin cytoskeleton.* Science, 1998. **279**(5350): p. 509-14.

308. Wittmann, T. and C.M. Waterman-Storer, *Cell motility: can Rho GTPases and microtubules point the way?* J Cell Sci, 2001. **114**(Pt 21): p. 3795-803.

309. Ridley, A.J., et al., *Cell migration: integrating signals from front to back.* Science, 2003. **302**(5651): p. 1704-9.

310. Bhadriraju, K., et al., *Activation of ROCK by RhoA is regulated by cell adhesion, shape, and cytoskeletal tension.* Exp Cell Res, 2007. **313**(16): p. 3616-23.

311. Kolodney, M.S. and E.L. Elson, *Contraction due to microtubule disruption is associated with increased phosphorylation of myosin regulatory light chain.* Proc Natl Acad Sci U S A, 1995. **92**(22): p. 10252-6.

312. Liu, B.P., M. Chrzanowska-Wodnicka, and K. Burridge, *Microtubule depolymerization induces stress fibers, focal adhesions, and DNA synthesis via the GTP-binding protein Rho.* Cell Adhes Commun, 1998. **5**(4): p. 249-55.

313. Enomoto, T., *Microtubule disruption induces the formation of actin stress fibers and focal adhesions in cultured cells: possible involvement of the rho signal cascade.* Cell Struct Funct, 1996. **21**(5): p. 317-26.

314. Amano, M., et al., *Formation of actin stress fibers and focal adhesions enhanced by Rho-kinase.* Science, 1997. **275**(5304): p. 1308-11.

315. Grinnell, F., *Fibroblast biology in three-dimensional collagen matrices.* Trends Cell Biol, 2003. **13**(5): p. 264-9.

316. Zemel, A. and S.A. Safran, *Active self-polarization of contractile cells in asymmetrically shaped domains.* Phys Rev E Stat Nonlin Soft Matter Phys, 2007. **76**(2 Pt 1): p. 021905.

317. Wang, H.B., M. Dembo, and Y.L. Wang, *Substrate flexibility regulates growth and apoptosis of normal but not transformed cells.* Am J Physiol Cell Physiol, 2000. **279**(5): p. C1345-50.

318. Yeung, T., et al., *Effects of substrate stiffness on cell morphology, cytoskeletal structure, and adhesion.* Cell Motil Cytoskeleton, 2005. **60**(1): p. 24-34.

319. Califano, J.P. and C.A. Reinhart-King, *Substrate Stiffness and Cell Area Predict Cellular Traction Stresses in Single Cells and Cells in Contact.* Cell Mol Bioeng, 2010. **3**(1): p. 68-75.

320. Shewan, A.M., et al., *Myosin 2 is a key Rho kinase target necessary for the local concentration of E-cadherin at cell-cell contacts.* Mol Biol Cell, 2005. **16**(10): p. 4531-42.

321. Liu, Z., et al., *Mechanical tugging force regulates the size of cell-cell junctions.* Proc Natl Acad Sci U S A, 2010. **107**(22): p. 9944-9.

322. Maruthamuthu, V., et al., *Cell-ECM traction force modulates endogenous tension at cell-cell contacts.* Proc Natl Acad Sci U S A, 2011. **108**(12): p. 4708-13.

323. Carmeliet, P., *Angiogenesis in health and disease.* Nature Medicine, 2003. **9**(6): p. 653-660.

324. Folkman, J., *Angiogenesis in cancer, vascular, rheumatoid and other disease.* Nat Med, 1995. **1**(1): p. 27-31.

325. Carmeliet, P. and R.K. Jain, *Angiogenesis in cancer and other diseases.* Nature, 2000. **407**(6801): p. 249-257.

326. Holderfield, M.T. and C.C. Hughes, *Crosstalk between vascular endothelial growth factor, notch, and transforming growth factor-beta in vascular morphogenesis.* Circ Res, 2008. **102**(6): p. 637-52.

327. Davis, G.E. and D.R. Senger, *Endothelial extracellular matrix - Biosynthesis, remodeling, and functions during vascular morphogenesis and neovessel stabilization.* Circulation Research, 2005. **97**(11): p. 1093-1107.

328. Lee, H., E.J. Goetzl, and S. An, *Effects of lysophosphatidic acid and sphingosine 1-phosphate on endothelial cells.* Faseb Journal, 1999. **13**(5): p. A706-A706.

329. Lee, H., E.J. Goetzl, and S.Z. An, *Lysophosphatidic acid and sphingosine 1-phosphate stimulate endothelial cell wound healing.* American Journal of Physiology-Cell Physiology, 2000. **278**(3): p. C612-C618.

330. Bayless, K.J. and G.E. Davis, *Sphingosine-1-phosphate markedly induces matrix metalloproteinase and integrin-dependent human endothelial cell invasion and lumen formation in three-dimensional collagen and fibrin matrices.* Biochemical and Biophysical Research Communications, 2003. **312**(4): p. 903-913.

331. Lafleur, M.A., et al., *Endothelial tubulogenesis within fibrin gels specifically requires the activity of membrane-type-matrix metalloproteinases (MT-MMPs).* J Cell Sci, 2002. **115**(Pt 17): p. 3427-38.

332. Hotary, K.B., et al., *Matrix metalloproteinases (MMPs) regulate fibrin-invasive activity via MT1-MMP-dependent and -independent processes.* Journal of Experimental Medicine, 2002. **195**(3): p. 295-308.

333. Saunders, W.B., et al., *Coregulation of vascular tube stabilization by endothelial cell TIMP-2 and pericyte TIMP-3.* Journal of Cell Biology, 2006. **175**(1): p. 179-191.

334. Freund, I., M. Deutsch, and A. Sprecher, *Connective-Tissue Polarity - Optical 2nd-Harmonic Microscopy, Crossed-Beam Summation, and Small-Angle Scattering in Rat-Tail Tendon.* Biophysical Journal, 1986. **50**(4): p. 693-712.

335. Williams, R.M., W.R. Zipfel, and W.W. Webb, *Multiphoton microscopy in biological research.* Current Opinion in Chemical Biology, 2001. **5**(5): p. 603-608.

336. Zoumi, A., A. Yeh, and B.J. Tromberg, *Imaging cells and extracellular matrix in vivo by using second-harmonic generation and two-photon excited fluorescence.* Proceedings of the National Academy of Sciences of the United States of America, 2002. **99**(17): p. 11014-11019.

337. Campagnola, P.J., et al., *Three-dimensional high-resolution second-harmonic generation imaging of endogenous structural proteins in biological tissues.* Biophysical Journal, 2002. **82**(1): p. 493-508.

338. Brown, E., et al., *Dynamic imaging of collagen and its modulation in tumors in vivo using second-harmonic generation.* Nature Medicine, 2003. **9**(6): p. 796-800.

339. Yeh, A.T., et al., *Imaging wound healing using optical coherence tomography and multiphoton microscopy in an in vitro skin-equivalent tissue model.* Journal of Biomedical Optics, 2004. **9**(2): p. 248-253.

340. Provenzano, P.P., et al., *Collagen reorganization at the tumor-stromal interface facilitates local invasion.* BMC Med, 2006. **4**(1): p. 38.

341. Brown, E.B., et al., *In vivo measurement of gene expression, angiogenesis and physiological function in tumors using multiphoton laser scanning microscopy.* Nat Med, 2001. **7**(7): p. 864-8.

342. Lin, S.J., et al., *Discrimination of basal cell carcinoma from normal dermal stroma by quantitative multiphoton imaging.* Opt Lett, 2006. **31**(18): p. 2756-8.

343. Provenzano, P.P., et al., *Contact guidance mediated three-dimensional cell migration is regulated by Rho/ROCK-dependent matrix reorganization.* Biophys J, 2008. **95**(11): p. 5374-84.

344. Ingman, W.V., et al., *Macrophages promote collagen fibrillogenesis around terminal end buds of the developing mammary gland.* Dev Dyn, 2006. **235**(12): p. 3222-9.

345. Schenke-Layland, K., et al., *Imaging of cardiovascular structures using near-infrared femtosecond multiphoton laser scanning microscopy.* J Biomed Opt, 2005. **10**(2): p. 024017.

346. Kirkpatrick, N.D., et al., *Live imaging of collagen remodeling during angiogenesis.* Am J Physiol Heart Circ Physiol, 2007. **292**(6): p. H3198-206.

347. Konig, K., et al., *In vivo drug screening in human skin using femtosecond laser multiphoton tomography.* Skin Pharmacol Physiol, 2006. **19**(2): p. 78-88.

348. Pena, A.M., et al., *Three-dimensional investigation and scoring of extracellular matrix remodeling during lung fibrosis using multiphoton microscopy.* Microsc Res Tech, 2007. **70**(2): p. 162-70.

349. Wu, Q. and A.T. Yeh, *Rabbit cornea microstructure response to changes in intraocular pressure visualized by using nonlinear optical microscopy.* Cornea, 2008. **27**(2): p. 202-8.

350. Denk, W., J.H. Strickler, and W.W. Webb, *Two-photon laser scanning fluorescence microscopy.* Science, 1990. **248**(4951): p. 73-6.

351. Burridge, K. and M. Chrzanowska-Wodnicka, *Focal adhesions, contractility, and signaling.* Annu Rev Cell Dev Biol, 1996. **12**: p. 463-518.

352. Tapon, N. and A. Hall, *Rho, Rac and Cdc42 GTPases regulate the organization of the actin cytoskeleton.* Curr Opin Cell Biol, 1997. **9**(1): p. 86-92.

353. Aspenstrom, P., *Effectors for the Rho GTPases.* Curr Opin Cell Biol, 1999. **11**(1): p. 95-102.

354. Ridley, A.J., *Rho family proteins: coordinating cell responses.* Trends Cell Biol, 2001. **11**(12): p. 471-7.

355. Barrett, K., M. Leptin, and J. Settleman, *The Rho GTPase and a putative RhoGEF mediate a signaling pathway for the cell shape changes in Drosophila gastrulation.* Cell, 1997. **91**(7): p. 905-15.

356. Hacker, U. and N. Perrimon, *DRhoGEF2 encodes a member of the Dbl family of oncogenes and controls cell shape changes during gastrulation in Drosophila.* Genes Dev, 1998. **12**(2): p. 274-84.

357. Ridley, A.J., *Stress fibres take shape.* Nat Cell Biol, 1999. **1**(3): p. E64-6.

358. Riveline, D., et al., *Focal contacts as mechanosensors: externally applied local mechanical force induces growth of focal contacts by an mDia1-dependent and ROCK-independent mechanism.* J Cell Biol, 2001. **153**(6): p. 1175-86.

359. Maciag, T., et al., *Endothelial Cell-Growth Factor from Bovine Hypothalamus - Identification and Partial Characterization.* Proceedings of the National Academy of Sciences of the United States of America, 1979. **76**(11): p. 5674-5678.

360. Su, S.C., et al., *Molecular profile of endothelial invasion of three-dimensional collagen matrices: insights into angiogenic sprout induction in wound healing.* Am J Physiol Cell Physiol, 2008. **295**(5): p. C1215-29.

361. Larson, A.M. and A.T. Yeh, *Ex vivo characterization of sub-10-fs pulses.* Opt Lett, 2006. **31**(11): p. 1681-3.

362. Davis, G.E., S.M. Black, and K.J. Bayless, *Capillary morphogenesis during human endothelial cell invasion of three-dimensional collagen matrices.* In Vitro Cellular & Developmental Biology-Animal, 2000. **36**(8): p. 513-519.

363. Baker, A.H., D.R. Edwards, and G. Murphy, *Metalloproteinase inhibitors: biological actions and therapeutic opportunities.* Journal of Cell Science, 2002. **115**(19): p. 3719-3727.

364. Kim, A., N. Lakshman, and W.M. Petroll, *Quantitative assessment of local collagen matrix remodeling in 3-D culture: the role of Rho kinase.* Exp Cell Res, 2006. **312**(18): p. 3683-92.

365. Ghajar, C.M., et al., *Mesenchymal stem cells enhance angiogenesis in mechanically viable prevascularized tissues via early matrix metalloproteinase upregulation.* Tissue Eng, 2006. **12**(10): p. 2875-88.

366. Nehls, V. and R. Herrmann, *The configuration of fibrin clots determines capillary morphogenesis and endothelial cell migration.* Microvasc Res, 1996. **51**(3): p. 347-64.

367. Pizzo, A.M., et al., *Extracellular matrix (ECM) microstructural composition regulates local cell-ECM biomechanics and fundamental fibroblast behavior: a multidimensional perspective.* J Appl Physiol, 2005. **98**(5): p. 1909-21.

368. Rhee, S. and F. Grinnell, *Fibroblast mechanics in 3D collagen matrices.* Adv Drug Deliv Rev, 2007. **59**(13): p. 1299-305.

369. Wang, J., et al., *Mechanical force regulation of myofibroblast differentiation in cardiac fibroblasts.* Am J Physiol Heart Circ Physiol, 2003. **285**(5): p. H1871-81.

370. Carmeliet, P., *Fibroblast growth factor-1 stimulates branching and survival of myocardial arteries - A goal for therapeutic angiogenesis?* Circulation Research, 2000. **87**(3): p. 176-178.

371. Topper, J.N., et al., *Identification of vascular endothelial genes differentially responsive to fluid mechanical stimuli: cyclooxygenase-2, manganese superoxide dismutase, and endothelial cell nitric oxide synthase are selectively up-regulated by steady laminar shear stress.* Proc Natl Acad Sci U S A, 1996. **93**(19): p. 10417-22.

372. Hynes, R.O., *Integrins: bidirectional, allosteric signaling machines.* Cell, 2002. **110**(6): p. 673-87.

373. Lubarsky, B. and M.A. Krasnow, *Tube morphogenesis: Making and shaping biological tubes.* Cell, 2003. **112**(1): p. 19-28.

374. Davis, G.E., K.J. Bayless, and A. Mavila, *Molecular basis of endothelial cell morphogenesis in three-dimensional extracellular matrices.* Anatomical Record, 2002. **268**(3): p. 252-275.

375. Humphries, M.J., et al., *Mechanisms of integration of cells and extracellular matrices by integrins.* Biochem Soc Trans, 2004. **32**(Pt 5): p. 822-5.

376. Ingber, D.E., *Mechanical signaling and the cellular response to extracellular matrix in angiogenesis and cardiovascular physiology.* Circ Res, 2002. **91**(10): p. 877-87.

377. Friedl, P., *Dynamic imaging of cellular interactions with extracellular matrix.* Histochem Cell Biol, 2004. **122**(3): p. 183-90.

378. Friedl, P. and E.B. Brocker, *The biology of cell locomotion within three-dimensional extracellular matrix.* Cell Mol Life Sci, 2000. **57**(1): p. 41-64.

379. Niggemann, B., et al., *Tumor cell locomotion: differential dynamics of spontaneous and induced migration in a 3D collagen matrix.* Exp Cell Res, 2004. **298**(1): p. 178-87.

380. Kwon, G.P., et al., *Contribution of macromolecular structure to the retention of low-density lipoprotein at arterial branch points.* Circulation, 2008. **117**(22): p. 2919-27.

381. Syeda, B., et al., *Arterial compliance: a diagnostic marker for atherosclerotic plaque burden?* Am J Hypertens, 2003. **16**(5 Pt 1): p. 356-62.

382. Bonapace, S., et al., *Aortic stiffness correlates with an increased extracellular matrix turnover in patients with dilated cardiomyopathy.* Am Heart J, 2006. **152**(1): p. 93 e1-6.

383. Wolf, K., et al., *Multi-step pericellular proteolysis controls the transition from individual to collective cancer cell invasion.* Nature Cell Biology, 2007. **9**(8): p. 893-U39.

384. Gerhardt, H., et al., *VEGF guides angiogenic sprouting utilizing endothelial tip cell filopodia.* J Cell Biol, 2003. **161**(6): p. 1163-77.

385. Folkman, J., *Angiogenesis.* Annu Rev Med, 2006. **57**: p. 1-18.

386. Su, S.C. and K.J. Bayless, *Utilizing sphingosine-1-phosphate to stimulate sprouting angiogenesis.* Methods Mol Biol, 2012. **874**: p. 201-13.

387. Saunders, W.B., K.J. Bayless, and G.E. Davis, *MMP-1 activation by serine proteases and MMP-10 induces human capillary tubular network collapse and regression in 3D collagen matrices.* Journal of Cell Science, 2005. **118**(10): p. 2325-2340.

388. Erler, J.T. and V.M. Weaver, *Three-dimensional context regulation of metastasis.* Clin Exp Metastasis, 2009. **26**(1): p. 35-49.

389. Wells, R.G., *The role of matrix stiffness in regulating cell behavior.* Hepatology, 2008. **47**(4): p. 1394-400.

390. Reinhart-King, C.A., M. Dembo, and D.A. Hammer, *Cell-cell mechanical communication through compliant substrates.* Biophys J, 2008. **95**(12): p. 6044-51.

391. Stroka, K.M. and H. Aranda-Espinoza, *A biophysical view of the interplay between mechanical forces and signaling pathways during transendothelial cell migration.* FEBS J, 2010. **277**(5): p. 1145-58.

392. Peyton, S.R. and A.J. Putnam, *Extracellular matrix rigidity governs smooth muscle cell motility in a biphasic fashion.* J Cell Physiol, 2005. **204**(1): p. 198-209.

393. Engler, A., et al., *Substrate compliance versus ligand density in cell on gel responses.* Biophysical Journal, 2004. **86**(1): p. 617-628.

394. Pelham, R.J., Jr. and Y. Wang, *Cell locomotion and focal adhesions are regulated by substrate flexibility.* Proc Natl Acad Sci U S A, 1997. **94**(25): p. 13661-5.

395. Fereol, S., et al., *Sensitivity of alveolar macrophages to substrate mechanical and adhesive properties.* Cell Motil Cytoskeleton, 2006. **63**(6): p. 321-40.

396. Stroka, K.M. and H. Aranda-Espinoza, *Neutrophils display biphasic relationship between migration and substrate stiffness.* Cell Motil Cytoskeleton, 2009. **66**(6): p. 328-41.

397. Pathak, A. and S. Kumar, *Independent regulation of tumor cell migration by matrix stiffness and confinement.* Proc Natl Acad Sci U S A, 2012. **109**(26): p. 10334-9.

398. Pathak, A. and S. Kumar, *Biophysical regulation of tumor cell invasion: moving beyond matrix stiffness.* Integr Biol (Camb), 2011. **3**(4): p. 267-78.

399. Ulrich, T.A., E.M. de Juan Pardo, and S. Kumar, *The mechanical rigidity of the extracellular matrix regulates the structure, motility, and proliferation of glioma cells.* Cancer Res, 2009. **69**(10): p. 4167-74.

400. Saha, K., et al., *Substrate modulus directs neural stem cell behavior.* Biophys J, 2008. **95**(9): p. 4426-38.

401. An, S.S., et al., *Cell stiffness, contractile stress and the role of extracellular matrix.* Biochem Biophys Res Commun, 2009. **382**(4): p. 697-703.

402. Sieminski, A.L., et al., *The stiffness of three-dimensional ionic self-assembling peptide gels affects the extent of capillary-like network formation.* Cell Biochem Biophys, 2007. **49**(2): p. 73-83.

403. Vailhe, B., et al., *In vitro angiogenesis is modulated by the mechanical properties of fibrin gels and is related to alpha(v)beta3 integrin localization.* In Vitro Cell Dev Biol Anim, 1997. **33**(10): p. 763-73.

404. Kanzawa, S., H. Endo, and N. Shioya, *Improved in vitro angiogenesis model by collagen density reduction and the use of type III collagen.* Ann Plast Surg, 1993. **30**(3): p. 244-51.

405. Hoying, J.B., C.A. Boswell, and S.K. Williams, *Angiogenic potential of microvessel fragments established in three-dimensional collagen gels.* In Vitro Cell Dev Biol Anim, 1996. **32**(7): p. 409-19.

406. Gribova, V., T. Crouzier, and C. Picart, *A material's point of view on recent developments of polymeric biomaterials: control of mechanical and biochemical properties.* Journal of Materials Chemistry, 2011(21): p. 14354-14366.

407. Lee, P.F., A.T. Yeh, and K.J. Bayless, *Nonlinear optical microscopy reveals invading endothelial cells anisotropically alter three-dimensional collagen matrices.* Exp Cell Res, 2009. **315**(3): p. 396-410.

408. Wu, Q., B.E. Applegate, and A.T. Yeh, *Cornea microstructure and mechanical responses measured with nonlinear optical and optical coherence microscopy using sub-10-fs pulses.* Biomed Opt Express, 2011. **2**(5): p. 1135-46.

409. Gonzales, R.C., R.E. Woods, and S.L. Eddins, *Digital Image Processing using MATLAB*. 2nd ed. 2009: GATESMARK.

410. Hu, J.J., J.D. Humphrey, and A.T. Yeh, *Characterization of Engineered Tissue Development under Biaxial Stretch Using Nonlinear Optical Microscopy.* Tissue Eng Part A, 2008.

411. Fujimoto, D., *Isolation and characterization of a fluorescent material in bovine achilles tendon collagen.* Biochem Biophys Res Commun, 1977. **76**(4): p. 1124-9.

412. Sell, D.R. and V.M. Monnier, *Isolation, purification and partial characterization of novel fluorophores from aging human insoluble collagen-rich tissue.* Connect Tissue Res, 1989. **19**(1): p. 77-92.

413. Migneault, I., et al., *Glutaraldehyde: behavior in aqueous solution, reaction with proteins, and application to enzyme crosslinking.* Biotechniques, 2004. **37**(5): p. 790-6, 798-802.

414. Hiiragi, T., et al., *Transglutaminase type 1 and its cross-linking activity are concentrated at adherens junctions in simple epithelial cells.* J Biol Chem, 1999. **274**(48): p. 34148-54.

415. ChrzanowskaWodnicka, M. and K. Burridge, *Rho-stimulated contractility drives the formation of stress fibers and focal adhesions.* Journal of Cell Biology, 1996. **133**(6): p. 1403-1415.

416. Borghi, N., et al., *Regulation of cell motile behavior by crosstalk between cadherin- and integrin-mediated adhesions.* Proc Natl Acad Sci U S A, 2010. **107**(30): p. 13324-9.

417. Toriseva, M. and V.M. Kahari, *Proteinases in cutaneous wound healing.* Cell Mol Life Sci, 2009. **66**(2): p. 203-24.

418. Guo, S. and L.A. Dipietro, *Factors affecting wound healing.* J Dent Res, 2010. **89**(3): p. 219-29.

419. Barrientos, S., et al., *Growth factors and cytokines in wound healing.* Wound Repair Regen, 2008. **16**(5): p. 585-601.

420. Midwood, K.S., L.V. Williams, and J.E. Schwarzbauer, *Tissue repair and the dynamics of the extracellular matrix.* Int J Biochem Cell Biol, 2004. **36**(6): p. 1031-7.

421. Martin, P., *Wound healing--aiming for perfect skin regeneration.* Science, 1997. **276**(5309): p. 75-81.

422. Tonnesen, M.G., X. Feng, and R.A. Clark, *Angiogenesis in wound healing.* J Investig Dermatol Symp Proc, 2000. **5**(1): p. 40-6.

423. Rowe, S.L., S. Lee, and J.P. Stegemann, *Influence of thrombin concentration on the mechanical and morphological properties of cell-seeded fibrin hydrogels.* Acta Biomater, 2007. **3**(1): p. 59-67.

424. Eyrich, D., et al., *Long-term stable fibrin gels for cartilage engineering.* Biomaterials, 2007. **28**(1): p. 55-65.

425. Kjaergard, H.K. and U.S. Weis-Fogh, *Important factors influencing the strength of autologous fibrin glue; the fibrin concentration and reaction time--comparison of strength with commercial fibrin glue.* Eur Surg Res, 1994. **26**(5): p. 273-6.

426. Sun, Y., O. Giraudier, and V.L. Garde, *Rheological characterization and dissolution kinetics of fibrin gels crosslinked by a microbial transglutaminase.* Biopolymers, 2005. **77**(5): p. 257-63.

427. Kronek, J., et al., *Mechanical properties of artery-artery connection based upon transglutaminase cross-linked gelatin.* METALURGIJA, 2010. **49**(2): p. 356-360.

428. McDermott, M.K., et al., *Mechanical properties of biomimetic tissue adhesive based on the microbial transglutaminase-catalyzed crosslinking of gelatin.* Biomacromolecules, 2004. **5**(4): p. 1270-1279.

429. Yao, L., et al., *The effect of laminin peptide gradient in enzymatically cross-linked collagen scaffolds on neurite growth.* J Biomed Mater Res A, 2009(92): p. 484-492.

430. Nomura, Y., et al., *Effect of transglutaminase on reconstruction and physicochemical properties of collagen gel from shark type I collagen.* Biomacromolecules, 2001. **2**(1): p. 105-110.

431. Chau, D.Y.S., et al., *The cellular response to transglutaminase-cross-linked collagen.* Biomaterials, 2005. **26**(33): p. 6518-6529.

432. Garcia, Y., et al., *Towards development of a dermal rudiment for enhanced wound healing response.* Biomaterials, 2008. **29**(7): p. 857-868.

433. Mammoto, A., et al., *A mechanosensitive transcriptional mechanism that controls angiogenesis.* Nature, 2009. **457**(7233): p. 1103-U57.

434. Sant, S., et al., *Biomimetic Gradient Hydrogels for Tissue Engineering.* Can J Chem Eng, 2010. **88**(6): p. 899-911.

435. Yang, P.J. and J.S. Temenoff, *Engineering orthopedic tissue interfaces.* Tissue Eng Part B Rev, 2009. **15**(2): p. 127-41.

436. Miserez, A., et al., *The transition from stiff to compliant materials in squid beaks.* Science, 2008. **319**(5871): p. 1816-9.

437. Seidi, A., et al., *Gradient biomaterials for soft-to-hard interface tissue engineering.* Acta Biomater, 2011. **7**(4): p. 1441-51.

438. Seidi, A. and M. Ramalingam, *Impact of gradient biomaterials on interface tissue engineering.* Journal of Biomaterials and Tissue Engineering, 2012. **2**: p. 89-99.

439. Place, E.S., N.D. Evans, and M.M. Stevens, *Complexity in biomaterials for tissue engineering.* Nat Mater, 2009. **8**(6): p. 457-70.

440. Mikos, A.G., et al., *Engineering complex tissues.* Tissue Eng, 2006. **12**(12): p. 3307-39.

441. Peret, B.J. and W.L. Murphy, *Controllable Soluble Protein Concentration Gradients in Hydrogel Networks.* Adv Funct Mater, 2008. **18**(21): p. 3410-3417.

442. Phillips, J.E., et al., *Engineering graded tissue interfaces.* Proc Natl Acad Sci U S A, 2008. **105**(34): p. 12170-5.

443. Kutejova, E., J. Briscoe, and A. Kicheva, *Temporal dynamics of patterning by morphogen gradients.* Curr Opin Genet Dev, 2009. **19**(4): p. 315-22.

444. Wang, F., *The signaling mechanisms underlying cell polarity and chemotaxis.* Cold Spring Harb Perspect Biol, 2009. **1**(4): p. a002980.

445. Makarenkova, H.P., et al., *Differential interactions of FGFs with heparan sulfate control gradient formation and branching morphogenesis.* Sci Signal, 2009. **2**(88): p. ra55.

446. DeLong, S.A., J.J. Moon, and J.L. West, *Covalently immobilized gradients of bFGF on hydrogel scaffolds for directed cell migration.* Biomaterials, 2005. **26**(16): p. 3227-34.

447. Chung, S., et al., *Cell migration into scaffolds under co-culture conditions in a microfluidic platform.* Lab Chip, 2009. **9**(2): p. 269-75.

448. Vickerman, V., et al., *Design, fabrication and implementation of a novel multi-parameter control microfluidic platform for three-dimensional cell culture and real-time imaging.* Lab Chip, 2008. **8**(9): p. 1468-77.

449. Kloxin, A.M., J.A. Benton, and K.S. Anseth, *In situ elasticity modulation with dynamic substrates to direct cell phenotype.* Biomaterials, 2010. **31**(1): p. 1-8.

450. Choquet, D., D.P. Felsenfeld, and M.P. Sheetz, *Extracellular matrix rigidity causes strengthening of integrin-cytoskeleton linkages.* Cell, 1997. **88**(1): p. 39-48.

451. Oh, S.H., et al., *In vitro and in vivo characteristics of PCL scaffolds with pore size gradient fabricated by a centrifugation method.* Biomaterials, 2007. **28**(9): p. 1664-71.

452. Dubruel, P., et al., *Porous gelatin hydrogels: 2. In vitro cell interaction study.* Biomacromolecules, 2007. **8**(2): p. 338-44.

453. Wu, J., et al., *Gradient biomaterials and their influences on cell migration.* Interface Focus, 2012. **2**: p. 337-355.

454. Gillette, B.M., et al., *Engineering extracellular matrix structure in 3D multiphase tissues.* Biomaterials, 2011. **32**(32): p. 8067-76.

455. Nam, K., et al., *Fabrication of a heterostructural fibrillated collagen matrix for the regeneration of soft tissue function.* Soft Matter, 2012. **8**: p. 472-480.

456. He, J., et al., *Rapid generation of biologically relevant hydrogels containing long-range chemical gradients.* Adv Funct Mater, 2010. **20**(1): p. 131-137.

457. Abhyankar, V.V., et al., *Characterization of a membrane-based gradient generator for use in cell-signaling studies.* Lab Chip, 2006. **6**(3): p. 389-93.

458. Lo, C.T., et al., *Photopolymerized diffusion-defined polyacrylamide gradient gels for on-chip protein sizing.* Lab Chip, 2008. **8**(8): p. 1273-9.